

อันตรกิริยาของพีริดีนคาลิก[4]อาร์นกับแคทไอออนและโมเลกุลอินทรีย์โดยการคำนวณทางเคมีควอนตัม



ประชาน ฤกษ์เมธา

สถาบันวิทยบริการ

จุฬาลงกรณ์มหาวิทยาลัย

วิทยานิพนธ์นี้เป็นส่วนหนึ่งของการศึกษาตามหลักสูตรปริญญาวิทยาศาสตรมหาบัณฑิต

สาขาวิชาเคมี ภาควิชาเคมี


คณะวิทยาศาสตร์ จุฬาลงกรณ์มหาวิทยาลัย

ปีการศึกษา 2543

ISBN 974-346-741-6

ลิขสิทธิ์ของจุฬาลงกรณ์มหาวิทยาลัย

INTERACTIONS OF PYRIDINOCALIX[4]ARENE WITH CATIONS AND ORGANIC MOLECULES BY  
QUANTUM CHEMICAL CALCULATIONS



PRATAN RUEKMETHA

สถาบันวิทยบริการ  
จุฬาลงกรณ์มหาวิทยาลัย

A Thesis Submitted in Partial Fulfillment of the Requirements  
for the Degree of Master of Science in Chemistry

Department of Chemistry

Faculty of Science

Chulalongkorn University

Academic Year 2000

ISBN 974-346-741-6

Thesis Title                      Interactions of Pyridinocalix[4]arene with Cations and Organic  
Molecules by Quantum Chemical Calculations  
By                                      Pratan Ruekmetha  
Department                        Chemistry  
Thesis Advisor                    Assistant Professor Thawatchai Tuntulani, Ph.D.  
Thesis Co-advisor               Associate Professor Vithaya Ruangpornvisuti, Dr. rer. nat.

---

Accepted by the Faculty of Science, Chulalongkorn University in Partial  
Fulfillment of the Requirements for the Master 's Degree

..... Dean of Faculty of Science  
(Associate Professor Wanchai Phothiphichi, Ph.D.)

THESIS COMMITTEE

..... Chairman  
(Associate Professor Supot Hannongbua, Ph.D.)

..... Thesis Advisor  
(Assistant Professor Thawatchai Tuntulani, Ph.D.)

..... Thesis Co-advisor  
(Associate Professor Vithaya Ruangpornvisuti, Dr. rer. nat.)

..... Member  
(Associate Professor Chai Hok Eab, Ph.D.)

..... Member  
(Nongnuj Jaiboon, Ph.D.)

ประธาน ฤกษ์เมธา : อันตรกิริยาของพิริดีนคาลิก[4]เอรีนกับแคทไอออนและโมเลกุลอินทรีย์โดยการคำนวณทางเคมีควอนตัม (INTERACTIONS OF PYRIDINOCALIX[4]ARENE WITH CATIONS AND ORGANIC MOLECULES BY QUANTUM CHEMICAL CALCULATIONS) อ. ที่ปรึกษา : ผศ.ดร. รัชชชัย ต้นทุลานี, อ. ที่ปรึกษาร่วม : รศ.ดร.วิทยา เรืองพรวิสุทธิ, 109 หน้า. ISBN 974-346-741-6.

โครงสร้างของสารประกอบ 25,27-ได(4-เมทิล-ไพริดีน)พาราเทอร์เซียร์บิวทิลคาลิก[4]เอรีน (L) สองแบบที่ถูกตรึงไว้ คือ แบบ  $L_{\perp}$  ที่หมู่ไพริดีนเมทิลชี้ไปในทิศทางตรงกันข้าม กับแบบ  $L_{\parallel}$  ซึ่งหมู่ไพริดีนเมทิลชี้เข้าหากันหาได้โดยวิธี AM1 คำนวณพลังงานศักย์ที่เสถียรที่สุดระหว่างโครงสร้างแบบ  $L_{\perp}$  กับโปรตอน, เมทานอล,  $Li^+$ ,  $Na^+$ ,  $K^+$ ,  $Be^{2+}$ ,  $Mg^{2+}$  ได้โดยวิธีแอบ อินิซิโอ ที่ระดับเบซิส เซต STO-3G และ 6-31G พบว่า  $L_{\perp}$  จะเกิดสารประกอบเชิงซ้อนกับ  $Na^+$  และ  $K^+$  โดยอันตรกิริยา 2 ประเภทคือ อันตรกิริยาระหว่าง  $Na^+$  และ  $K^+$  กับออกซิเจน และอันตรกิริยา  $Na^+-\pi$  และ  $K^+-\pi$  อย่างไรก็ตามพบว่า  $L_{\perp}$  จะเกิดสารประกอบเชิงซ้อนกับ  $Li^+$ ,  $Be^{2+}$  และ  $Mg^{2+}$  โดยใช้อันตรกิริยาระหว่างไอออนของโลหะกับออกซิเจน การหาค่าพลังงานเสถียรของการเกิดสารประกอบเชิงซ้อนระหว่างโครงสร้างแบบ  $L_{\parallel}$  กับ รีซอร์ซินอล และกรดพทาสิก พบว่ามีค่าพลังงานความเสถียรเท่ากับ -16.1 และ -17.5 กิโลคาลอรีต่อโมลตามลำดับ ความยาวพันธะ  $N\cdots H$  ระหว่างไพริดีนไนโตรเจนกับโปรตอนกรดของกรดพทาสิกมีความยาวเท่ากับ 1.90 Å ส่วนความยาวพันธะระหว่างไพริดีนไนโตรเจนกับไฮดรอกซีโปรตอนของรีซอร์ซินอลมีความยาวเท่ากับ 1.90 Å การคำนวณทางควอนตัมแสดงให้เห็นว่ารีซอร์ซินอลกับกรดพทาสิกจะไม่เกิดสารประกอบเชิงซ้อนแบบอินคลูชันกับ  $L_{\parallel}$  ในสถานะแก๊ส

สถาบันวิทยบริการ  
จุฬาลงกรณ์มหาวิทยาลัย

ภาควิชา .....เคมี.....  
สาขาวิชา ...เคมี.....  
ปีการศึกษา ...2543.....

ลายมือชื่อนิสิต .....  
ลายมือชื่ออาจารย์ที่ปรึกษา .....  
ลายมือชื่ออาจารย์ที่ปรึกษาร่วม .....

## 4072299323 : MAJOR CHEMISTRY

KEY WORD: *p-tert*-BUTYLCALIX[4]ARENES / 25,27-DI(4-METHYL-PYRIDINE)-*p-tert*-BUTYLCALIX[4]ARENE /

*AB INITIO* ENERGY / COMPLEXES / CONFORMATIONAL ANALYSIS

PRATAN RUEKMETHA : INTERACTIONS OF PYRIDINOCALIX[4]ARENE WITH CATIONS AND ORGANIC MOLECULES BY QUANTUM CHEMICAL CALCULATIONS. THESIS ADVISOR : ASSIST. PROF. THAWATCHAI TUNTULANI, Ph.D., THESIS COADVISOR ASSOC. PROF. VITHAYA RUANGPORNVISUTI, Dr. rer. nat., 109 pp. ISBN 974-346-741-6.

Two rigidity configurations of 25,27-di(4-methyl-pyridine)-*p-tert*-butylcalix[4]arene (**L**), **L<sub>I</sub>** which possesses pyridine methyl groups pointing in the opposite direction and **L<sub>II</sub>** which possesses pyridine methyl groups pointing towards each other were obtained by structural optimization using AM1 method. Potential energies of interactions between the configuration **L<sub>I</sub>** and proton, methanol, Li<sup>+</sup>, Na<sup>+</sup>, K<sup>+</sup>, Be<sup>2+</sup> and Mg<sup>2+</sup> were calculated by *ab initio* methods using STO-3G and 6-31G basis sets. It was found that **L<sub>I</sub>** could form a complex with Na<sup>+</sup> and K<sup>+</sup> by two types of interactions: Na<sup>+</sup> and K<sup>+</sup>-oxygen interaction and a Na<sup>+</sup> and K<sup>+</sup>- $\pi$  interaction. Nevertheless, **L<sub>I</sub>** could form complexes with Li<sup>+</sup>, Be<sup>2+</sup> and Mg<sup>2+</sup> using metal-oxygen interactions. Complexation studies of **L<sub>II</sub>** with resorcinol and phthalic acid were found to have stabilization energies of -16.1 and -17.5 kcal mol<sup>-1</sup>, respectively. The N...H bond distance between the pyridine nitrogen and the acidic protons of phthalic acid was 1.90 Å while that between the pyridine nitrogen and the hydroxy protons of resorcinol was 1.90 Å. Quantum calculations also showed that resorcinol and phthalic acid could not be included into the cavity of **L<sub>II</sub>** in the gas phase.

สถาบันวิทยบริการ  
จุฬาลงกรณ์มหาวิทยาลัย

Department ...Chemistry.....	Student's signature .....
Field of study ...Chemistry.....	Advisor's signature .....
Academic year ...2000.....	Co-advisor's signature .....

## ACKNOWLEDGMENTS

I would like to express my sincerest gratitude to my advisor, Assist. Prof. Dr. Thawatchai Tuntulani, my co-advisor, Assoc. Prof. Dr. Vithaya Ruangpornvisuti and Dr. Buncha Pulpoka for their guidance, kindness, suggestions, supports and also aids in my writing and discussion in this thesis. In addition, I thank the thesis committee for their valuable suggestions and attention.

I would like to thank the Department of Chemistry, Faculty of Science and the Graduate School, Chulalongkorn University for providing the basic facilities and financial support.

Finally, I would like to express much appreciation to my family members for their encouragement and supports to make my study successful.



สถาบันวิทยบริการ  
จุฬาลงกรณ์มหาวิทยาลัย

## CONTENTS

	Pages
Abstract in Thai .....	iv
Abstract in English .....	v
Acknowledgement .....	vi
List of Figures .....	ix
List of Tables .....	xii
<b>CHAPTER I : INTRODUCTION</b> .....	1
1.1    Macrocyclic ligand and cyclic supermolecules.....	1
1.2    The macrocyclic effect and effect of solvation.....	2
1.3    Calixarenes.....	3
1.4    Hydrogen bonding interaction.....	4
1.5    Interaction of nitrogen containing ligand and metal ions.....	4
1.6    Quantum Calculations for Calixarenes.....	6
1.7    Objective and Scope of The Research.....	7
<b>CHAPTER II : METHOD OF CALCULATION</b> .....	8
2.1    Initial structure building.....	8
2.2    Quantum Chemical Calculations.....	8
2.3    Basis Set Effects.....	9
2.3.1    Minimal Basis Sets.....	10
2.3.2    Split Valence Basis Sets.....	10
2.4    Practical considerations when performing <i>ab initio</i> calculations.....	11
2.4.1    Setting up the calculation and the choice of coordinates.....	12
2.4.2    Calculating derivatives of the energy.....	12
2.4.3    Basis set superposition error.....	13

<b>CHAPTER III : RESULTS AND DISCUSSION</b> .....	14
3.1 Structure of <i>p-tert</i> -butylcalix[4]arenes.....	14
3.2 Structure of 25,27-di(4-methyl-pyridine)- <i>p-tert</i> -butylcalix[4]arene.....	17
3.3 Stability of $L_I \cdot H^+$ complex.....	18
3.4 Stability of $L_I \cdot$ methanol complex .....	23
3.5 Stability of $L_I \cdot Li^+$ complex .....	28
3.6 Stability of $L_I \cdot Na^+$ complex.....	33
3.7 Stability of $L_I \cdot K^+$ complex.....	38
3.8 Stability of $L_I \cdot Be^{2+}$ complex .....	41
3.9 Stability of $L_I \cdot Mg^{2+}$ complex.....	46
3.10 Stability of $L_{II}$ and Resorcinol Molecule.....	51
3.11 Stability of $L_{II}$ and Phthalic acid.....	55
<b>CHAPTER V : CONCLUSION</b> .....	59
<b>REFERENCES</b> .....	62
<b>APPENDICES</b> .....	65
<b>VITA</b> .....	93

สถาบันวิทยบริการ  
จุฬาลงกรณ์มหาวิทยาลัย



## LIST OF FIGURES

	Pages
<b>Figure 1.1</b> The conformations of calix[4]arenes.....	3
<b>Figure 1.2</b> Interconversion between various conformations of calix[4]arenes. Energies in kcal mol <sup>-1</sup> .....	6
<b>Figure 2.1</b> represent rotational reference plane of L <sub>I</sub> (a), and center point center of the plane of the 4 carbons of <i>p</i> -tert-butylcalix[4]arene (pointed by arrow), (b).....	9
<b>Figure 3.1</b> The conformations of <i>p</i> -tert-butylcalix[4]arene.....	15
<b>Figure 3.2</b> The two most stable configurations of 25,27-di(4-methylpyridine)- <i>p</i> -tert-butylcalix[4]arene (L), L <sub>I</sub> and L <sub>II</sub> .....	17
<b>Figure 3.3</b> Structure of protonated L <sub>I</sub> .....	18
<b>Figure 3.4</b> The potential curve for proton and the ligand L <sub>I</sub> at the pyridine plane.....	19
<b>Figure 3.5</b> Proton interacting with L <sub>I</sub> along the principle molecular axis.....	21
<b>Figure 3.6</b> The potential curve for interactions between a proton and L <sub>I</sub> along the principal molecular axis.....	21
<b>Figure 3.7</b> Methanol interacting with L <sub>I</sub> .....	23
<b>Figure 3.8</b> The potential curve for methanol and the ligand L <sub>I</sub> at the pyridine plane.....	24
<b>Figure 3.9</b> Methanol interacting with L <sub>I</sub> along the molecular axis.....	26
<b>Figure 3.10</b> The potential curve for interactions between L <sub>I</sub> and methanol along the molecular axis.....	26
<b>Figure 3.11</b> Methanol, points the methoxy unit towards framework interacting with L <sub>I</sub> along the molecular axis.....	27
<b>Figure 3.12</b> The potential curve for interactions between L <sub>I</sub> and methanol, points the methoxy unit towards framework.....	27
<b>Figure 3.13</b> Lithium ion interacting with L <sub>I</sub> .....	28
<b>Figure 3.14</b> The potential curve for interactions of L <sub>I</sub> and Li <sup>+</sup> at the pyridine plane.....	29
<b>Figure 3.15</b> Lithium ion interacting with L <sub>I</sub> along the Z-axis.....	31
<b>Figure 3.16</b> The potential curve for interaction between lithium ion and L <sub>I</sub> along the Z-axis.....	31

	Pages
<b>Figure 3.17</b> The sodium ion interacting with $L_I$ .....	33
<b>Figure 3.18</b> The potential curve for interaction between sodium ion and $L_I$ at the pyridine plane.....	34
<b>Figure 3.19</b> Sodium ion interacting with $L_I$ and along the principal axis.....	36
<b>Figure 3.20</b> The potential curve for interactions between sodium ion and $L_I$ along the principal axis. ....	36
<b>Figure 3.21</b> Potassium ion interacting with $L_I$ .....	38
<b>Figure 3.22</b> The potential curve for potassium ion and the ligand $L_I$ along the $Z$ -axis.....	39
<b>Figure 3.23</b> Beryllium ion interacting with $L_I$ . ....	41
<b>Figure 3.24</b> The potential curve for interaction between beryllium ion and $L_I$ at the pyridine plane. ....	42
<b>Figure 3.25</b> Beryllium ion interacting with $L_I$ along the principal axis.....	44
<b>Figure 3.26</b> The potential curve for interaction between beryllium ion and $L_I$ along the $Z$ -axis. ....	44
<b>Figure 3.27</b> Magnesium ion interacting with $L_I$ . ....	46
<b>Figure 3.28</b> The potential curve for interaction between magnesium ion and $L_I$ at the pyridine plane. ....	47
<b>Figure 3.29</b> Magnesium ion interacting with $L_I$ along the principal axis.....	49
<b>Figure 3.30</b> The potential curve for interaction between magnesium ion and $L_I$ along $Z$ -axis. ....	49
<b>Figure 3.31</b> The resorcinol interacting with the ligand $L_{II}$ .....	51
<b>Figure 3.32</b> The potential curve for interaction between resorcinol and nitrogen atom of $L_{II}$ along the $Z$ -axis. ....	52
<b>Figure 3.33</b> Resorcinol, points the molecular unit below calix[4]arene framework interacting with $L_I$ along the molecular axis.....	54
<b>Figure 3.34</b> The potential curve for interactions between $L_I$ and resorcinol, points the molecular unit below calix[4]arene framework.....	54
<b>Figure 3.35</b> Phthalic acid interacting with $L_{II}$ . ....	55
<b>Figure 3.36</b> The potential curve for interaction between phthalic acid and the ligand $L_{II}$ along the $Z$ -axis. ....	56
<b>Figure 3.37</b> Phthalic acid, points the aromatic unit towards framework interacting with $L_I$ along the molecular axis. ....	58
<b>Figure 3.38</b> The potential curve for interactions between $L_I$ and phthalic acid, points the aromatic unit towards framework.. ....	58
<b>Figure B1</b> Rotational barrier curve of methanol and the ligand $L_I$ .....	84

<b>Figure B2</b>	Rotational barrier curve of methanol which but points the methoxy unit towards the calix[4]arene framework and the ligand L <sub>II</sub> . .....	85
<b>Figure B3</b>	Potential curve of methanol which but points the methoxy unit towards the calix[4]arene framework and the ligand L <sub>II</sub> . .....	86
<b>Figure B4</b>	Rotational barrier curve of resorcinol and the ligand L <sub>II</sub> . .....	87
<b>Figure B5</b>	Rotational barrier curve of resorcinol which points the molecular unit below the calix[4]arene framework included in ligand L <sub>II</sub> . .....	88
<b>Figure B6</b>	Potential curve of resorcinol which points the molecular unit below the calix[4]arene framework and the ligand L <sub>II</sub> . .....	89
<b>Figure B7</b>	Rotational barrier curve of phthalic acid and the ligand L <sub>II</sub> . .....	90
<b>Figure B8</b>	Rotational barrier curve of phthalic acid which points the aromatic unit towards the calix[4]arene framework and the ligand L <sub>II</sub> . .....	91
<b>Figure B9</b>	Potential curve of phthalic acid which points the aromatic unit towards the calix [4]arene framework and the ligand L <sub>II</sub> . .....	92

## LIST OF TABLES

	Pages
<b>Table 1.1</b> Functional groups that form strong and moderate hydrogen bonds.....	5
<b>Table 3.1</b> The SCF energies of <i>p-tert</i> -butylcalix[4]arene conformations evaluated by using <i>ab initio</i> calculations with 6-31G basis set.....	14
<b>Table 3.2</b> Total Energies (in au) of the Cone Calix[4]arene Conformer at Different Theoretical Levels.....	16
<b>Table 3.3</b> The SCF energies of L <sub>I</sub> and L <sub>II</sub> evaluated by using <i>ab initio</i> calculations with 6-31G basis set. ....	17
<b>Table 3.4</b> Total energies and stabilization energies of protonation of L <sub>I</sub> at the pyridine plane.....	19
<b>Table 3.5</b> <i>Ab initio</i> energies with STO-3G and 6-31G basis sets of each counterpoise components and interaction energies with counterpoise procedure of the protonation system.....	20
<b>Table 3.6</b> Total energies and stabilization energies of the protonation of L <sub>I</sub> .....	22
<b>Table 3.7</b> <i>Ab initio</i> energies with STO-3G and 6-31G basis sets of each counterpoise components and interaction energy with counterpoise procedure of the protonation L <sub>I</sub> .....	22
<b>Table 3.8</b> Total energies and stabilization energies of the L <sub>I</sub> · methanol complex.....	24
<b>Table 3.9</b> <i>Ab initio</i> energies with STO-3G and 6-31G basis sets of each counterpoise components and interaction energies with counterpoise procedure of the L <sub>I</sub> · methanol complex.....	25
<b>Table 3.10</b> Total energies and stabilization energies of the L <sub>I</sub> /Li <sup>+</sup> complex system at the pyridine plane.....	29
<b>Table 3.11</b> <i>Ab initio</i> energies with STO-3G and 6-31G basis sets of each counterpoise components and interaction energies with counterpoise procedure of the L <sub>I</sub> /Li <sup>+</sup> complex system at the pyridine plane.....	30
<b>Table 3.12</b> Total energies and stabilization energies of the L <sub>I</sub> /Li <sup>+</sup> complex system at the optimum distance along the Z-axis.....	32

<b>Table 3.13</b>	<i>Ab initio</i> energies with STO-3G and 6-31G basis sets of each counterpoise components and interaction energies with counterpoise procedure of the $L_I/Li^+$ complex system at the optimum distance along the Z-axis.....	32
<b>Table 3.14</b>	Total energies and stabilization energies of the $Na^+/L_I$ complex system at the pyridine plane.....	34
<b>Table 3.15</b>	<i>Ab initio</i> energies with STO-3G and 6-31G basis sets of each counterpoise components and interaction energies with counterpoise procedure of the $Na^+/L_I$ complex system at the pyridine plane orientation.....	35
<b>Table 3.16</b>	Total energies and stabilization energies of the $L_I/Na^+$ complex system at the optimum distance along the Z-axis.....	37
<b>Table 3.17</b>	<i>Ab initio</i> energies with STO-3G and 6-31G basis sets of each counterpoise components and interaction energies with counterpoise procedure of the $L_I/Na^+$ complex system at the optimum distance along the Z-axis.....	38
<b>Table 3.18</b>	Total energies and stabilization energies of the $L_I/K^+$ complex system at the optimum distance along the Z-axis.....	39
<b>Table 3.19</b>	<i>Ab initio</i> energy with STO-3G basis set of each counterpoise components and interaction energies with counterpoise procedure of the $L_I/K^+$ complex system at the optimum distance along the Z-axis.....	40
<b>Table 3.20</b>	Total energies and stabilization energies of the $L_I/Be^{2+}$ complex system at the pyridine plane orientation.....	42
<b>Table 3.21</b>	<i>Ab initio</i> energies with STO-3G and 6-31G basis sets of each counterpoise components and interaction energies with counterpoise procedure of the $L_I/Be^{2+}$ complex system at the pyridine plane.....	43
<b>Table 3.22</b>	Total energies and stabilization energies of the $L_I/Be^{2+}$ complex system at the optimum distance along the Z-axis.....	45
<b>Table 3.23</b>	<i>Ab initio</i> energies with STO-3G and 6-31G basis sets of each counterpoise components and interaction energies with counterpoise procedure of the $L_I/Be^{2+}$ complex system at the optimum distance along the Z-axis.....	45
<b>Table 3.24</b>	Total energies and stabilization energies of the $L_I/Mg^{2+}$ complex system at the pyridine plane orientation.....	47
<b>Table 3.25</b>	<i>Ab initio</i> energies with STO-3G and 6-31G basis sets of each counterpoise components and interaction energies with counterpoise procedure of the $L_I/Mg^{2+}$ complex system at the pyridine plane.....	48



<b>Table 3.26</b>	Total energies and stabilization energies of the $L_I/Mg^{2+}$ complex system at the optimum distance along the Z-axis.....	50
<b>Table 3.27</b>	<i>Ab initio</i> energies with STO-3G and 6-31G basis sets of each counterpoise components and interaction energies with counterpoise procedure of the $L_I/Mg^{2+}$ complex system at the optimum distance along the Z-axis.....	50
<b>Table 3.28</b>	Total energies and stabilization energies of $L_{II}$ /resorcinol complex system at the optimum distance along the Z-axis.....	52
<b>Table 3.29</b>	<i>Ab initio</i> energies with STO-3G and 6-31G basis sets of each counterpoise components and interaction energies with counterpoise procedure of $L_{II}$ /resorcinol complex system at the optimum distance along the Z-axis.....	53
<b>Table 3.30</b>	Total energies and stabilization energies of $L_{II}$ /phthalic acid complex system at the optimum distance along the Z-axis.....	56
<b>Table 3.31</b>	<i>Ab initio</i> energies with STO-3G and 6-31G basis sets of each counterpoise components and interaction energies with counterpoise procedure of $L_{II}$ /phthalic acid complex system at the optimum distance along the Z-axis.....	57
<b>Table 4.1</b>	Summary of the potential energies of interactions between $L_I$ and guest molecules (Type A).....	59
<b>Table 4.2</b>	Summary of the potential energies of interactions between $L_I$ and guest molecules (Type B).....	60
<b>Table 4.3</b>	Summary of interactions between $L_{II}$ and neutral guest molecules. ....	60
<b>Table A1</b>	Interaction data for the ligand $L_I$ and proton. ....	65
<b>Table A2</b>	Interaction data obtained from <i>ab initio</i> calculations with 6-31G basis set, at orientation of proton locating in the Z-axis.....	66
<b>Table A3</b>	Interaction data obtained from <i>ab initio</i> calculations with 6-31G basis set, which methanol locating on the axis along a nitrogen atom of the pyridine plane.....	67
<b>Table A4</b>	Interaction data obtained from <i>ab initio</i> calculations with 6-31G basis set, at orientation of methanol locating in the Z-axis.....	68
<b>Table A5</b>	Interaction data obtained from <i>ab initio</i> calculations with 6-31G basis set, at orientation of methanol which points the methoxy unit towards the calix[4]arene framework locating in the Z-axis. ....	69

	Pages
<b>Table A6</b> Interaction data obtained from <i>ab initio</i> calculations with 6-31G basis set, which lithium locating on the axis along a nitrogen atom of the pyridine plane.....	70
<b>Table A7</b> Interaction data obtained from <i>ab initio</i> calculations with 6-31G basis set, at orientation of lithium locating in the Z-axis.....	71
<b>Table A8</b> Interaction data obtained from <i>ab initio</i> calculations with 6-31G basis set, which sodium locating on the axis along a nitrogen atom of the pyridine plane. ....	72
<b>Table A9</b> Interaction data obtained from <i>ab initio</i> calculations with 6-31G basis set, at orientation of sodium locating in the Z-axis.....	73
<b>Table A10</b> Interaction data obtained from <i>ab initio</i> calculations with 6-31G basis set, at orientation of potassium locating in the Z-axis.....	75
<b>Table A11</b> Interaction data obtained from <i>ab initio</i> calculations with 6-31G basis set, which beryllium locating on the axis along a nitrogen atom of the pyridine plane.....	76
<b>Table A12</b> Interaction data obtained from <i>ab initio</i> calculations with 6-31G basis set, at orientation of beryllium locating in the Z-axis.....	77
<b>Table A13</b> Interaction data obtained from <i>ab initio</i> calculations with 6-31G basis set, which magnesium locating on the axis along a nitrogen atom of the pyridine plane. ....	78
<b>Table A14</b> Interaction data obtained from <i>ab initio</i> calculations with 6-31G basis set, at orientation of magnesium locating in the Z-axis.....	79
<b>Table A15</b> Interaction data obtained from <i>ab initio</i> calculations with 6-31G basis set, at orientation of resorcinol locating in the Z-axis.....	80
<b>Table A16</b> Interaction data obtained from <i>ab initio</i> calculations with 6-31G basis set, at orientation of resorcinol which points the molecular unit below the calix[4]arene framework locating in the Z-axis.....	81
<b>Table A17</b> Interaction data obtained from <i>ab initio</i> calculations with 6-31G basis set, at orientation of phthalic acid locating in the Z-axis.....	82
<b>Table A18</b> Interaction data obtained from <i>ab initio</i> calculations with 6-31G basis set, at orientation of phthalic acid locating in the Z-axis.....	83
<b>Table B1</b> Rotational barrier data obtained from <i>ab initio</i> calculations with STO-3G basis set, of interaction between methanol and the ligand L <sub>1</sub> .....	84

<b>Table B2</b>	Rotational barrier data obtained from <i>ab initio</i> calculations with STO-3G basis set, of interaction between methanol which but points the methoxy unit towards the calix[4]arene framework and the ligand L <sub>II</sub> .....	85
<b>Table B3</b>	Inclusion data obtained from <i>ab initio</i> calculations with STO-3G basis set, of interaction between methanol which but points the methoxy unit towards the calix[4]arene framework and the ligand L <sub>I</sub> .....	86
<b>Table B4</b>	Rotational barrier data obtained from <i>ab initio</i> calculations with STO-3G basis set, of interaction between resorcinol and the ligand L <sub>II</sub> .....	87
<b>Table B5</b>	Rotational barrier data obtained from <i>ab initio</i> calculations with STO-3G basis set, of interaction between resorcinol which points the molecular unit below the calix[4]arene framework and the ligand L <sub>II</sub> .....	88
<b>Table B6</b>	Energies data obtained from <i>ab initio</i> calculations with STO-3G basis set, of interaction between resorcinol which points the molecular unit below the calix[4]arene framework and the ligand L <sub>II</sub> .....	89
<b>Table B7</b>	Rotational barrier data obtained from <i>ab initio</i> calculations with STO-3G basis set, of interaction between phthalic acid and the ligand L <sub>II</sub> .....	90
<b>Table B8</b>	Rotational barrier data obtained from <i>ab initio</i> calculations with STO-3G basis set, of interaction between phthalic acid which points the aromatic unit towards the calix[4]arene framework and the ligand L <sub>II</sub> .....	91
<b>Table B9</b>	Energies data obtained from <i>ab initio</i> calculations with STO-3G basis set, of interaction between phthalic acid which points the aromatic unit towards the calix[4]arene framework and the ligand L <sub>II</sub> .....	92



## CHAPTER I

### INTRODUCTION

#### 1.1 Macrocyclic ligands and cyclic supermolecules

Macrocyclic ligands consist of donating atoms connecting with alkyl or aryl chains in a cyclic manner. The macrocyclic compounds containing electron donating atoms such as nitrogen, oxygen, and sulfur, called as aza, oxa, and thia compounds respectively, have ability to bind cations. The complexation is principally controlled by the structural features of the ligand cavity and size of the cation. The oxidation number and the size of cation usually indicate the stability of complexes<sup>1</sup>.

In general, the magnitude of the protonation constant of macrocyclic ligands depends strongly on the electron donating ability of the binding sites. In the case of highly symmetrical macrocyclic compounds, the magnitude of the successive protonation constants (multiple binding sites) probably depends also on the molecular symmetry<sup>2</sup>. For the binding sites of macrocyclic ligands, oxygen sites provide normally higher electron density but lower polarizability than nitrogen sites.

Complex stability constants are controlled by the nature of ion-ligand interaction, such as the ion-dipole and charge-induced dipole type<sup>3</sup>. The selectivity of the complexation is related further to the "fit" of cations into the ring cavity of the macrocyclic ligand or the cyclic supermolecule. However, both stability and selectivity of complexation are also strongly affected by solvation and counterion<sup>4</sup>.

## 1.2 The macrocyclic effect and effect of solvation

The enhanced stability of the metal ion complex of macrocyclic ligands as compared to their open-chain analogues, has been termed the "macrocyclic effect"<sup>5</sup>. This effect has been firstly attributed to the smaller configurational entropy of the macrocyclic ligands<sup>5</sup>. The most frequent suggestions postulate that the stability of macrocyclic complexes arises from:

(a) the "prestrained" conformation of cyclic ligands, which are already in a conformation most suitable for complex formation<sup>6,7</sup>.

(b) the higher ligand field strength of the cyclic ligands due to the presence of more secondary nitrogen atoms than in the non-cyclic analogues<sup>8</sup>.

(c) the large number of fixed atoms of the cyclic ligands, for which Busch et al.<sup>9</sup> suggested the term "multiple juxtapositional fixiness".

(d) the steric hindrance to solvation of the donor atoms, which are oriented into the ring cavity in the center of the ligands<sup>10,11</sup>.

However, the main source of macrocyclic effect was attributed to the internal interactions of metal and donor groups and, the external interactions between the cyclic ligand and the solvent molecules, which led to the "ligand solvation effect". In an aqueous solution, the complex was supposed to be less hydrated than the metal ion because of the ligand coordination, the decreased charge to radius ratio and hydrophobic exterior presented by the "bound ligand". The release of water from the metal ion and the ligand should result in a positive entropy contribution because the number of free solvent particles has increased, but a negative contribution to the entropy change should come from the loss of configurational entropy of the ligand upon coordination. However, Izatt, et al. suggested that the factors which determine the magnitude of entropy change can be nearly compensated by the change of ligand conformation upon complexation as well as the change in ligand and metal ion hydration and total number of particles<sup>12</sup>.

Nowadays, macrocyclic ligands have played an important role in supramolecular chemistry. The well-known and useful supramolecular building blocks are calixarenes<sup>13</sup>.

### 1.3 Calixarenes

Calixarenes have proved to be very useful building blocks in supramolecular chemistry. They are the cavity-containing-cyclic molecules made up of phenolic units linked *via* methylene bridges. The name *calixarenes* is chosen for these compounds because it clearly describes the shape of these cyclic molecules (calix: beaker, arene: aryl<sup>14</sup>) when they orientate in the cone conformation. Such conformation is very stable because of intramolecular hydrogen bondings of all phenolic hydroxy groups. Calixarenes possess an upper rim defined by the *para* substituents of the phenolic moieties and a lower rim defined by the phenolic hydroxy groups. One of the most important properties of calixarenes is their ability to include smaller molecules and ions reversibly and selectively. Calixarenes have many sizes of cavity for including substrates depending on the number of phenolic moieties. Calix[4]arene, the smallest member of this family, is a very popular one since it provides a cavity and can be prepared with ease. In addition they have different positions that can be selectively functionalized *i.e.*, the phenolic oxygens at the lower rim and the aromatic *para* positions at the upper rim. Calix[4]arene can adopt four different conformations: cone, partial cone, 1,2-alternate and 1,3-alternate<sup>14</sup>, shown in Figure 1.1. This enlarges the number of potentially useful geometries of these molecules as building blocks. Calixarenes and especially calix[4]arenes are widely used in supramolecular chemistry because they are useful in the design and synthesis of artificial receptors for the selective recognition of ions and neutral molecules. Some of the molecular complexes of calixarenes are a class of inclusion compounds in which the receptors enclose other molecules without the formation of covalent or ionic bonds. Molecules which do the enclosing are referred to as hosts, while included molecules are guests. The hosts form a lattice type structure with voids, which are large enough to accommodate the guests.

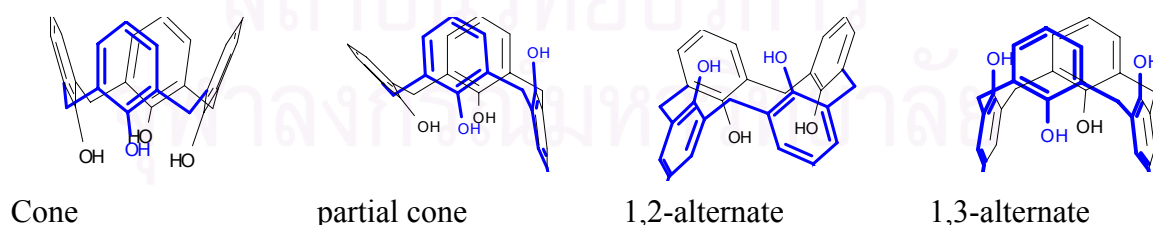


**Figure 1.1** The conformations of calix[4]arenes.

#### 1.4 Hydrogen bonding interaction<sup>14</sup>

A main goal of supramolecular chemistry is the use of specific non-covalent binding forces to obtain selectively stable host-guest complexes and their hydrogen bonding interactions. Hydrogen bonding is known to be one of the most important non-covalent interactions not merely in supramolecular chemistry but also in molecular biology. Hydrogen bondings have three different types of interactions, strong, moderate and weak, depending on the functional groups of donors and acceptors. The properties of hydrogen bondings are therefore classified into three classes. All types of hydrogen bonding can be intramolecular when donor and acceptor groups are on the same molecule or intermolecular when they are on different molecules. Very strong hydrogen bonds resemble covalent bonds, while very weak hydrogen bonds are close to van der Waals forces. A wide variety of both intermolecular and intramolecular hydrogen bonds is described having O-H or N-H as donor and O or N as acceptor atom. The nature of a hydrogen bond depends on the nature of the donors and acceptor groups. The strong and moderate hydrogen bonds, most influential bonds, shown in Table 1.1 are the interaction between the donor and acceptor groups of different type containing nitrogen atom. The inclusion compounds containing hydrogen bond are carried out not exclusively in metal cation guest molecules but also anion as well as neutral molecules. In comparison with the large variety of ligands which has been described for cations, the development of selective hosts for anions and neutral molecules is still in its infancy. This is also true for calixarene-based receptors.

#### 1.5 Interaction of nitrogen containing ligand and metal ions

Electron donating atoms may form parts of a basic or an acidic functional group. A basic group is one that contains an atom carrying a lone pair of electrons which may interact with a metal ion or proton. Some important basic functional groups are amino (-NH<sub>2</sub>), imino (=NH), heterocyclic nitrogen (-N=), carbonyl (=O) and ether (-O-). The nitrogen containing groups prefer to interact with soft metal ion like most transition metal ions. The most important multidentate ligands that contain only nitrogen donors are those in which at least some of the nitrogen atoms form part of heterocyclic systems such as 2,2',6,2''-terpyridyl, pyridine-2-aldehyde-2'-pyridylhydrazone and hexapyridine derivatives<sup>15</sup>. Pyridyl groups can form hydrogen bonding with metal ions, especially with transition metal ions.

As a general rule, formation of stable complexes results from interactions between hard acids and hard bases, or soft acids and soft bases. The choice of chelating agent for complexing various metals can be rationalized on this basis. Thus a cyclic polyether contains a number of oxygen donors, which are not easily polarized, and it can therefore be classed as hard acids like  $K^+$  and  $Ca^{2+}$ . Conversely, sodium diethyldithiocarbamate contains readily polarized sulphur atoms as donors and so is most suitable for the chelation of soft acids like copper(I) ion, cadmium(II) ion, and mercury(II) ion.

**Table 1.1.** Functional groups that form strong and moderate hydrogen bonds.

Strength of Hydrogen bond	Groups species
<b>Strong hydrogen bonds</b>	
<i>Donors and acceptors</i>	
$[N^+ \text{---} H \text{---} N]$	Proton sponges
$[N \text{---} H \cdots N]$	
<b>Moderate hydrogen bonds</b>	
<i>Donors and acceptors</i>	
$\begin{array}{c} C \\ \diagdown \\ N-H \\ \diagup \\ C \end{array}, \quad \begin{array}{c} N \\ \diagdown \\ N-H \\ \diagup \\ C \end{array}$	Secondary amines, amides, carbamates, hydrazides, purines, pyrimidines, barbiturates, nucleosides, nucleotides, peptides, proteins (main chain and side chains)
<i>Donors only</i>	
$N^+(H_3)H$	Ammonium salts
$\text{---}N^+(H_2)H, \quad \begin{array}{c} \diagdown \\ N^+(H)H \\ \diagup \end{array}$	Zwitterion amino acids
$\begin{array}{c} C \\ \diagdown \\ N^+ \text{---} H \\ \diagup \\ C \end{array}$	Proteins (side chain, nucleic acids (at low pH))
$C \text{---} N(H)H$	Primary amines, pyrimidines, purines, barbiturates
<i>Acceptors only</i>	
$\begin{array}{c} \cdots \\ \diagdown \\ N \\ \diagup \end{array}$	Tertiary amines
$\begin{array}{c} \cdots \\ \diagdown \\ N \\ \diagup \end{array}$	Purines, pyrimidines, barbiturates, nucleosides, nucleotides, nucleic acid



## 1.6 Quantum Calculations for Calixarenes

Grootenhuis et al. have studied some properties of calix[4]arene such as structural, energetical and acid-base properties by various computational methods<sup>16</sup>. Due to conformational interconversion of calix[4]arenes, quantum calculations using CHARMM force field were employed to study the energy of each conformation and pathway of interconversion processes. Reinhoudt and coworkers have shown that in compounds **1** and **2** only ring flips were involved in their interconversion, giving the energy diagram in Figure 1.2<sup>16</sup>.

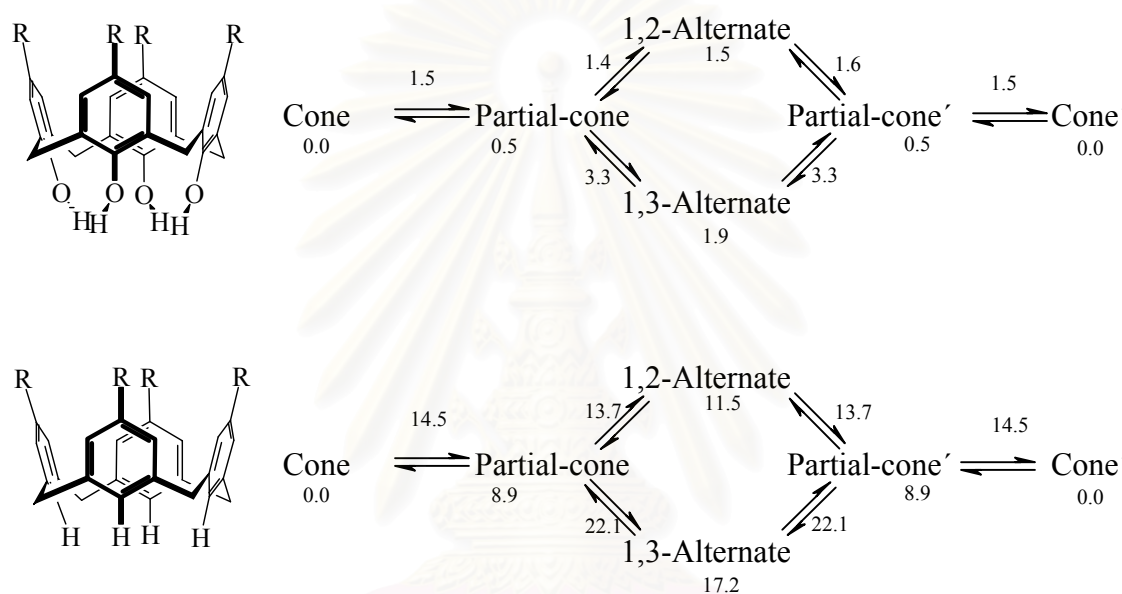


**Figure 1.2** Interconversion between various conformations of calix[4]arenes. Energies in kcal mol<sup>-1</sup>.

Thondorf and coworkers have used various computational methods to study conformation and rotational barriers of calix[4]arene derivatives<sup>17-20</sup>. Molecular mechanic methods such as MM3 force field were employed in these investigations.

The conformational distribution of tetramethoxycalix[4]arene has been studied by molecular modelling with the CHARMM force field<sup>21</sup>. Simulations show that the cavity of the cone of tetramethoxy-*p*-*tert*-butylcalix[4]arene contains a solvent molecule in dichloromethane, but not in chloroform. In both chloroform and dichloromethane, the partial cone conformer was stabilized by the possibility of CH...O hydrogen bonds.

## 1.7 Objective and Scope of The Research

Recently, Tumcharern and coworkers have synthesized 25,27-di(4-methyl-pyridine)-*p*-*tert*-butylcalix[4]arene (**L**) and studied its interactions with benzene dialcohols and benzene dicarboxylic acids<sup>22</sup>. From <sup>1</sup>H NMR experiments, **L** can form interesting supramolecular complexes with resorcinol, catichol and phthalic acid. However, these complexes cannot be crystallized to give suitable single crystals for X-ray analysis. Theoretical calculation may be a useful tool for obtaining such supramolecular structures of the mentioned complexes. Therefore, interactions of **L** towards guest molecules have been investigated using various quantum chemical calculations provided in GUASSIAN94W software<sup>23</sup>.



สถาบันวิทยบริการ  
จุฬาลงกรณ์มหาวิทยาลัย

## CHAPTER II

### METHOD OF CALCULATION

#### 2.1 Initial structure building

The initial structure of the calix[4]arene unit was built using standard geometrical parameters of the HyperChem Release 5.0 for Windows<sup>24</sup>. At first *p-tert*-butylcalix[4]arene in cone conformation was obtained from the structural optimization process using AM1 method. The structure of 25,27-di(4-methyl-pyridine)-*p-tert*-butylcalix[4]arenes (**L**) was built up and optimized using the AM1 and *ab initio* calculations with STO-3G basis set.

#### 2.2 Quantum Chemical Calculations

The semi-empirical computations of AM1 method and *ab initio* Hartree-Fock calculations with STO-3G and 6-31G basis sets were performed with the Gaussian 94W program<sup>23</sup>. Optimizations of the molecular structures were performed by the algorithm as the default tolerances. Interaction energies of the complexes of 2(4-ethylpyridine)calix[4]arene with proton, methanol, lithium ion, sodium ion, potassium ion, beryllium ion, magnesium ion, resocinol and phthalic acid were obtained from the *ab initio* calculations with difference theoretical levels by using the single point method. Configurations of interactions between the ligand **L**<sub>1</sub> and ions were determined, and their interaction energies were evaluated at different orientation paths of interacting ions. For interactions of guests with **L** along the principal Z axis, the original position of the guest was set at center of the plane of the 4 carbons (of *p-tert*-butylcalix[4]arene) to which -OH and -OR groups were attached. The rotational reference plane and the center of the plane are illustrated in Figure 2.1.



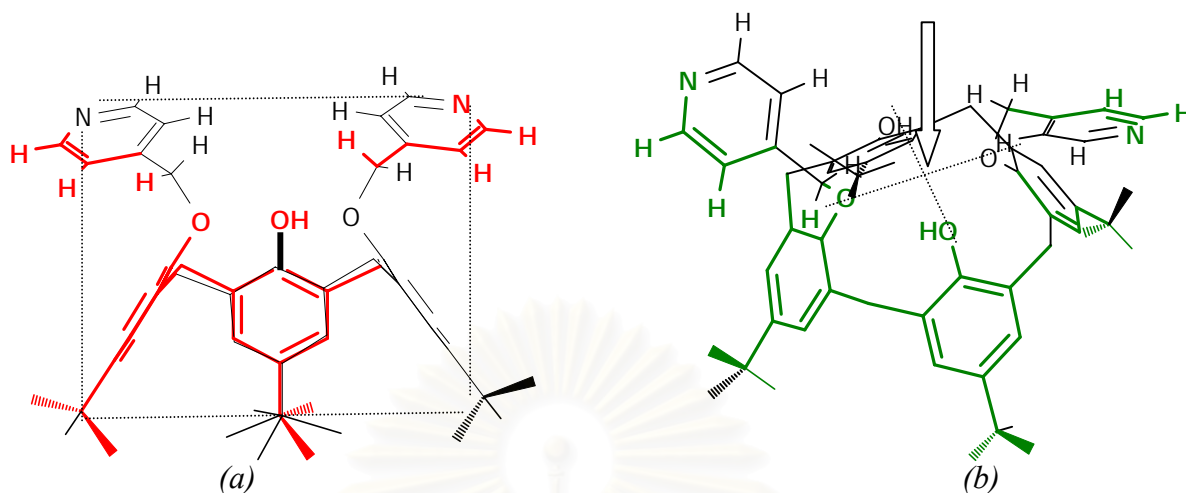


**Figure 2.1** (a) rotational reference plane of  $L_1$  (b) center of the plane of the 4 carbons of *p*-*tert*-butylcalix[4]arene (pointed by arrow).

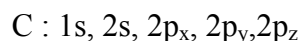
### 2.3 Basis Set Effects

A basis set is the mathematical description of the orbitals within a system which in turn combine to approximate the total electronic wavefunction, used to perform the theoretical calculation. Larger basis sets more accurately approximate the orbitals by imposing fewer restrictions on the locations of the electrons in space. In the true quantum mechanical picture, electrons have affinite probability of existing anywhere in space; this limit corresponds to the infinite basis set expansion.

Standard basis sets for electronic structure calculations use linear combinations of gaussian functions to form the orbitals. Gaussian program offers a wide range of pre-defined basis sets, which may be classified by the number and types of basis functions that they contain. Basis sets assign a group of basis functions to each atom within a molecule to approximate its orbitals. These basis functions themselves are composed of a linear combination of gaussian functions; such basis functions are referred to as contracted functions, and the component gaussian functions are referred to as primitives. A basis function consisting of a single gaussian function is termed uncontracted.

### 2.3.1 Minimal Basis Sets

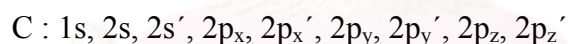
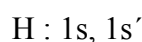
Minimal basis sets contain the minimum number of basis functions needed for each atom, as in these examples:



Minimal basis sets use fixed-size atomic-type orbitals. The STO-3G basis set<sup>20</sup> is a minimal basis set (although it is not the smallest possible basis set). It uses three gaussian primitives per basis function, which accounts for the “3G” in its name. “STO” stands for “Slater-type orbitals” and the STO-3 basis set approximates Slater orbitals with gaussian functions.

### 2.3.2 Split Valence Basis Sets

The first way that a basis set can be made larger is to increase the number of basis functions per atom. Split valence basis sets, such as 3-21G<sup>21-25</sup> and 6-31G<sup>26-32</sup>, have two or more sizes of basis function for each valence orbital. For example, hydrogen and carbon are represented as:



Where the primed and unprimed orbitals differ in size.

The double zeta basis sets, such as the Dunning-Huzinaga basis set<sup>29</sup> (D95), form all molecular orbitals from linear combinations of two sizes of functions for each atomic orbital. Similarly, triple split valence basis sets, like 6-311G<sup>30-37</sup>, use three sizes of contracted functions for each orbital-type.

## 2.4 Practical considerations when performing *ab initio* calculations

*Ab initio* calculations can be extremely time-consuming, especially when using the higher levels of theory or when the nuclei are free to move, as in a minimization calculation. Various “tricks” have been developed which can significantly reduce the computational effort involved. Many of these options are routinely available in the major software packages and are invoked by the specification of simple keywords. One common tactic is to combine different levels of theory for the various stages of a calculation<sup>37</sup>. For example, a lower level of theory can be used to provide the initial guess for the density matrix prior to the first SCF iteration. Lower levels of theory can also be used in other ways. Suppose we wish to determine some of the electronic properties of a molecule in a minimum energy structure. Energy minimization requires that the nuclei move, and is typically performed in a series of steps, at each of which the energy (and frequently the gradient of the energy) must be calculated. Minimization is therefore a computationally expensive procedure, particularly when performed at the high level of theory. To reduce this computational burden a lower level of theory can be employed for the geometry optimization. A “single point” calculation using a high level of theory is then performed at the geometry so obtained to give a wavefunction from which the properties are determined. The assumption here of course is that the geometry does not change much between the two levels of theory. Such calculations are denoted by slashes (/). For example, a calculation that is described as “6-31G\*/STO-3G” indicates that the geometry was determined using the STO-3G basis set and the wavefunction was obtained using the 6-31G\* basis set. Two slashes are used when each calculation is itself described using a slash, such as when electron correlation methods are used. For example, “MP2/6-31G\*//HF/6-31G\*” indicates a geometry optimization using a Hartree-Fock calculation with a 6-31G\* basis set followed by a single-point calculation using the MP2 method for incorporating electron correlation, again using a 6-31G\* basis set.

### 2.4.1 Setting up the calculation and the choice of coordinates

The traditional way to provide the nuclear coordinates to a quantum mechanical program is via a Z-matrix, in which the positions of the nuclei are defined in terms of a set of internal coordinates. Some programs also accept coordinates in Cartesian format, which can be more convenient for large systems. It can sometimes be important to choose an appropriate set of internal coordinates, especially when locating minima or transition points or when following reaction pathways.

### 2.4.2 Calculating derivatives of the energy

Considerable effort has been spent devising efficient ways of calculating the first and second derivatives of the energy with respect to the nuclear coordinates. Derivatives are primarily used during minimization procedures for finding equilibrium structures and are also used by methods, which locate transition structures and determine reaction pathways. To calculate derivatives of the energy it is necessary to calculate the derivatives of the various electron integrals. For Gaussian basis sets the derivatives can be obtained analytically, and it is relatively straightforward to obtain first derivatives for many levels of theory. The time taken to calculate the derivatives is comparable to that required for the calculation of the total energy. Second derivatives are more difficult and expensive to calculate, even at the lower levels of theory.

### 2.4.3 Basis set superposition error<sup>38</sup>

Suppose we wish to calculate the energy of formation of a bimolecular complex, such as the energy of formation of a hydrogen-bonded water dimer. Such complexes are sometimes referred to as “supermolecules”. One might expect that this energy value could be obtained by first calculating the energy of a single water molecule, then calculating the energy of the dimer, and finally subtracting the energy of the two isolated water molecules from that of the dimer. However, the energy difference obtained by such an approach will invariably be an overestimate of the true value. The discrepancy arises from a phenomenon known as basis set superposition error (BSSE). As the two water molecules approach, the energy of the system falls not only because of the favourable intermolecular interactions but also because the basis functions on each molecule provide a better description of the electronic structure around the other molecule. It is clear that the BSSE would be expected to be particularly significant when small, inadequate basis sets are used, e.g. the minimal basis STO-nG basis sets, which do not provide for an adequate representation of the electron distribution far from the nuclei, particularly in the region where non-covalent interactions are strongest. One way to estimate the basis set superposition error is via the counterpoise correction method of Boys and Bernardi in which the entire basis set is included in all calculations. Thus, in the general case:

$$A + B \equiv AB$$

$$\Delta E = E(AB) - [E(A) + E(B)]$$

The calculation of the energy of the individual species A is performed in the presence of “ghost” orbitals of B; that is, without the nuclei or electrons of B. A similar calculation is performed for B using ghost orbitals on A. An alternative approach is to use a basis set in which the orbital exponents and contraction coefficients have been optimized for molecular calculations rather than for atoms. The relevance of the basis set superposition error and its dependence upon the basis set and the level of theory employed, i.e. SCF or with electron correlation, remains a subject of much research.

## CHAPTER III

### RESULTS AND DISCUSSION

The optimized structures of *p-tert*-butylcalix[4]arenes and 25,27-di(4-methyl-pyridine)-*p-tert*-butylcalix[4]arene (**L**) were examined by semi-empirical and *ab initio* methods with various basis sets. The initial structure of the *p-tert*-butylcalix[4]arene unit was built using standard geometrical parameters of the reference<sup>24</sup> and their conformational structures were optimized using AM1 method and *ab initio* calculations with STO-3G basis set.

#### 3.1 Structure of *p-tert*-butylcalix[4]arenes

The total energy of four conformations of *p-tert*-butylcalix[4]arene shown in Figure 3.1 was calculated by *ab initio* method with 6-31G basis set and tabulated in Table 3.1.

**Table 3.1** The SCF energies of *p-tert*-butylcalix[4]arene conformations evaluated by using *ab initio* calculations with 6-31G basis set.

Conformation	Total energy	
	Hartree	kcal mol <sup>-1</sup>
Cone	-1997.51721	
Partial cone	-1997.50455	7.9
1,2-Alternate	-1997.50418	8.2
1,3-Alternate	-1997.49101	16.4

The order of stability of *p-tert*-butylcalix[4]arene conformation is in the same sequence of the previously reported results<sup>17</sup> : cone > partial cone > 1,2-alternate > 1,3-alternate.



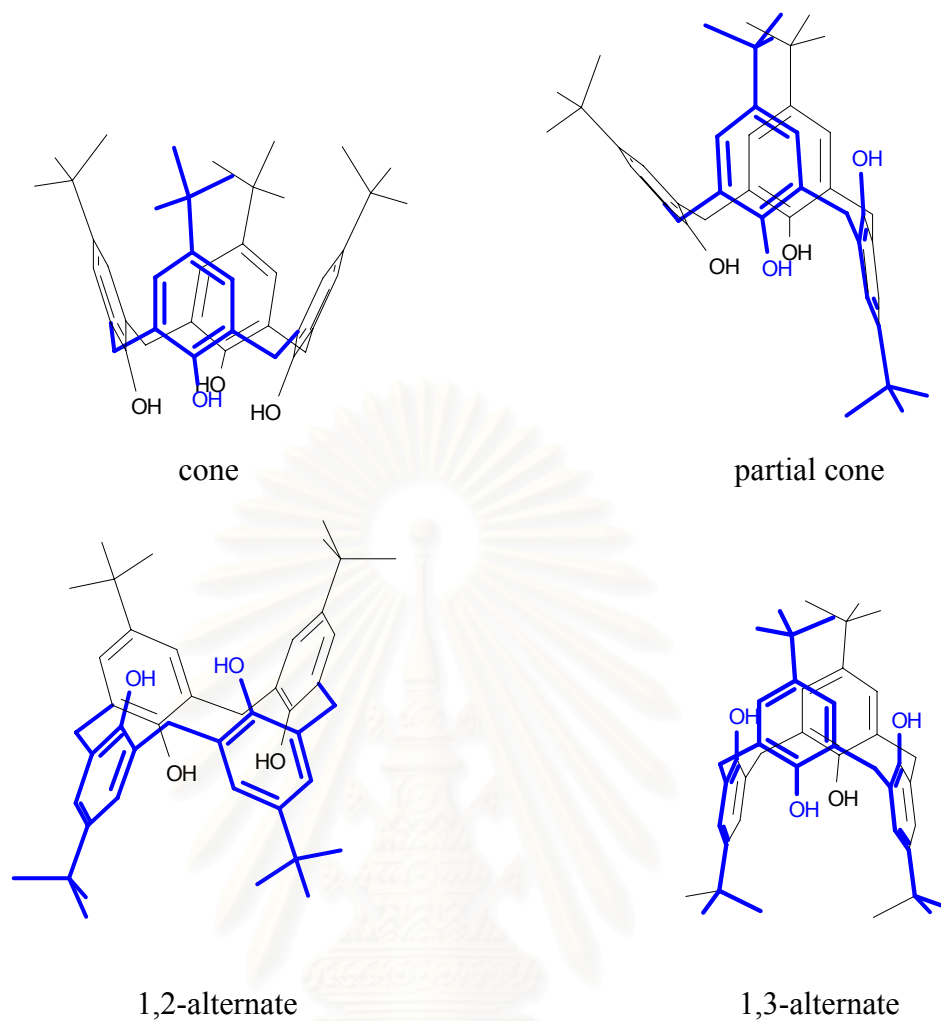


**Figure 3.1** The conformations of *p-tert*-butylcalix[4]arene.

สถาบันวิทยบริการ  
จุฬาลงกรณ์มหาวิทยาลัย

Table 3.2 presents results for the energy differences between the *p-tert*-butylcalix[4]arene conformers based on different theoretical levels.

**Table 3.2** Total Energies (in au) of the Cone Calix[4]arene Conformer at Different Theoretical Levels<sup>a</sup>.

	cone (total)	partial cone ( $\Delta E$ )	1,2-alternate ( $\Delta E$ )	1,3-alternate ( $\Delta E$ )
HFB/6-31G	-1373.86022	12.1	20.4	20.9
BLYP/6-31G	-1381.50877	16.0	26.2	27.8
	(-1381.86696)			
BLYP/6-31G* <sup>b</sup>	-1381.80462	9.7	17.2	16.3
BLYP/6-31G** <sup>b</sup>	-1381.85609	10.0	17.4	16.6
BLYP/6-31G*	-1381.81015	10.7	18.6	18.1
	(1382.15952)			
BLYP/6-31G** <sup>c</sup>	-1381.86109	10.7	18.3	17.7
B3LYP/6-31G** <sup>c</sup>	-1382.36033	10.5	18.4	17.6
AM1		7.4	10.4	11.5
PM3		7.4	12.4	11.1
CHARMM <sup>d</sup>		9.6	11.8	17.2
MM3(89) <sup>e</sup>		9.9	11.7	18.7
MM3(92) <sup>f</sup>		5.6	6.4	10.6
MM <sup>+b</sup>		7.4	9.3	13.6
Experiment <sup>g</sup>		14.9,13.8		

<sup>a</sup>Energy differences ( $\Delta E$ 's in kcal/mol) between the conformers (partial-cone, 1,2-alternate and 1,3-alternate) and the cone conformer. Total energies for the protonated cone are also reported (values in parentheses). <sup>b</sup>Geometry optimized at BLYP/6-31G. <sup>c</sup>Geometry optimized at BLYP/6-31G\* <sup>d</sup>From ref 17. <sup>e</sup>From ref 39. <sup>f</sup>From refs 40 and 41. <sup>g</sup>Free energies of activation  $\Delta G^\ddagger$  in a solvent (chloroform and benzene, respectively) from ref 42.



### 3.2 Structure of 25,27-di(4-methyl-pyridine)-*p*-*tert*-butylcalix[4]arene

The optimized structures of 25,27-di(4-methyl-pyridine)-*p*-*tert*-butylcalix[4]arene (**L**) are shown in Figure 3.2. These two optimized structures, **L<sub>I</sub>** which pyridine methyl groups point away from each other and **L<sub>II</sub>** which pyridine methyl groups point toward each other, were obtained from AM1 method. Both of them possess the C<sub>2</sub> rotation axis that agree well with the results from NOESY and ROESY experiments<sup>22</sup>.

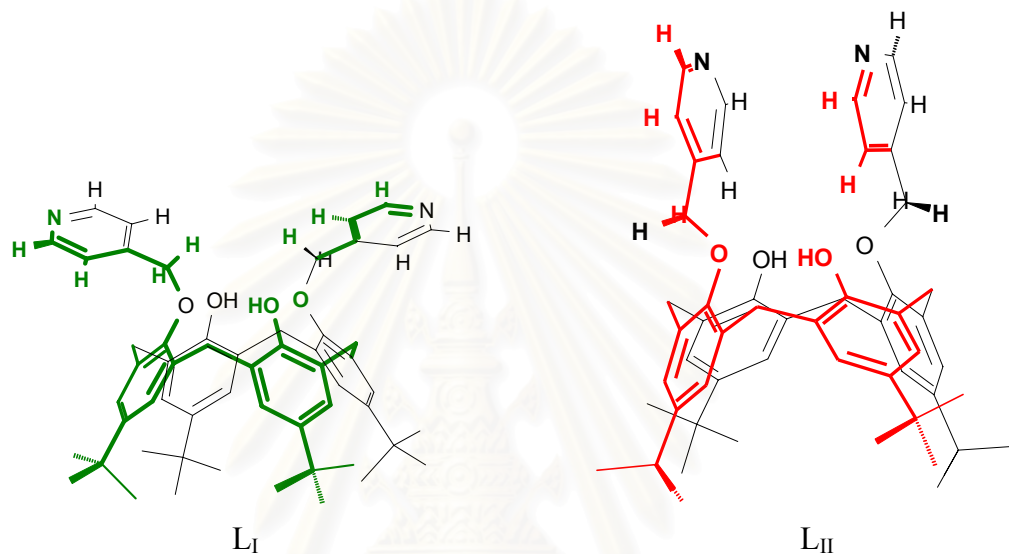


**Figure 3.2** The two most stable configurations of 25,27-di(4-methyl-pyridine)-*p*-*tert*-butylcalix[4]arene (**L**), **L<sub>I</sub>** and **L<sub>II</sub>**.

Total energies of the 25,27-di(4-methyl-pyridine)-*p*-*tert*-butylcalix[4]arene were evaluated by *ab initio* calculations with 6-31G basis set and shown in Table 3.2.

**Table 3.3** The SCF energies of **L<sub>I</sub>** and **L<sub>II</sub>** evaluated by using *ab initio* calculations with 6-31G basis set.

Configuration	Total energy	
	Hartree	kcal mol <sup>-1</sup>
<b>L<sub>I</sub></b>	-2566.373537	6.63
<b>L<sub>II</sub></b>	-2566.384108	

The results suggest that **L<sub>II</sub>** is even more stable than **L<sub>I</sub>**. This is probably due to the  $\pi$ - $\pi$  stacking and hydrophobic interactions between two pyridine rings.

### 3.3 Stability of $L_I \cdot H^+$ complex

#### a) Interactions along the axis of N-pyridine

The potential curve for an interaction between the ligand  $L_I$  and the proton locating on the axis along a nitrogen atom of the pyridine plane (see Figure 3.3) is shown in Figure 3.4. Interaction data from *ab initio* calculations with 6-31G basis set are collected in Table A1. The interaction energies of *ab initio* HF/STO-3G//HF/STO-3G and HF/6-31G//HF/STO-3G with and without counterpoise procedure are shown in Tables 3.4 and 3.5, respectively. In addition, the interactions of  $L_I$  and 2 protons have also been calculated and the result is accumulated in Table 3.4.

The results show that the most stable  $N \cdots H$  distance is 1.05 Å which is also pertinent to the standard bond length of N-H. The stabilization energies according to the first and second protonation obtained by *ab initio* calculations at HF/6-31G level are -233.4 and -209.2 kcal mol<sup>-1</sup>, respectively.

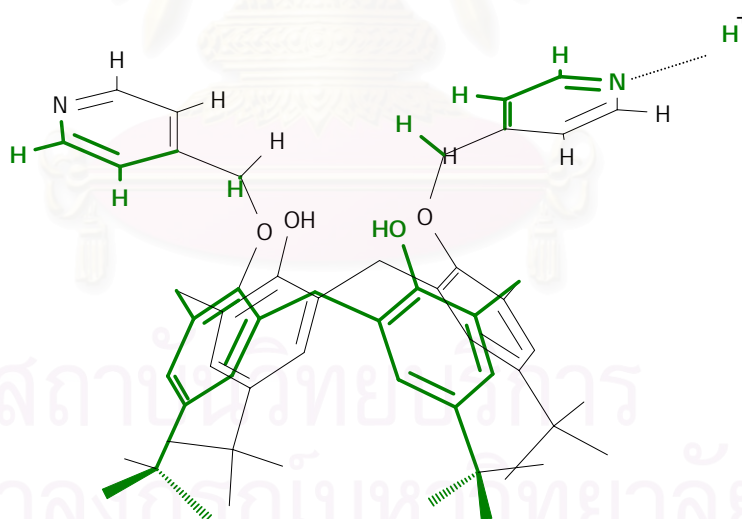


**Figure 3.3** Structure of protonated  $L_I$ .

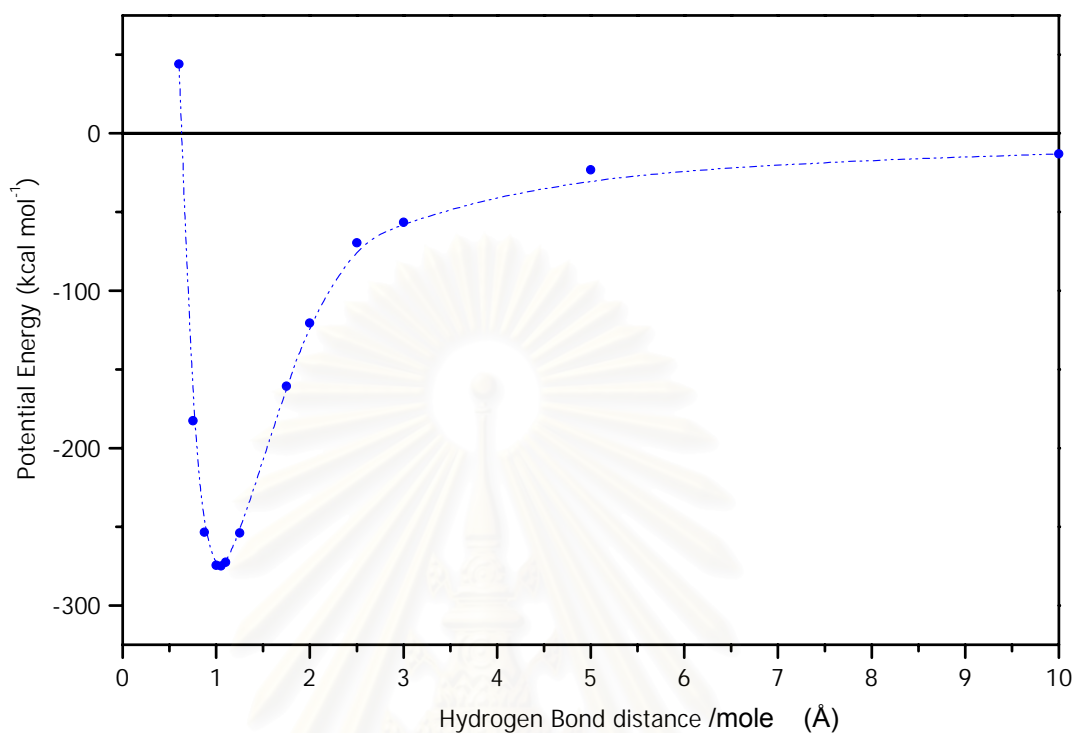


**Figure 3.4** The potential curve for proton and the ligand  $L_1$  at the pyridine plane.

**Table 3.4** Total energies and stabilization energies of protonation of  $L_1$  at the pyridine plane.

Configuration	HF/STO-3G// HF/STO-3G		HF/6-31G// HF/STO-3G	
	$E_{\text{Total}}$ (Hartree)	$\Delta E$ (kcal mol <sup>-1</sup> )	$E_{\text{Total}}$ (Hartree)	$\Delta E$ (kcal mol <sup>-1</sup> )
$L_1$	-2536.120307	-	-2566.373537	-
$L_1H^+$	-2536.558397	-274.9	-2566.754938	-239.3
$L_1H_2^{2+}$	-2536.946942	-243.8	-2567.089235	-209.8

**Table 3.5** *Ab initio* energies with STO-3G and 6-31G basis sets of each counterpoise components and interaction energies with counterpoise procedure of the protonation system.

System of A/B	HF/STO-3G// HF/STO-3G		HF/6-31G// HF/STO-3G	
	L <sub>I</sub> /H <sup>+</sup>	L <sub>I</sub> H <sup>+</sup> /H <sup>+</sup>	L <sub>I</sub> /H <sup>+</sup>	L <sub>I</sub> H <sup>+</sup> /H <sup>+</sup>
E <sub>A</sub> (Hartree)	-2536.128032	-2536.565827	-2566.383016	-2566.755867
E <sub>AB</sub> (Hartree)	-2536.558397	-2536.946942	-2566.754938	-2567.089235
ΔE <sub>cp</sub> (kcal mol <sup>-1</sup> )	-270.1	-239.2	-233.4	-209.2

$$E_B = E_{H^+} = 0, \Delta E_{cp} = \Delta E_{AB} - (E_A + E_B)$$

#### b) Interactions along the principal z axis

The interaction potential curve for L<sub>I</sub> and the proton locating in the molecular axis (Z-axis) of *p-tert*-butylcalix[4]arene (see Figure 3.5) is depicted in Figure 3.6. The stabilization energies of *ab initio* HF/STO-3G//HF/STO-3G and HF/6-31G//HF/STO-3G with and without counterpoise procedure are shown in Tables 3.6 and 3.7, respectively. Stabilization energy of H<sup>+</sup>/L<sub>I</sub> complex calculated by *ab initio* with 6-31G basis set and counterpoise procedure to be -128.4 kcal mol<sup>-1</sup>. The most stable configuration of H<sup>+</sup>/L<sub>I</sub> complex occurred when the proton was locating at 1.25 Å from the origin of the Z-axis. The result suggest that H<sup>+</sup> has interaction with the oxygen atoms of calix[4]arene.

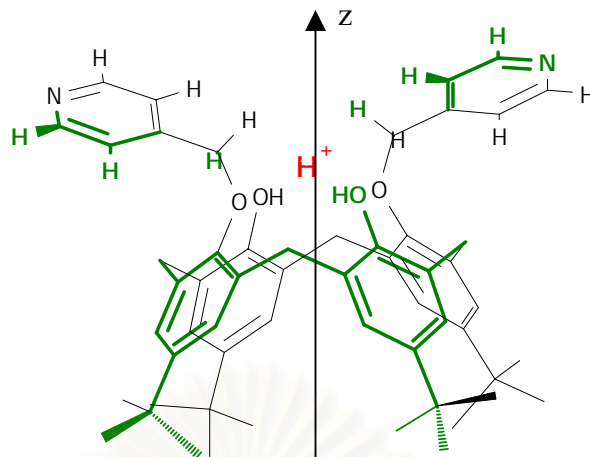


**Figure 3.5** Proton interacting with  $L_1$  along the principle molecular axis.

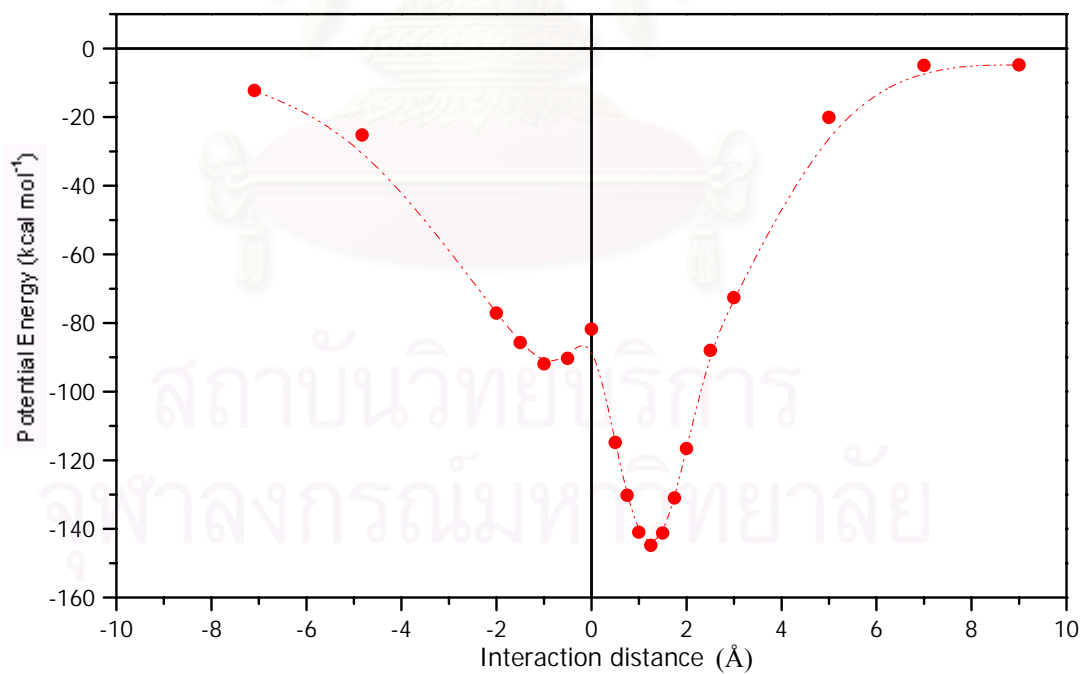


**Figure 3.6** The potential curve for interactions between a proton and  $L_1$  along the principal molecular axis.

**Table 3.6** Total energies and stabilization energies of the protonation of  $L_I$ .

Configuration	HF/STO-3G// HF/STO-3G		HF/6-31G// HF/STO-3G	
	$E_{\text{Total}}$ (Hartree)	$\Delta E$ (kcal mol <sup>-1</sup> )	$E_{\text{Total}}$ (Hartree)	$\Delta E$ (kcal mol <sup>-1</sup> )
$L_I$	-2536.120307	-	-2566.372828	-
$L_I H^+$	-2536.351129	-144.8	-2566.578552	-129.1

**Table 3.7** *Ab initio* energies with STO-3G and 6-31G basis sets of each counterpoise components and interaction energy with counterpoise procedure of the protonation  $L_I$ .

System of A/B	HF/STO-3G// HF/STO-3G	HF/6-31G// HF/STO-3G
	$L_I/H^+$	$L_I/H^+$
$E_A$ (Hartree)	-2536.123287	-2566.373885
$E_{AB}$ (Hartree)	-2536.351129	-2566.578552
$\Delta E_{\text{cp}}$ (kcal mol <sup>-1</sup> )	-143.0	-128.4

$$E_B = E_{H^+} = 0, \Delta E_{\text{cp}} = \Delta E_{AB} - (E_A + E_B).$$

### 3.4 Stability of $L_I$ ·methanol complex

#### a) Interactions along the axis of N-pyridine

The potential curve for interactions between  $L_I$  and methanol locating on the symmetrical axis along a nitrogen atom of the pyridine plane by pointing the  $H_{MeOH}$  towards to a pyridyl nitrogen (see Figure 3.7) is shown in Figure 3.8. The hydrogen bond distance between pyridyl nitrogen of ligand  $L_I$  and hydroxyl proton of methanol (Figure 3.7), expressed in terms of  $N\cdots H$  distance is 1.95 Å. Interaction data of *ab initio* calculations with 6-31G basis set are collected in Table A3. The interaction energies of *ab initio* HF/STO-3G//HF/STO-3G and HF/6-31G//HF/STO-3G with and without counterpoise procedures are shown in Tables 3.8 and 3.9, respectively. The optimization of the angle between the methanol molecular plane and the line connecting between two pyridyl nitrogens is shown in Figure B1 and Table B1.

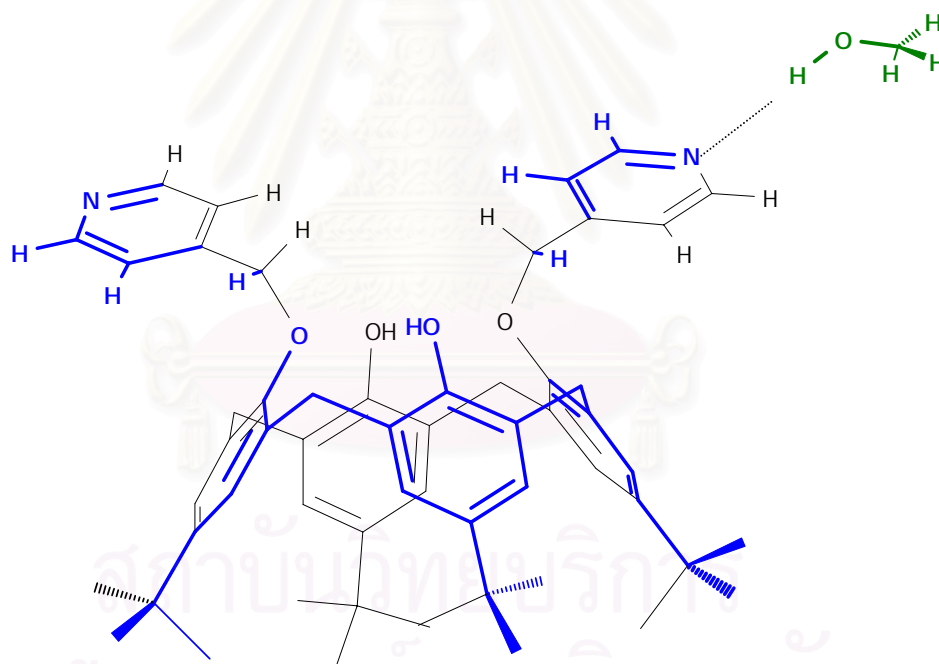


**Figure 3.7** Methanol interacting with  $L_I$ .

According to the stabilization energies of protonation model, computed by *ab initio* at different theoretical levels, with and without counterpoise correction as shown in Tables 3.8 and 3.9, the weak interactions between methanol and  $L_I$  have appeared. The stabilization energy of  $L_I$ .MeOH was calculated to be -0.8 and -5.0 kcal mol<sup>-1</sup> with and without counterpoise correction, respectively.

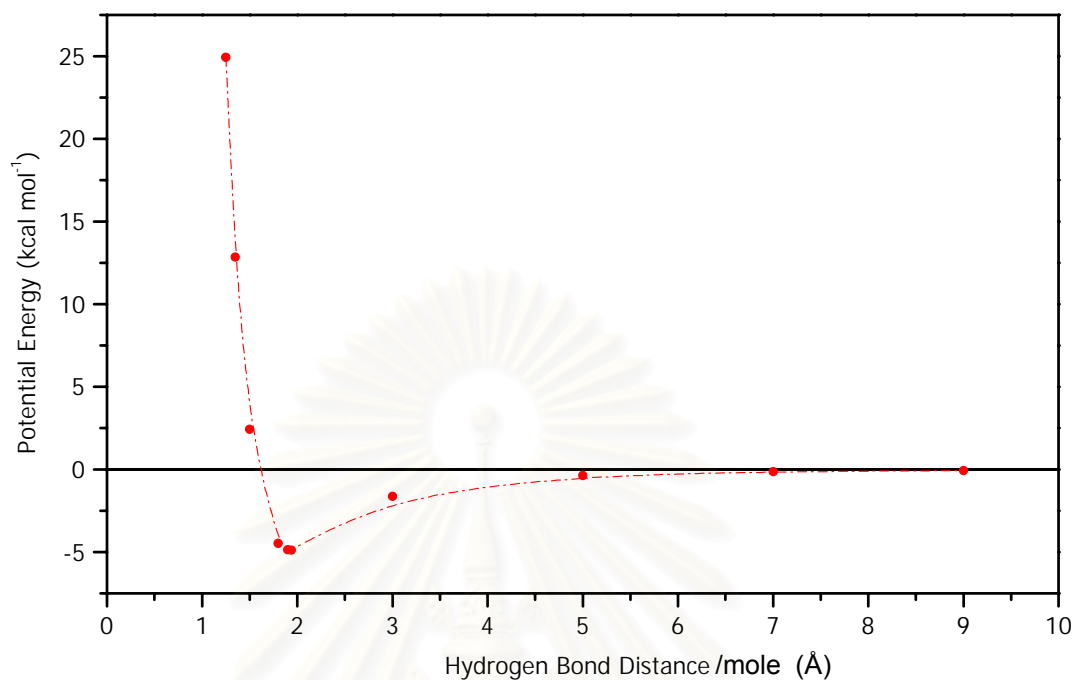


**Figure 3.8** The potential curve for methanol and the ligand  $L_1$  at the pyridine plane.

**Table 3.8** Total energies and stabilization energies of the  $L_1$ ·methanol complex.

Configuration	HF/STO-3G// HF/STO-3G		HF/6-31G// HF/STO-3G	
	$E_{\text{Total}}$ (Hartree)	$\Delta E$ (kcal mol <sup>-1</sup> )	$E_{\text{Total}}$ (Hartree)	$\Delta E$ (kcal mol <sup>-1</sup> )
$L_1$	-2536.120307	-	-2566.373537	-
MeOH	-113.549193	-	-114.983700	-
$L_1$ -MeOH	-2649.677292	-4.9	-2681.376791	-12.3
$L_1$ -(MeOH) <sub>2</sub>	-2763.234186	-4.8	-2796.361689	-0.8



**Table 3.9** *Ab initio* energies with STO-3G and 6-31G basis sets of each counterpoise components and interaction energies with counterpoise procedure of the  $L_I$  · methanol complex.

System of A/B	HF/STO-3G// HF/STO-3G		HF/6-31G// HF/STO-3G	
	$L_I$ /MeOH	$L_I$ -MeOH/MeOH	$L_I$ /MeOH	$L_I$ -MeOH/MeOH
$E_A$ (Hartree)	-2536.125235	-2649.682227	-2566.372828	-2681.369219
$E_B$ (Hartree)	-113.549463	-113.549463	-114.984473	-114.984473
$E_{AB}$ (Hartree)	-2649.677292	-2763.234186	-2681.376791	-2796.361689
$\Delta E_{cp}$ (kcal mol <sup>-1</sup> )	-1.6	-1.6	-12.2	-5.0

b) Interactions along the principal z axis

The interaction potential curve for  $L_I$  and methanol locating along the molecular axis (Z-axis) of *p-tert*-butylcalix[4]arene and pointing the proton towards the calix[4]arene unit (see Figure 3.9) is depicted in Figure 3.10. The interaction data of *ab initio* calculations with STO-3G basis set shown in Table A4 are all repulsion energies.

It can be noted from Figure 3.9 that methanol hardly exists within 5 Å above the center of calixarene (defined as a middle point of line connecting between two OH-moieties and two OR groups along the molecular axis). The result then suggests that methanol cannot be included into the cavity of  $L_I$ .

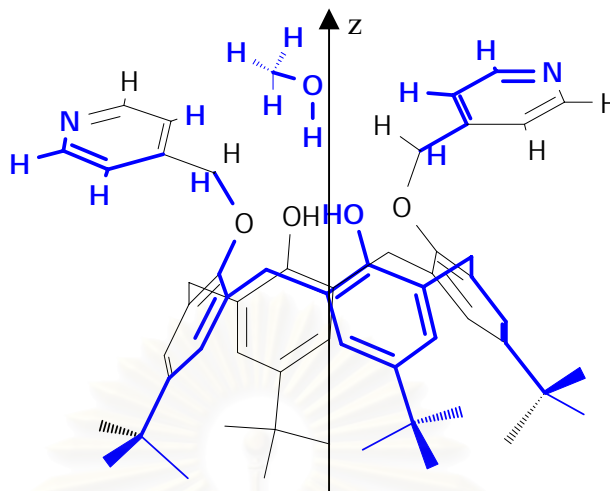


**Figure 3.9** Methanol interacting with  $L_1$  along the molecular axis.

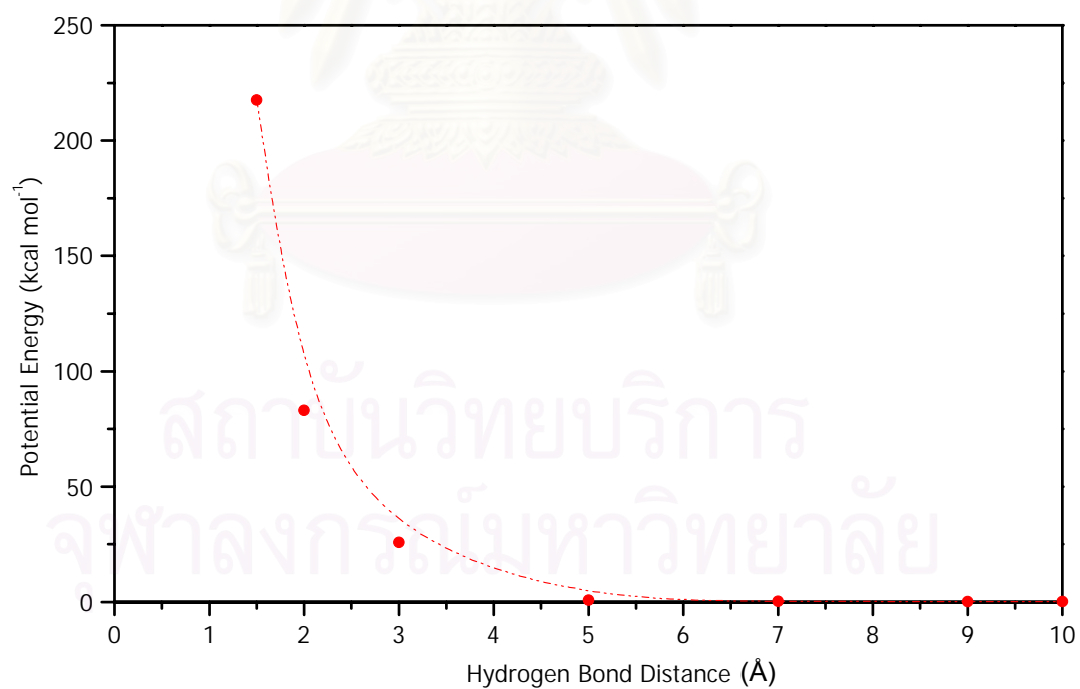


**Figure 3.10** The potential curve for interactions between  $L_1$  and methanol along the molecular axis.

When methanol locates along the principal molecular axis but points the methoxy unit towards the calix[4]arene framework, the interaction potential curve is shown in Figure 3.11. The result also indicates that there is not interaction between methanol and calix[4]arene in this manner.

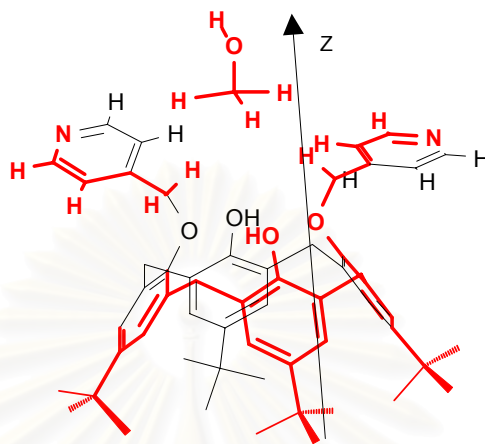


**Figure 3.11** Methanol, points the methoxy unit towards framework interacting with  $L_1$  along the molecular axis.

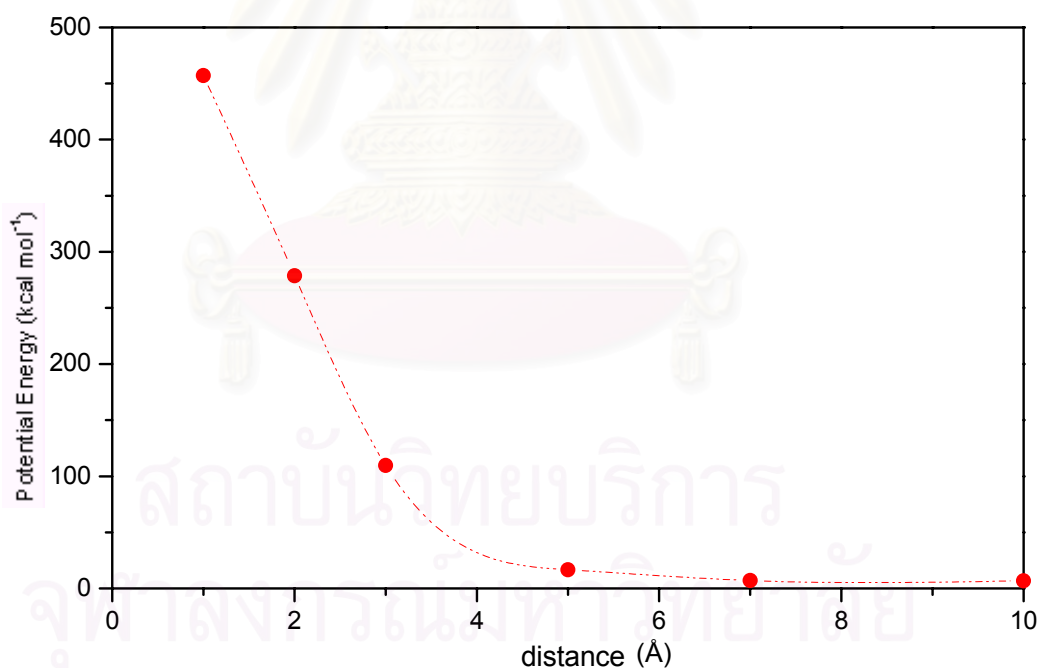


**Figure 3.12** The potential curve for interactions between  $L_1$  and methanol, points the methoxy unit towards framework.

It can be noted from Figure 3.12 that methanol hardly exists within 7 Å above the center of calixarene. The result suggests that methanol cannot be included into the cavity of  $L_1$  by pointing the methoxy unit into the calix[4]arene cavity.

### 3.5 Stability of $L_1 \cdot Li^+$ complex

#### a) Interactions along the axis of N-pyridine

The potential curve for an interaction between  $L_1$  and lithium ion locating on the axis along a nitrogen atom of the pyridine plane (see Figure 3.13) is shown in Figure 3.14. Interaction distance between pyridyl nitrogen of ligand  $L_1$  and lithium ion is 1.83 Å. Interaction data of *ab initio* calculations with 6-31G basis set are collected in Table A5. The stabilization energy of  $Li^+/L_1$  complex was calculated to be  $-81.7 \text{ kcal mol}^{-1}$ . Interaction energies of *ab initio* HF/STO-3G//HF/STO-3G and HF/6-31G//HF/STO-3G with and without counterpoise procedures are shown in Tables 3.10 and 3.11, respectively.

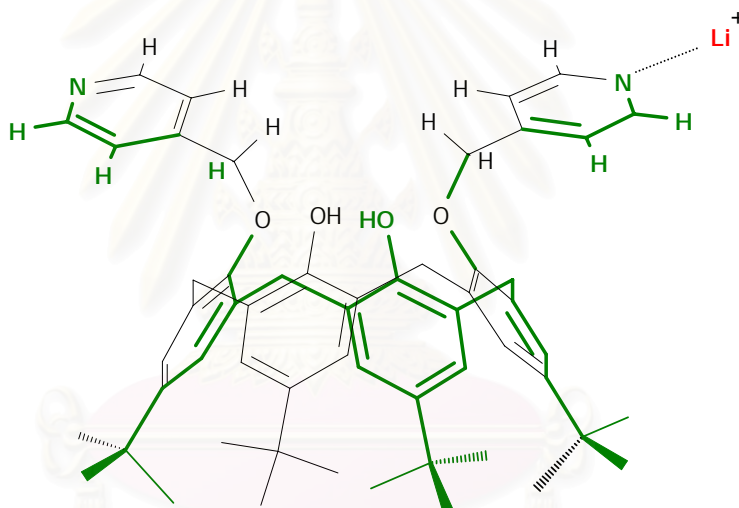


**Figure 3.13** Lithium ion interacting with  $L_1$ .

The stabilization energy of the  $Li^+/L_1$  obtained by *ab initio* calculations at the HF/6-31G theoretical level is acceptable value of  $-51.5 \text{ kcal mol}^{-1}$ .

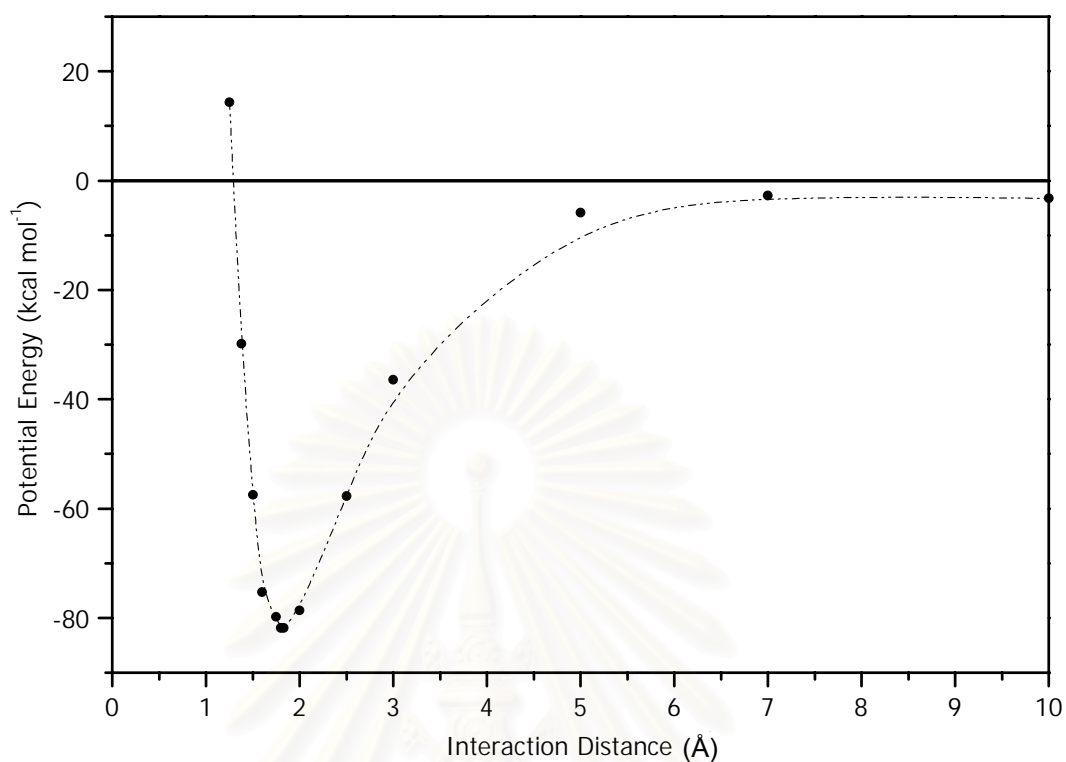


**Figure 3.14** The potential curve for lithium ion and the ligand  $L_1$  at the pyridine plane.

**Table 3.10** Total energies and stabilization energies of the  $L_1/Li^+$  complex system at the pyridine plane.

Configuration	HF/STO-3G// HF/STO-3G		HF/6-31G// HF/STO-3G	
	$E_{Total}$ (Hartree)	$\Delta E$ (kcal mol <sup>-1</sup> )	$E_{Total}$ (Hartree)	$\Delta E$ (kcal mol <sup>-1</sup> )
$L_1$	-2536.120307	-	-2566.373537	-
$Li^+$	-7.135448	-	-7.235480	-
$L_1-Li^+$	-2543.385914	-81.7	-2573.692996	-52.7

**Table 3.11** *Ab initio* energies with STO-3G and 6-31G basis sets of each counterpoise components and interaction energies with counterpoise procedure of the  $L_1/Li^+$  complex system at the pyridine plane.

System of A/B	HF/STO-3G// HF/STO-3G	HF/6-31G// HF/STO-3G
	$L_1/Li^+$	$L_1/Li^+$
$E_A$ (Hartree)	-2536.154485	-2566.375497
$E_B$ (Hartree)	-7.135646	-7.235487
$E_{AB}$ (Hartree)	-2543.385914	-2573.692996
$\Delta E_{cp}$ (kcal mol <sup>-1</sup> )	-60.1	-51.5

b) Interactions along the principal z axis

The potential curve for  $L_1$  and the lithium ion locating along the molecular axis (Z-axis) of *p-tert-butylcalix[4]arene* (Figure 3.15) is depicted in Figure 3.16. Stabilization energies of  $Li^+/L_1$  complex were calculated by *ab initio* with 6-31G basis set to be -141.9 kcal mol<sup>-1</sup>. Interaction data of *ab initio* HF/STO-3G//HF/STO-3G and HF/6-31G//HF/STO-3G with and without counterpoise procedures are shown in Table 3.12 and 3.13, respectively. The most stable configuration of  $Li/L_1$  complex occurred when the lithium ion was locating at 0.95 Å from the origin of the Z-axis suggesting that  $Li^+$  can interact with the O-atoms of calix[4]arene.



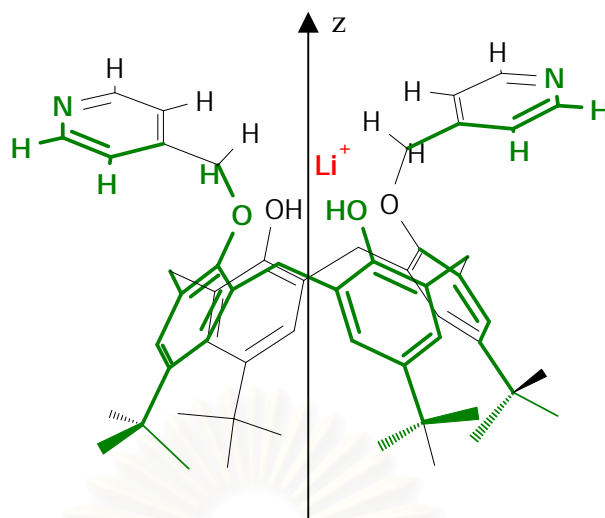


**Figure 3.15** Lithium ion interacting with  $\text{L}_1$  along the Z-axis.

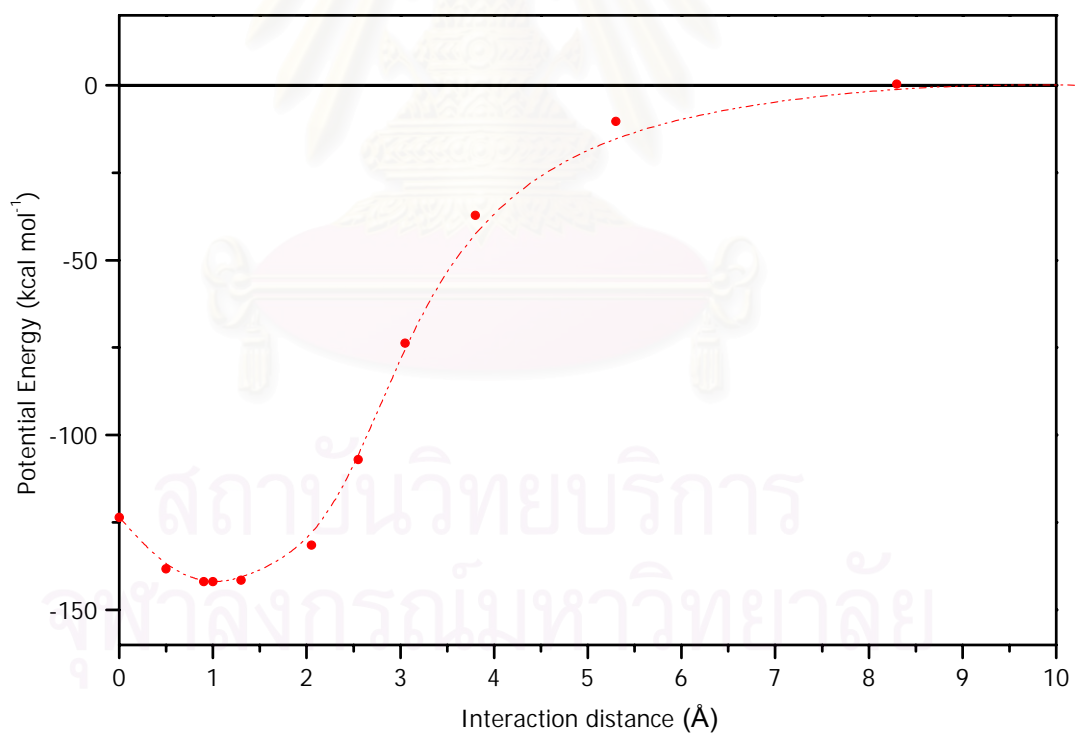


**Figure 3.16** The potential curve for lithium ion and the ligand  $\text{L}_1$  along the Z-axis.

**Table 3.12** Total energies and stabilization energies of the  $L_I/Li^+$  complex system at the optimum distance along the Z-axis.

Configuration	HF/STO-3G// HF/STO-3G		HF/6-31G// HF/STO-3G	
	$E_{Total}$ (Hartree)	$\Delta E$ (kcal mol <sup>-1</sup> )	$E_{Total}$ (Hartree)	$\Delta E$ (kcal mol <sup>-1</sup> )
$L_I$	-2536.120307	-	-2566.373537	-
$Li^+$	-7.135448	-	-7.235480	-
$L_I-Li^+$	-2543.481941	-141.9	-2573.706392	-61.1

**Table 3.13** *Ab initio* energies with STO-3G and 6-31G basis sets of each counterpoise components and interaction energies with counterpoise procedure of the  $L_I/Li^+$  complex system at the optimum distance along the Z-axis.

System of A/B	HF/STO-3G// HF/STO-3G	HF/6-31G// HF/STO-3G
	$L_I/Li^+$	$L_I/Li^+$
$E_A$ (Hartree)	-2536.154485	-2566.377212
$E_B$ (Hartree)	-7.135646	-7.235508
$E_{AB}$ (Hartree)	-2543.481941	-2573.706392
$\Delta E_{cp}$ (kcal mol <sup>-1</sup> )	-120.4	-58.8

### 3.6 Stability of $L_1 \cdot Na^+$ complex

#### a) Interactions along the axis of N-pyridine

The potential curve for an interaction between the ligand  $L_1$  and the sodium ion locating on symmetrical axis along the nitrogen atom of the pyridine plane (see Figure 3.17) is shown in Figure 3.18. Interaction distance between pyridyl nitrogen of ligand  $L_1$  and sodium ion is 2.12 Å. Interaction data of *ab initio* calculations with 6-31G basis set are collected in Table A7. The stabilization energy of  $Na^+/L_1$  complex was calculated to be  $-37.2 \text{ kcal mol}^{-1}$ . The interaction energies of *ab initio* HF/STO-3G//HF/STO-3G and HF/6-31G//HF/STO-3G with and without counterpoise procedures are shown in Tables 3.14 and 3.15, respectively.

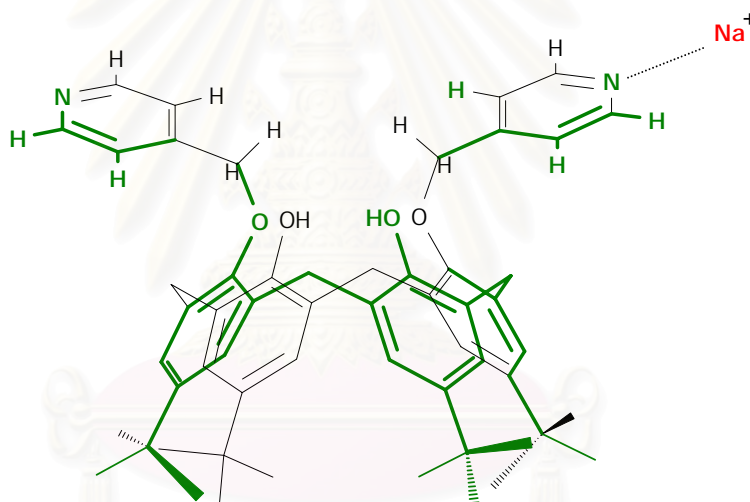


**Figure 3.17** The sodium ion interacting with  $L_1$ .

The stabilization energy of the  $Na^+/L_1$  obtained by *ab initio* calculations at the HF/6-31G theoretical level is acceptable value of  $-32.6 \text{ kcal mol}^{-1}$ .

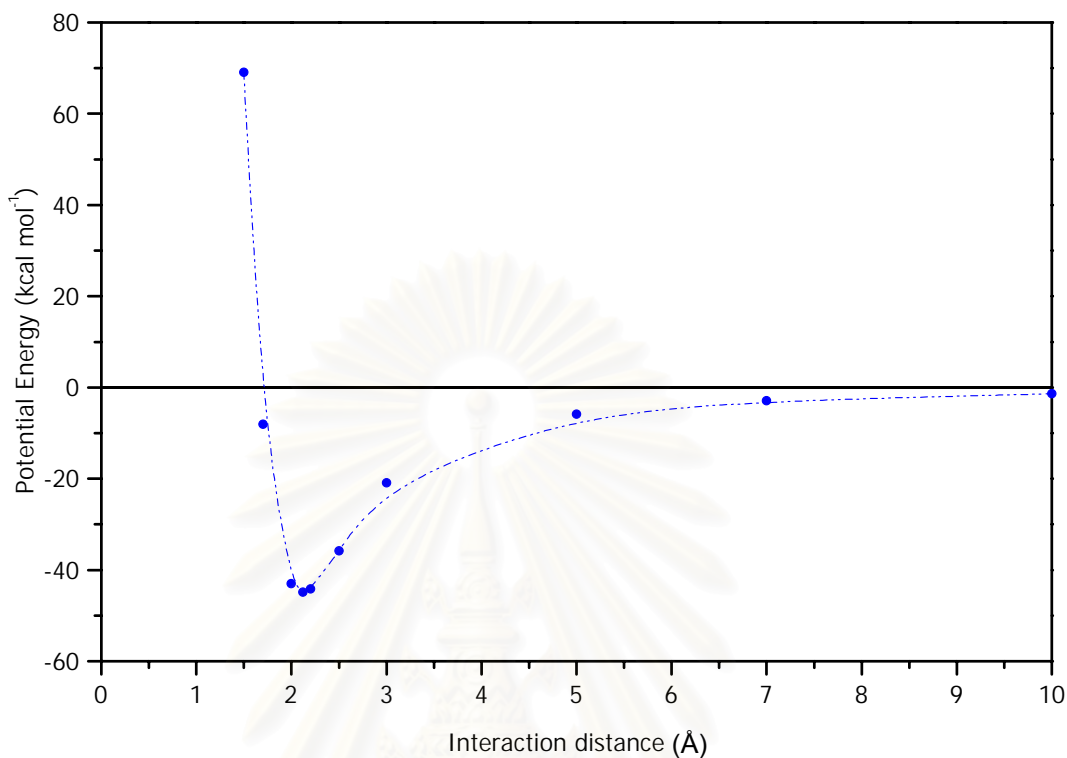


**Figure 3.18** The potential curve for sodium ion and the ligand  $L_1$  at the pyridine plane orientation.

**Table 3.14** Total energies and stabilization energies of the  $\text{Na}^+/\text{L}_1$  complex system at the pyridine plane.

Configuration	HF/STO-3G// HF/STO-3G		HF/6-31G// HF/STO-3G	
	$E_{\text{Total}}$ (Hartree)	$\Delta E$ (kcal mol <sup>-1</sup> )	$E_{\text{Total}}$ (Hartree)	$\Delta E$ (kcal mol <sup>-1</sup> )
$L_1$	-2536.120307	-	-2566.373537	-
$\text{Na}^+$	-159.784616	-	-161.659368	-
$L_1\text{-Na}^+$	-2695.976231	-44.7	-2728.092148	-37.2

**Table 3.15** *Ab initio* energies with STO-3G and 6-31G basis sets of each counterpoise components and interaction energies with counterpoise procedure of the Na<sup>+</sup>/L<sub>I</sub> complex system at the pyridine plane orientation.

System of A/B	HF/STO-3G// HF/STO-3G	HF/6-31G// HF/STO-3G
	L <sub>I</sub> /Na <sup>+</sup>	L <sub>I</sub> /Na <sup>+</sup>
E <sub>A</sub> (Hartree)	-2536.137325	-2566.380962
E <sub>B</sub> (Hartree)	-159.785494	-161.659277
E <sub>AB</sub> (Hartree)	-2695.976231	-2728.092148
ΔE <sub>cp</sub> (kcal mol <sup>-1</sup> )	-33.5	-32.6

b) Interactions along the principal z axis

The potential curve for L<sub>I</sub> and the sodium ion locating along the molecular axis (Z-axis) of *p-tert-butylcalix[4]arene* (see Figure 3.19) is depicted in Figure 3.20. Interaction data of Na<sup>+</sup>/L<sub>I</sub> complex was calculated by *ab initio* with 6-31G basis set to be -53.1 kcal mol<sup>-1</sup>. The stabilization energies of *ab initio* HF/STO-3G//HF/STO-3G and HF/6-31G//HF/STO-3G with and without counterpoise procedures are shown in Table 3.16 and 3.17, respectively. Interestingly, the potential curve shows 2 bumps at 0.25 and 2.25 Å indicating two stable positions of the Na<sup>+</sup> ion in L<sub>I</sub>. The first position which is more stable can be ascribed as a Na<sup>+</sup>-π interaction while the latter is a normal Na<sup>+</sup>-O interaction.

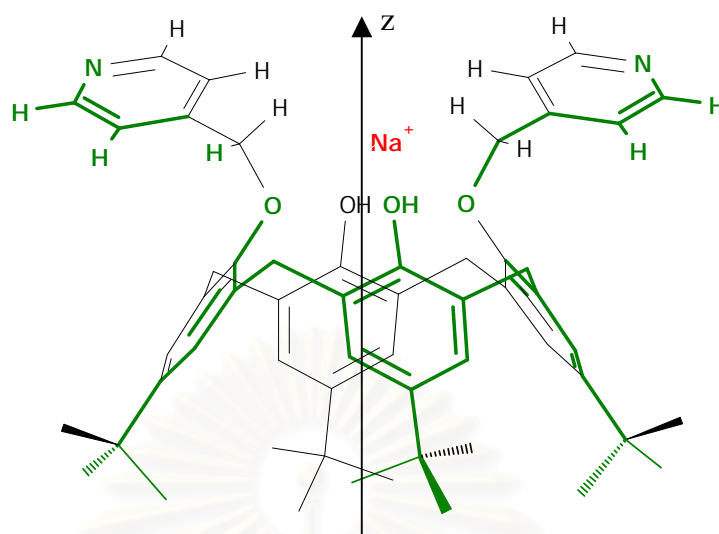


**Figure 3.19** Sodium ion interacting with  $L_1$ .

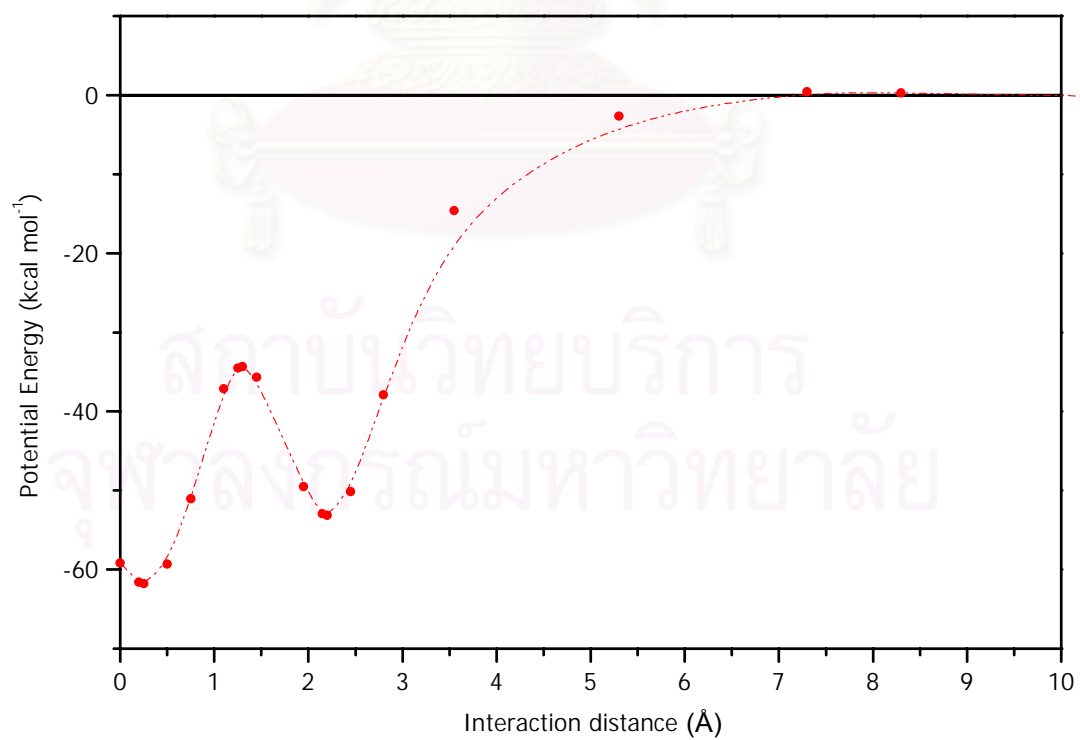


**Figure 3.20** The potential curve for sodium ion and the ligand  $L_1$  along the  $Z$ -axis.



**Table 3.16** Total energies and stabilization energies of the  $L_I/Na^+$  complex system at the optimum distance along the Z-axis.

Configuration	HF/STO-3G// HF/STO-3G		HF/6-31G// HF/STO-3G	
	$E_{Total}$ (Hartree)	$\Delta E$ (kcal mol <sup>-1</sup> )	$E_{Total}$ (Hartree)	$\Delta E$ (kcal mol <sup>-1</sup> )
$L_I$	-2536.120307	-	-2566.373537	-
$Na^+$	-159.784616	-	-161.659277	-
$L_I-Na^+$	-2695.989614	-53.1	-2728.094436	-38.7

**Table 3.17** *Ab initio* energies with STO-3G and 6-31G basis sets of each counterpoise components and interaction energies with counterpoise procedure of the  $L_I/Na^+$  complex system at the optimum distance along the Z-axis.

System of A/B	HF/STO-3G// HF/STO-3G	HF/6-31G// HF/STO-3G
	$L_I/Na^+$	$L_I/Na^+$
$E_A$ (Hartree)	-2536.137325	-2566.380990
$E_B$ (Hartree)	-159.785494	-161.659573
$E_{AB}$ (Hartree)	-2695.989614	-2728.094428
$\Delta E_{cp}$ (kcal mol <sup>-1</sup> )	-41.9	-33.8

### 3.7 Stability of $L_1 \cdot K^+$ complex

Interactions along the principal z axis

The potential curve for  $L_1$  and the potassium ion locating along the molecular axis (Z-axis) of *p-tert-butylcalix[4]arene* (see Figure 3.21) is depicted in Figure 3.22. Interaction data of  $K^+/L_1$  complex was calculated by *ab initio* with 6-31G basis set to be  $\text{kcal mol}^{-1}$ . The stabilization energies of *ab initio* HF/STO-3G//HF/STO-3G and HF/6-31G//HF/STO-3G with and without counterpoise procedures are shown in Table 3.18 and 3.19, respectively. Interestingly, the potential curve shows 2 bumps at 2.75 Å above and 0.63 Å under reference plane indicating two stable positions of the  $K^+$  ion in  $L_1$ . The second position which is more stable can be ascribed as a  $K^+-\pi$  interaction while the latter is a normal  $K^+-O$  interaction.

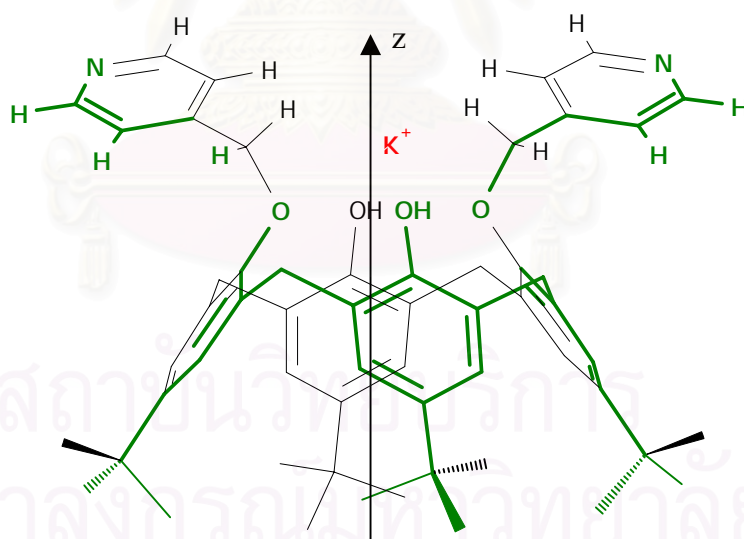


**Figure 3.21** Potassium ion interacting with  $L_1$ .

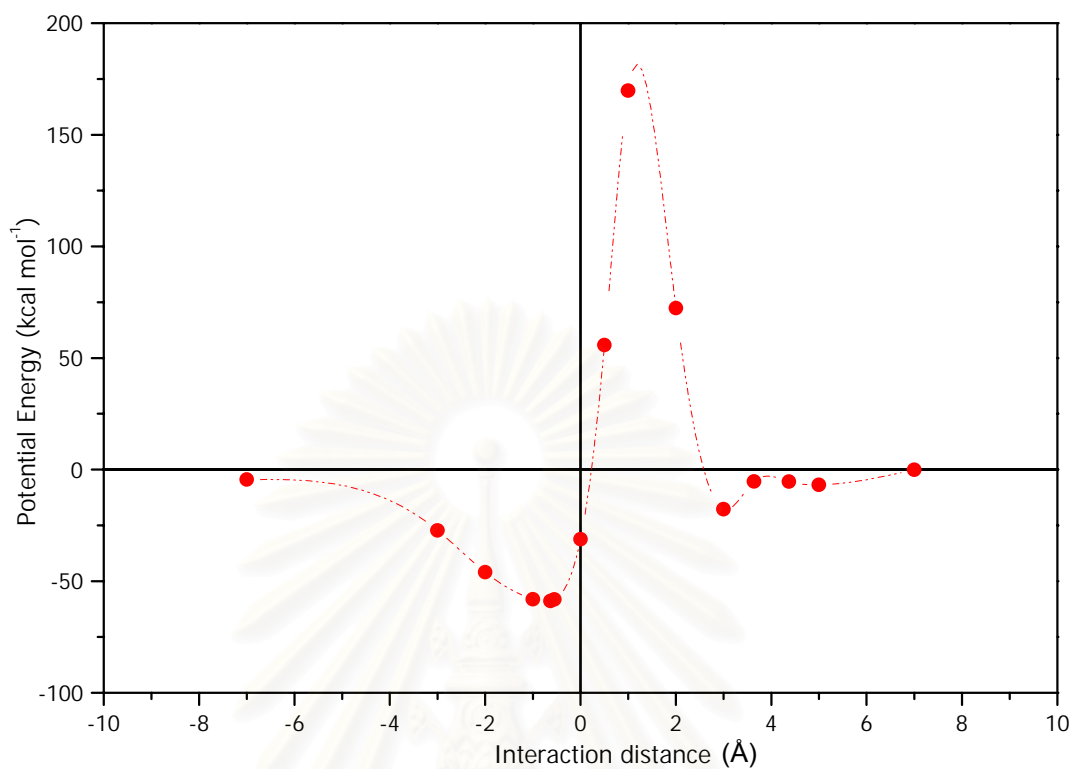


**Figure 3.22** The potential curve for potassium ion and the ligand  $L_1$  along the Z-axis.

**Table 3.18** Total energies and stabilization energies of the  $L_1/K^+$  complex system at the optimum distance along the Z-axis.

HF/STO-3G// HF/STO-3G		
Configuration	$E_{\text{Total}}$ (Hartree)	$\Delta E$ (kcal mol <sup>-1</sup> )
$L_1$	-2536.120307	-
$K^+$	-159.784616	-
$L_1-K^+$	-2695.989614	-53.1

**Table 3.19** *Ab initio* energy with STO-3G basis set of each counterpoise components and interaction energies with counterpoise procedure of the  $L_1/K^+$  complex system at the optimum distance along the Z-axis.

System of A/B	HF/STO-3G// HF/STO-3G
	$L_1/K^+$
$E_A$ (Hartree)	-2536.137325
$E_B$ (Hartree)	-159.785494
$E_{AB}$ (Hartree)	-2695.989614
$\Delta E_{cp}$ (kcal mol <sup>-1</sup> )	-41.9

สถาบันวิทยบริการ  
จุฬาลงกรณ์มหาวิทยาลัย

### 3.8 Stability of $L_I \cdot Be^{2+}$ complex

#### a) Interactions along the axis of N-pyridine

The potential curve between the ligand  $L_I$  and the beryllium ion locating on symmetrical axis along the nitrogen atom of the pyridine plane (see Figure 3.23) is shown in Figure 3.24. Interaction distance between pyridyl nitrogen of ligand  $L_I$  and beryllium ion (Figure 3.24) is 1.65 Å. Interaction data of *ab initio* calculations with 6-31G basis set are collected in Table A9. The stabilization energy of  $Be^{2+}/L_I$  complex was calculated to be  $-292.5 \text{ kcal mol}^{-1}$ . The interaction energies of *ab initio* HF/STO-3G//HF/STO-3G and HF/6-31G//HF/STO-3G with and without counterpoise procedures are shown in Tables 3.20 and 3.21, respectively.

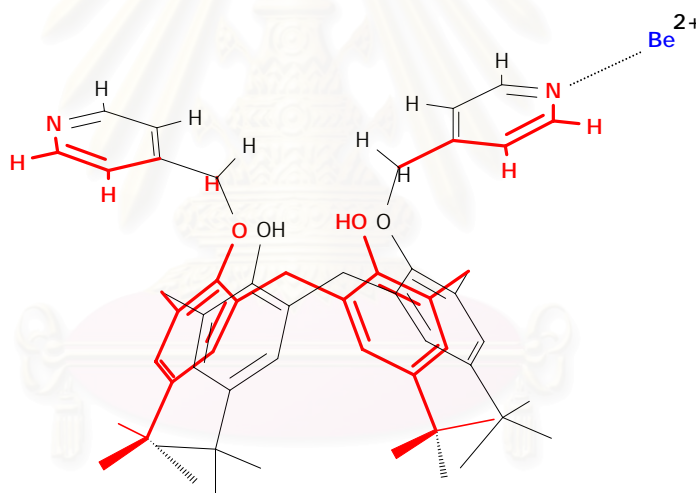


**Figure 3.23** Beryllium ion interacting with  $L_I$ .

The stabilization energy of the  $Be^{2+}/L_I$  obtained by *ab initio* calculations at the HF/6-31G theoretical level is acceptable values of  $-239.9 \text{ kcal mol}^{-1}$ .

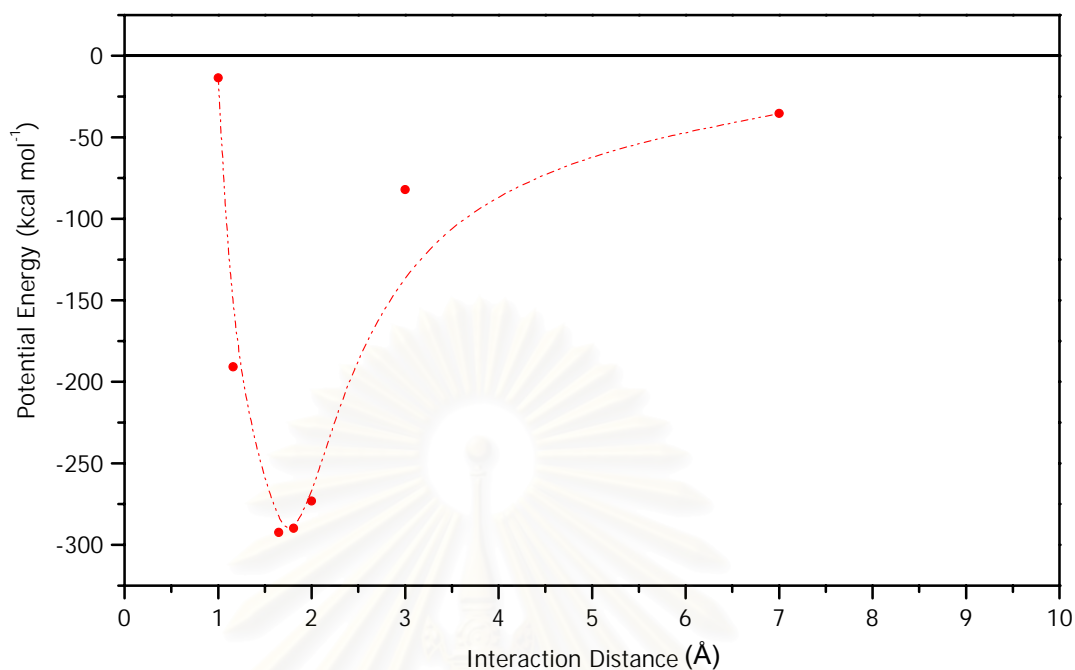


**Figure 3.24** The potential curve for beryllium ion and the ligand  $L_1$  at the pyridine plane orientation.

**Table 3.20** Total energies and stabilization energies of the  $L_1/Be^{2+}$  complex system at the pyridine plane orientation.

Configuration	HF/STO-3G// HF/STO-3G		HF/6-31G// HF/STO-3G	
	$E_{Total}$ (Hartree)	$\Delta E$ (kcal mol <sup>-1</sup> )	$E_{Total}$ (Hartree)	$\Delta E$ (kcal mol <sup>-1</sup> )
$L_1$	-2536.120307	-	-2566.373537	-
$Be^{2+}$	-13.439758	-	-13.609735	-
$L_1-Be^{2+}$	-2550.026209	-292.5	-2580.365510	-239.9



**Table 3.21** *Ab initio* energies with STO-3G and 6-31G basis sets of each counterpoise components and interaction energies with counterpoise procedure of the  $L_1/Be^{2+}$  complex system at the pyridine plane.

System of A/B	HF/STO-3G// HF/STO-3G	HF/6-31G// HF/STO-3G
	$L_1/Be^{2+}$	$L_1/Be^{2+}$
$E_A$ (Hartree)	-2536.149339	-2566.375013
$E_B$ (Hartree)	-13.439963	-13.609735
$E_{AB}$ (Hartree)	-2550.026209	-2580.365510
$\Delta E_{cp}$ (kcal mol <sup>-1</sup> )	-274.2	-238.9

b) Interactions along the principal z-axis

The interaction potential curve for  $L_1$  and the beryllium ion locating in the molecular axis (Z-axis) of *p-tert-butylcalix[4]arene* (Figure 3.25) is depicted in Figure 3.26. Stabilization energies of  $Be^{2+}/L_1$  complex was calculated by *ab initio* with 6-31G basis set to be -389.6 kcal mol<sup>-1</sup>. The stabilization energies of *ab initio* HF/STO-3G//HF/STO-3G and HF/6-31G//HF/STO-3G with and without counterpoise procedures are shown in Tables 3.22 and 3.23, respectively. The most stable configuration of  $Be^{2+}/L_1$  complex occurred when the beryllium ion was locating at 1.22 Å from the origin of the Z-axis suggesting the existence of  $Be^{2+}$  and oxygen atoms of calix[4]arene.

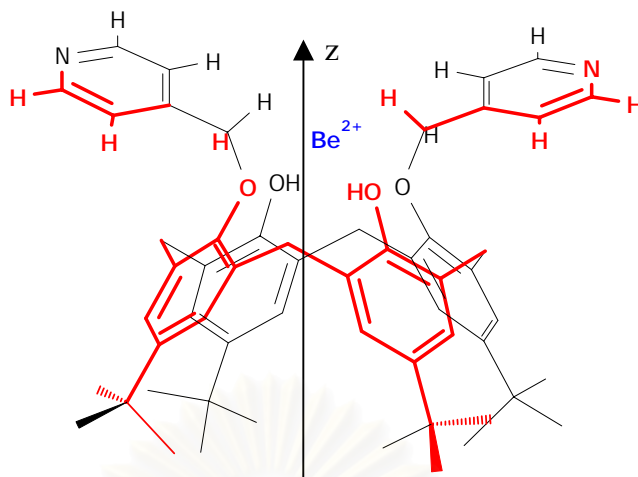


**Figure 3.25** Beryllium ion interacting with  $L_1$ .

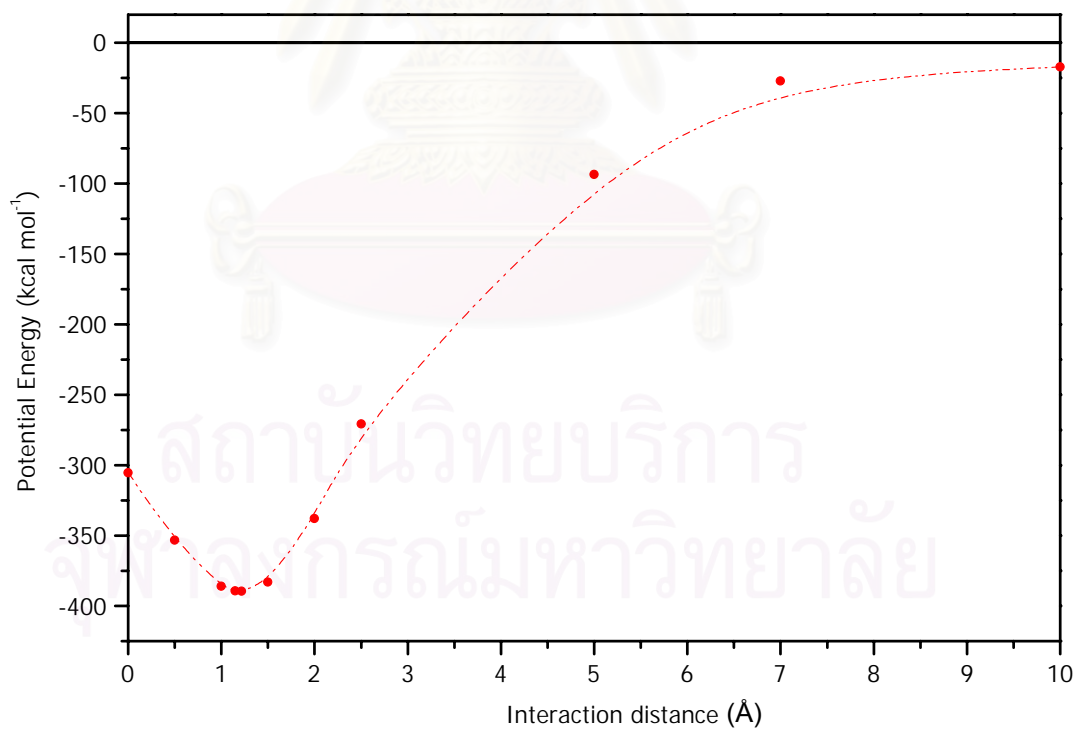


**Figure 3.26** The potential curve for beryllium ion and the ligand  $L_1$  along the  $Z$ -axis.

**Table 3.22** Total energies and stabilization energies of the  $L_I/Be^{2+}$  complex system at the optimum distance along the Z-axis.

Configuration	HF/STO-3G// HF/STO-3G		HF/6-31G// HF/STO-3G	
	$E_{Total}$ (Hartree)	$\Delta E$ (kcal mol <sup>-1</sup> )	$E_{Total}$ (Hartree)	$\Delta E$ (kcal mol <sup>-1</sup> )
$L_I$	-2536.120307	-	-2566.373537	-
$Be^{2+}$	-13.439758	-	-13.609735	-
$L_I-Be^{2+}$	-2550.180937	-389.6	-2580.45633	-296.8

**Table 3.23** *Ab initio* energies with STO-3G and 6-31G basis sets of each counterpoise components and interaction energies with counterpoise procedure of the  $L_I/Be^{2+}$  complex system at the optimum distance along the Z-axis.

System of A/B	HF/STO-3G// HF/STO-3G		HF/6-31G// HF/STO-3G	
	$L_I/Be^{2+}$		$L_I/Be^{2+}$	
$E_A$ (Hartree)	-2536.203393		-2566.378202	
$E_B$ (Hartree)	-13.440448		-13.609754	
$E_{AB}$ (Hartree)	-2550.180937		-2580.456327	
$\Delta E_{cp}$ (kcal mol <sup>-1</sup> )	-337.0		-293.9	

### 3.9 Stability of $L_I \cdot Mg^{2+}$ complex

#### a) Interactions along the axis of N-pyridine

The potential curve between the ligand  $L_I$  and the magnesium ion locating on symmetrical axis along a nitrogen atom of the pyridine plane (see Figure 3.27) is shown in Figure 3.28. The magnesium ion interaction distance between pyridyl nitrogen of ligand  $L_I$  and magnesium ion (see Figure 3.27) is 1.88 Å. Interaction data of *ab initio* calculations with 6-31G basis set are collected in Table A11. Stabilization energy of  $Be^{2+}/L_I$  complex was calculated to be  $-154.3 \text{ kcal mol}^{-1}$ . Interaction energies of *ab initio* HF/STO-3G//HF/STO-3G and HF/6-31G//HF/STO-3G with and without counterpoise procedures are shown in Tables 3.24 and 3.25, respectively.

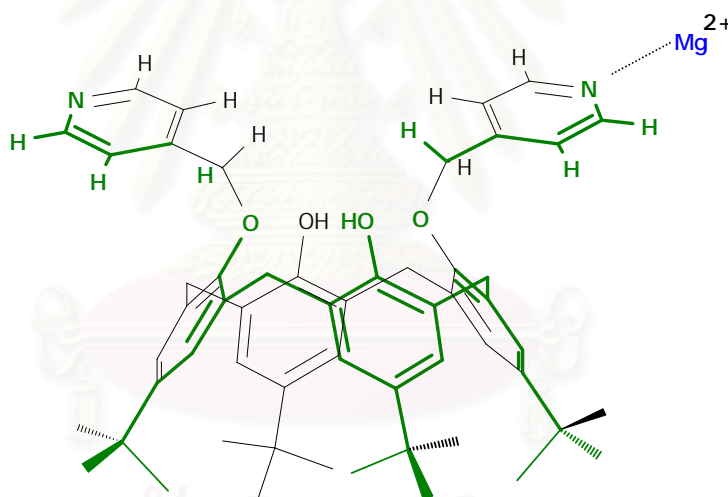


**Figure 3.27** Magnesium ion interacting with  $L_I$ .

The stabilization energy of the  $Mg^{2+}/L_I$  obtained by *ab initio* calculations at the HF/6-31G theoretical level is acceptable value of  $-139.6 \text{ kcal mol}^{-1}$ .

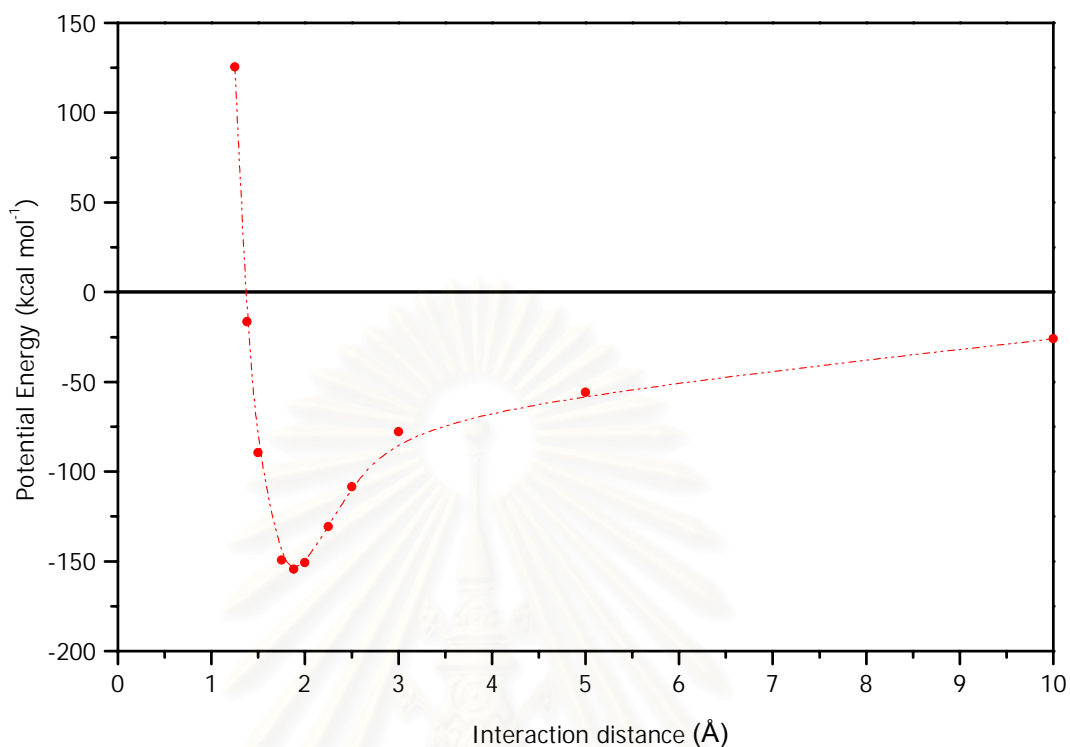


**Figure 3.28** The potential curve for magnesium ion and the ligand  $L_1$  at the pyridine plane orientation.

**Table 3.24** Total energies and stabilization energies of the  $L_1/Mg^{2+}$  complex system at the pyridine plane orientation.

Configuration	HF/STO-3G// HF/STO-3G		HF/6-31G// HF/STO-3G	
	$E_{\text{Total}}$ (Hartree)	$\Delta E$ (kcal mol <sup>-1</sup> )	$E_{\text{Total}}$ (Hartree)	$\Delta E$ (kcal mol <sup>-1</sup> )
$L_1$	-2536.120307	-	-2566.37350	-
$Mg^{2+}$	-196.511931	-	-198.81171	-
$L_1-Mg^{2+}$	-2732.87807	-154.3	-2765.4077	-139.6

**Table 3.25** *Ab initio* energies with STO-3G and 6-31G basis sets of each counterpoise components and interaction energies with counterpoise procedure of the  $L_I/Mg^{2+}$  complex system at the pyridine plane.

System of A/B	HF/STO-3G// HF/STO-3G	HF/6-31G// HF/STO-3G
	$L_I/Mg^{2+}$	$L_I/Mg^{2+}$
$E_A$ (Hartree)	-2536.143720	-2566.377920
$E_B$ (Hartree)	-196.514445	-198.811769
$E_{AB}$ (Hartree)	-2732.8781	-2765.4077
$\Delta E_{cp}$ (kcal mol <sup>-1</sup> )	-138.0	-136.8

b) Interactions along the principal z axis

The potential curve for  $L_I$  and the magnesium ion locating in the molecular axis (Z-axis) of *p-tert-butylcalix[4]arene* (see Figure 3.29) is depicted in Figure 3.30. Stabilization energies of  $Mg^{2+}/L_I$  complex were calculated by *ab initio* with 6-31G basis set to be -239.8 kcal mol<sup>-1</sup>. The stabilization energies of *ab initio* HF/STO-3G//HF/STO-3G and HF/6-31G//HF/STO-3G with and without counterpoise procedures are shown in Tables 3.26 and 3.27, respectively. The most stable configuration of  $Mg^{2+}/L_I$  complex occurred when the magnesium ion was locating at 0.88 Å from the origin of the Z-axis. The stabilization at this position can be resulted from either a metal- $\pi$  interaction or a metal-oxygen interaction.



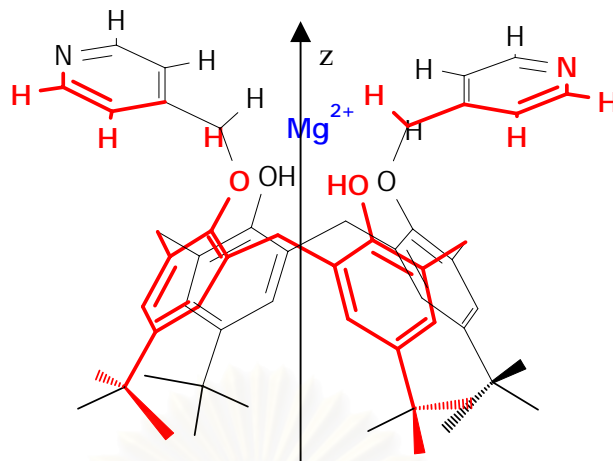


**Figure 3.29** Magnesium ion interacting with  $L_1$ .

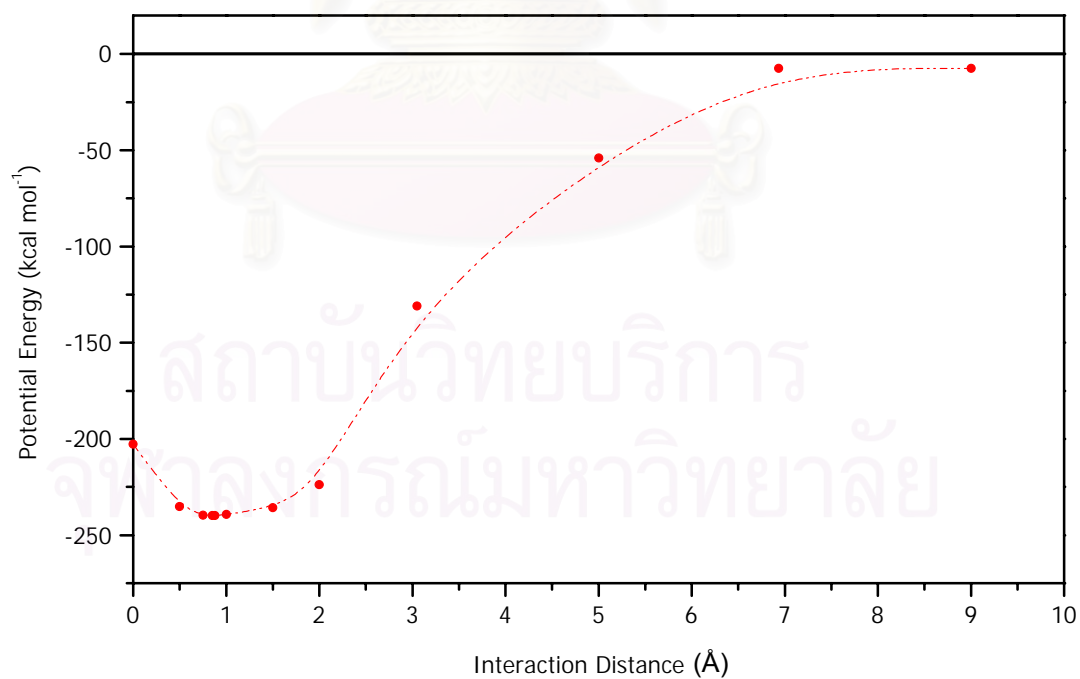


**Figure 3.30** The potential curve for magnesium ion and the ligand  $L_1$  along Z-axis.

**Table 3.26** Total energies and stabilization energies of the  $L_I/Mg^{2+}$  complex system at the optimum distance along the Z-axis.

Configuration	HF/STO-3G// HF/STO-3G		HF/6-31G// HF/STO-3G	
	$E_{Total}$ (Hartree)	$\Delta E$ (kcal mol <sup>-1</sup> )	$E_{Total}$ (Hartree)	$\Delta E$ (kcal mol <sup>-1</sup> )
$L_I$	-2536.120307	-	-2566.373537	-
$Mg^{2+}$	-196.511931	-	-198.811709	-
$L_I-Mg^{2+}$	-2733.014332	-239.8	-2765.477870	-183.6

**Table 3.27** *Ab initio* energies with STO-3G and 6-31G basis sets of each counterpoise components and interaction energies with counterpoise procedure of the  $L_I/Mg^{2+}$  complex system at the optimum distance along the Z-axis.

System of A/B	HF/STO-3G// HF/STO-3G		HF/6-31G// HF/STO-3G	
	$L_I/Mg^{2+}$		$L_I/Mg^{2+}$	
$E_A$ (Hartree)	-2535.647659		-2566.383600	
$E_B$ (Hartree)	-196.521875		-198.811899	
$E_{AB}$ (Hartree)	-2733.014332		-2765.477870	
$\Delta E_{cp}$ (kcal mol <sup>-1</sup> )	-530.1		-177.2	

### 3.10 Stability of L<sub>II</sub> and Resorcinol Molecule

The potential curve between the ligand L<sub>II</sub> and the resorcinol locating on symmetrical axis along the nitrogen atom of the pyridine plane (see Figure 3.31) is shown in Figure 3.32. Interaction distance between pyridyl nitrogen of ligand L<sub>I</sub> and hydroxyl proton of resorcinol (Figure 3.32) is 1.90 Å. The stabilization energy of resorcinol/L<sub>II</sub> complex calculated by *ab initio* with 6-31G basis set (Table A13) -12.6 kcal mol<sup>-1</sup>. The stabilization energies of *ab initio* HF/STO-3G//HF/STO-3G and HF/6-31G//HF/STO-3G with and without counterpoise procedures are shown in Tables 3.28 and 3.29, respectively. The optimization of the angle between the resorcinol molecular plane and the line connecting between two pyridyl nitrogens is shown in Figure B2 and Table B2.

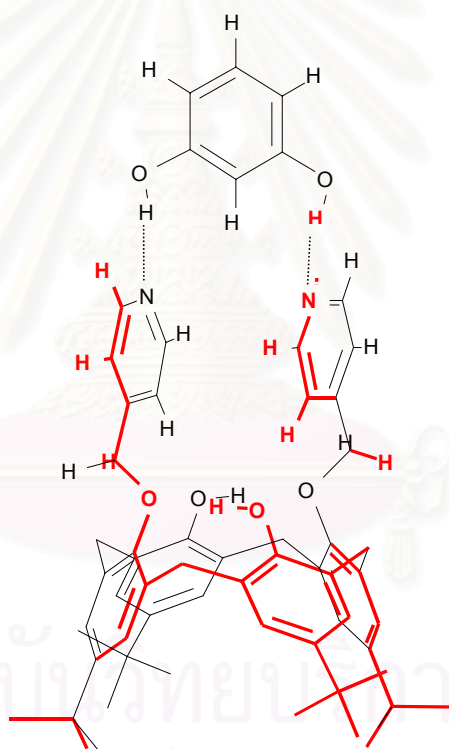


**Figure 3.31** The resorcinol interacting with the ligand L<sub>II</sub>.

According to the stabilization energies of protonation model, computed by different theoretical levels, with and without counterpoise corrections as shown in Table 3.28 and 3.29, the weak interaction between resorcinol and the ligand L<sub>II</sub> has been appeared. The structural configuration of interaction between L<sub>II</sub> and resorcinol molecule has well agreed with the experimental diagram of NOESY and ROESY<sup>41</sup>.

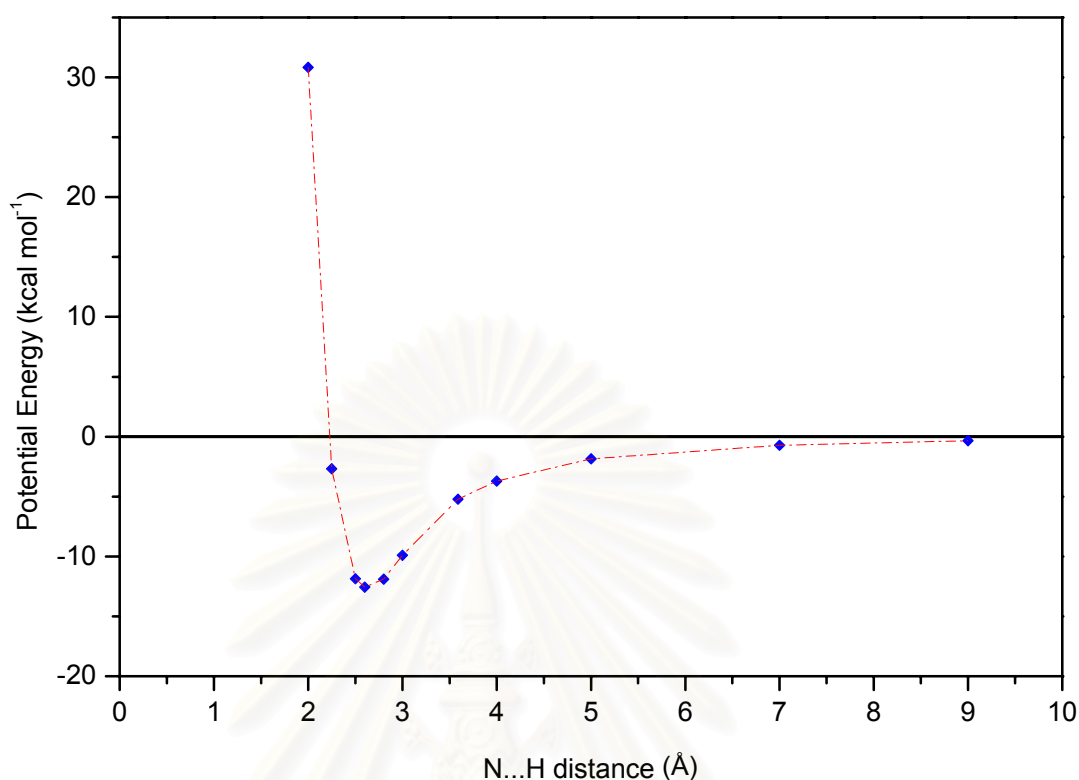


**Figure 3.32** The potential curve for interaction between resorcinol and nitrogen atom of the ligand L<sub>II</sub> along the Z-axis.

**Table 3.28** Total energies and stabilization energies of L<sub>II</sub>/resorcinol complex system at the optimum distance along the Z-axis.

Configuration	HF/STO-3G// HF/STO-3G		HF/6-31G// HF/STO-3G	
	E <sub>Total</sub> (Hartree)	ΔE (kcal mol <sup>-1</sup> )	E <sub>Total</sub> (Hartree)	ΔE (kcal mol <sup>-1</sup> )
L <sub>II</sub>	-2536.124793	-	-2566.384108	-
Resorcinol	-375.574828	-	-380.268382	-
L <sub>II</sub> -Resorcinol	-2911.719637	-12.6	-2946.671978	-12.2

**Table 3.29** *Ab initio* energies with STO-3G and 6-31G basis sets of each counterpoise components and interaction energies with counterpoise procedure of L<sub>II</sub>/resorcinol complex system at the optimum distance along the Z-axis.

System of A/B	HF/STO-3G// HF/STO-3G	HF/6-31G// HF/STO-3G
	L <sub>II</sub> /Resorcinol	L <sub>II</sub> /Resorcinol
E <sub>A</sub> (Hartree)	-2536.136502	-2566.384520
E <sub>B</sub> (Hartree)	-375.575596	-380.261868
E <sub>AB</sub> (Hartree)	-2911.735524	-2946.671978
ΔE <sub>cp</sub> (kcal mol <sup>-1</sup> )	-14.7	-16.1

When resorcinol is resided in the upper rim of *p-tert*-butylcalix[4]arene, its interaction potential curve is depicted in Figure 3.33 which shows that there is no interaction within 10 Å. The result thus suggests that in the gas phase resorcinol cannot be included into the upper rim cavity of the calix[4]arene.

สถาบันวิทยบริการ  
จุฬาลงกรณ์มหาวิทยาลัย

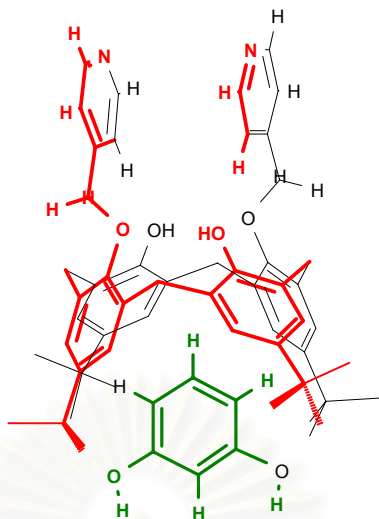


**Figure 3.33** Resorcinol, points the molecular unit below calix[4]arene framework interacting with  $L_1$  along the molecular axis.

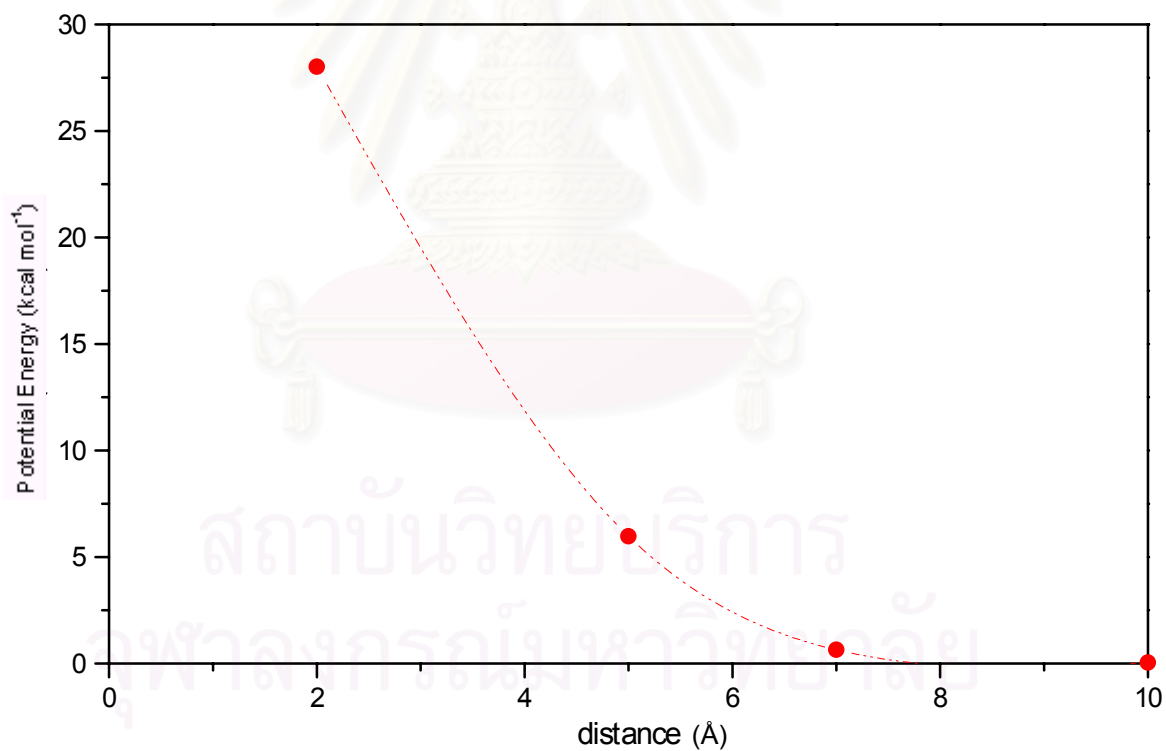


**Figure 3.34** The potential curve for interactions between  $L_1$  and resorcinol, points the molecular unit below calix[4]arene framework.

### 3.11 Stability of L<sub>II</sub> and Phthalic acid

The potential curve between the ligand L<sub>II</sub> and the phthalic acid locating on symmetrical axis along the nitrogen atom of the pyridine plane (see Figure 3.35) is shown in Figure 3.36. The hydrogen bond distance between pyridyl nitrogen of ligand L<sub>I</sub> and hydroxy proton of phthalic acid (Figure 3.35) is 1.90 Å. The stabilization energy of phthalic acid/L<sub>I</sub> complex calculated by *ab initio* with 6-31G basis set (Table A14) is -13.0 kcal mol<sup>-1</sup>. The stabilization energies of *ab initio* HF/STO-3G//HF/STO-3G and HF/6-31G//HF/STO-3G with and without counterpoise procedures are shown in Table 3.30 and 3.31, respectively. The optimization of the angle between the phthalic molecular plane and the line connecting between two pyridyl nitrogens is shown in Figure B3 and Table B3.

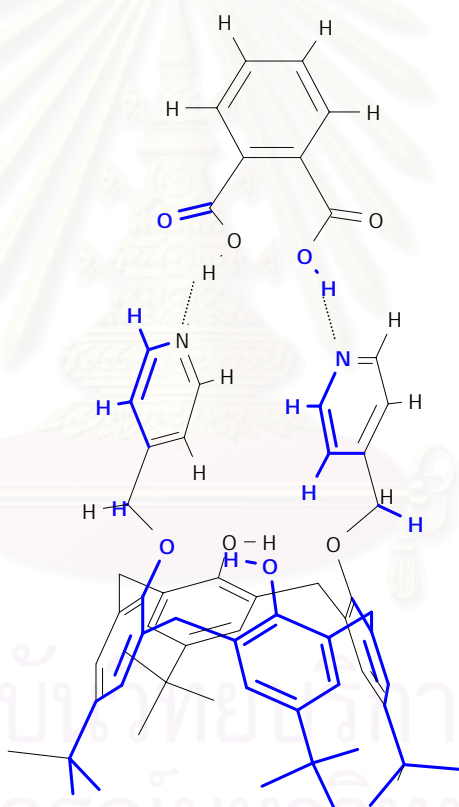


**Figure 3.35** Phthalic acid interacting with L<sub>II</sub>.

According to the stabilization energies of protonation model, computed by different theoretical levels, with and without counterpoise corrections as shown in Table 3.30 and 3.31, the weak interaction between phthalic acid and the ligand L<sub>II</sub> has been appeared. The structural configuration of interaction between L<sub>II</sub> and phthalic acid has well agreed with the experimental diagram of NOESY and ROESY<sup>41</sup>.



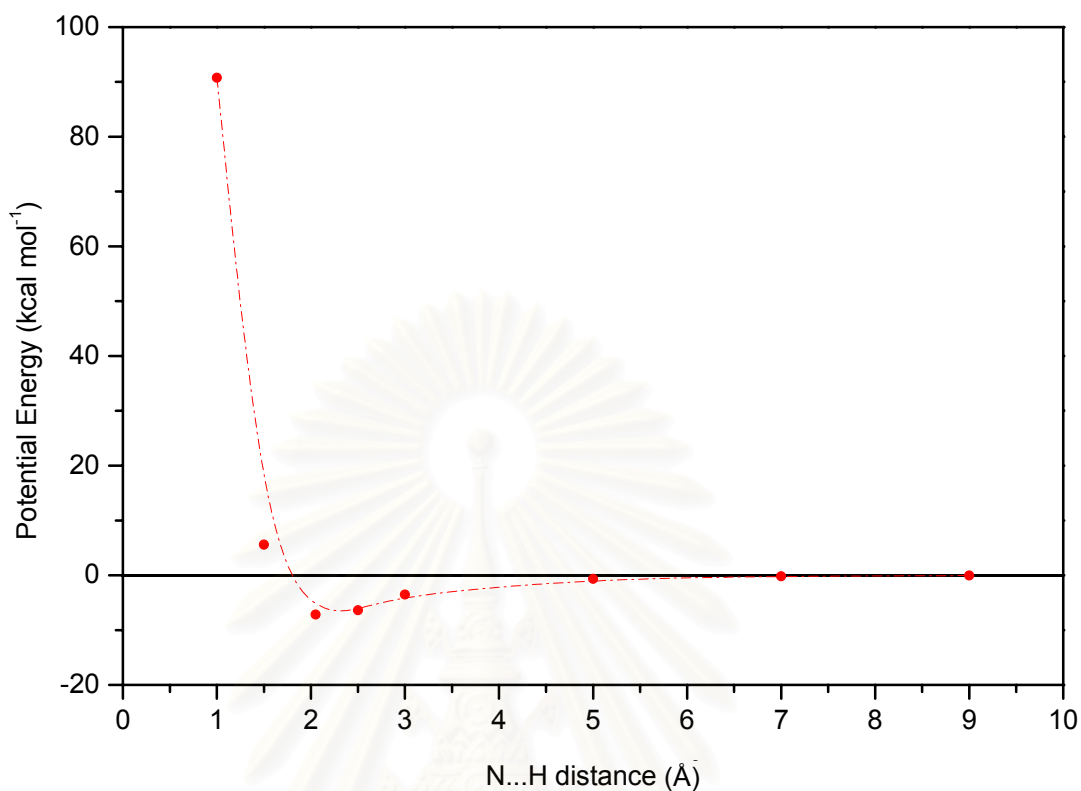


**Figure 3.36** The potential curve for interaction between phthalic acid and the ligand L<sub>II</sub> along the Z-axis.

**Table 3.30** Total energies and stabilization energies of L<sub>II</sub>/phthalic acid complex system at the optimum distance along the Z-axis.

Configuration	HF/STO-3G// HF/STO-3G		HF/6-31G// HF/STO-3G	
	E <sub>Total</sub> (Hartree)	ΔE (kcal mol <sup>-1</sup> )	E <sub>Total</sub> (Hartree)	ΔE (kcal mol <sup>-1</sup> )
L <sub>II</sub>	-2536.120307	-	-2566.384108	-
Phathlic acid	-598.066890	-	-605.658196	-
L <sub>II</sub> -Phthalic acid	-3134.212381	-13.0	-3172.066033	-15.0

**Table 3.31** *Ab initio* energies with STO-3G and 6-31G basis sets of each counterpoise components and interaction energies with counterpoise procedure of L<sub>II</sub>/phthalic acid complex system at the optimum distance along the Z-axis.

System of A/B	HF/STO-3G// HF/STO-3G	HF/6-31G// HF/STO-3G
	L <sub>II</sub> /Phthalic acid	L <sub>II</sub> /Phthalic acid
E <sub>A</sub> (Hartree)	-2536.135643	-2566.382549
E <sub>B</sub> (Hartree)	-598.068862	-605.655570
E <sub>AB</sub> (Hartree)	-3134.228250	-3172.066033
ΔE <sub>cp</sub> (kcal mol <sup>-1</sup> )	-14.9	-17.5

When phthalic acid points the benzene unit into methylpyridyl calix[4]arene frame work, its interaction potential curve is depicted in Figure 3.37 which shows that the most stable interaction can occur at more than 10 Å away from the calix[4]arene unit. The result suggests that phthalic acid cannot be included into the cavity of L<sub>II</sub> in the gas phase.

สถาบันวิทยบริการ  
จุฬาลงกรณ์มหาวิทยาลัย

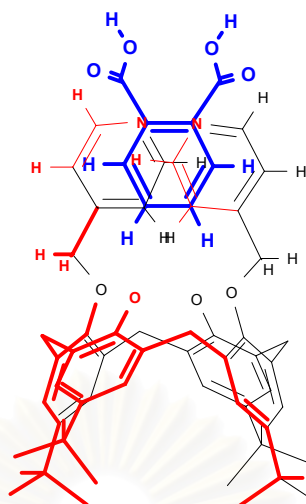


**Figure 3.37** Phthalic acid, points the aromatic unit towards framework interacting with  $L_1$  along the molecular axis.

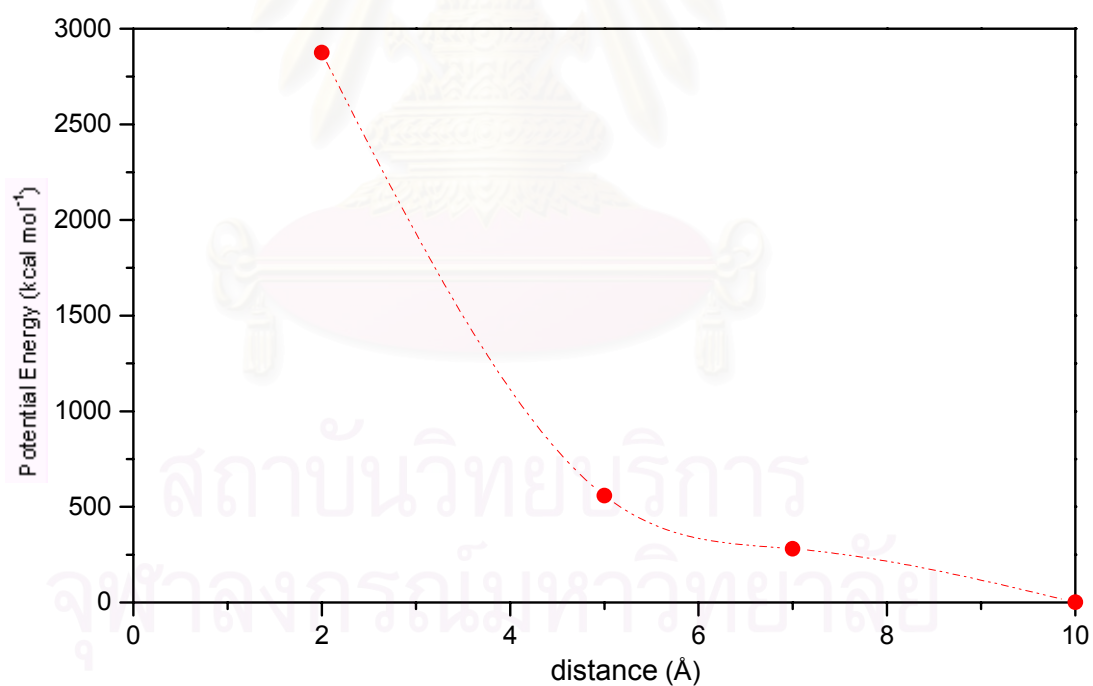


**Figure 3.38** The potential curve for interactions between  $L_1$  and phthalic acid, points the aromatic unit towards framework..

## CHAPTER IV

### CONCLUSION

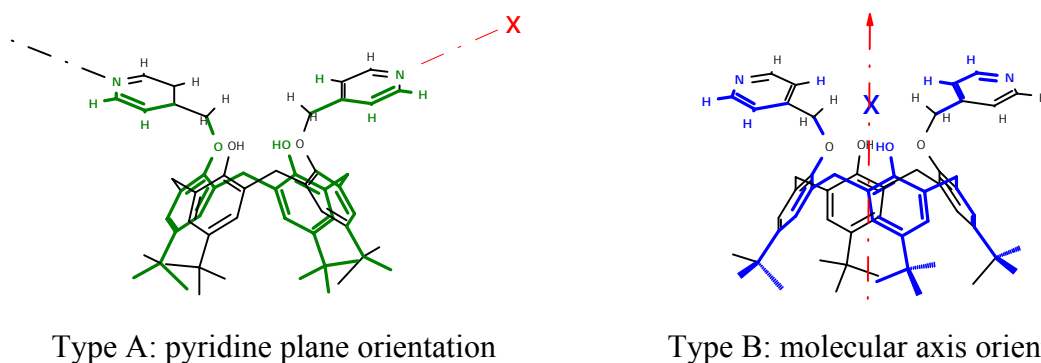
The stability order of the *p-tert*-butylcalix[4]arene conformations is in the sequence of cone > partial cone > 1,2-alternate > 1,3-alternate. The stability of these conformations is in the same sequence as concluded by Reinhoudt<sup>17</sup>. The most stable configuration of 25,27-di(4-methyl-pyridine)-*p-tert*-butylcalix[4]arene is the cone conformation of L<sub>II</sub> type (as shown in Figure 4.2).

The potential energies of interactions between the ligand L<sub>I</sub> and guest molecules, in type A orientation, obtained by *ab initio* calculations and corresponding bond distance are shown in Table 4.1.

**Table 4.1** Summary of the potential energies of interactions between L<sub>I</sub> and guest molecules (Type A).

Intermolecular bond	(Å)	Potential Energy (kcal mol <sup>-1</sup> )	
		Without counterpoise corrections	with counterpoise corrections
L <sub>I</sub> -H <sup>+</sup>	1.05 <sup>b</sup>	-274.9 <sup>a</sup> , -239.3 <sup>b</sup>	-270.1 <sup>a</sup> , -239.2 <sup>b</sup>
L <sub>I</sub> -H <sub>2</sub> <sup>2+</sup>	1.05 <sup>b</sup>	-243.8 <sup>a</sup> , -209.8 <sup>b</sup>	-233.4 <sup>a</sup> , -209.2 <sup>b</sup>
L <sub>I</sub> -MeOH	1.95 <sup>b</sup>	-4.9 <sup>a</sup> , -12.3 <sup>b</sup>	-4.8 <sup>a</sup> , -10.8 <sup>b</sup>
L <sub>I</sub> -(MeOH) <sub>2</sub>	1.95 <sup>b</sup>	-1.6 <sup>a</sup> , -1.6 <sup>b</sup>	-2.2 <sup>a</sup> , -5.0 <sup>b</sup>
L <sub>I</sub> -Li <sup>+</sup>	1.83 <sup>b</sup>	-81.7 <sup>a</sup> , -52.7 <sup>b</sup>	-60.1 <sup>a</sup> , -51.5 <sup>b</sup>
L <sub>I</sub> -Na <sup>+</sup>	2.12 <sup>b</sup>	-44.7 <sup>a</sup> , -37.2 <sup>b</sup>	-33.5 <sup>a</sup> , -32.6 <sup>b</sup>
L <sub>I</sub> -Be <sup>2+</sup>	1.65 <sup>b</sup>	-292.5 <sup>a</sup> , -274.2 <sup>b</sup>	-239.9 <sup>a</sup> , -238.9 <sup>b</sup>
L <sub>I</sub> -Mg <sup>2+</sup>	1.88 <sup>b</sup>	-154.3 <sup>a</sup> , -139.6 <sup>b</sup>	-138.0 <sup>a</sup> , -136.8 <sup>b</sup>

<sup>a</sup>calculations at STO-3G, <sup>b</sup>at 6-31G theoretical level.



The interaction between the ligand  $L_I$  and guest molecule along type B orientation is shown in Table 4.2.

**Table 4.2** Summary of the potential energies of interactions between  $L_I$  and guest molecules (Type B).

Intermolecular bond (Å)	Potential Energy (kcal mol <sup>-1</sup> )		
	without counterpoise corrections	with counterpoise corrections	
$L_I-H^+$	1.25 <sup>b</sup>	-144.8 <sup>a</sup> , -129.1 <sup>b</sup>	-143.0 <sup>a</sup> , -128.4 <sup>b</sup>
$L_I-Li^+$	0.95 <sup>b</sup>	-141.9 <sup>a</sup> , -61.1 <sup>b</sup>	-120.4 <sup>a</sup> , -58.8 <sup>b</sup>
$L_I-Na^+$	0.25 <sup>b</sup>	-53.1 <sup>a</sup> , -38.7 <sup>b</sup>	-41.9 <sup>a</sup> , -33.8 <sup>b</sup>
$L_I-Be^{2+}$	1.22 <sup>b</sup>	-389.6 <sup>a</sup> , -289.6 <sup>b</sup>	-337.0 <sup>a</sup> , -293.9 <sup>b</sup>
$L_I-Mg^{2+}$	0.88 <sup>b</sup>	-239.8 <sup>a</sup> , -183.6 <sup>b</sup>	-300.1 <sup>a</sup> , -177.2 <sup>b</sup>

<sup>a</sup>calculations at STO-3G, <sup>b</sup>at 6-31G theoretical level.

The interactions between the ligand  $L_{II}$  and neutral guest molecules the molecular axis  $L_{II}$  by pointing its pyridyl nitrogens toward to the protons of guest molecule is shown in Table 4.3.

**Table 4.3** Summary of interactions between  $L_{II}$  and neutral guest molecules.

Intermolecular bond (Å)	Potential Energy (kcal mol <sup>-1</sup> )		
	without counterpoise corrections	with counterpoise corrections	
$L_{II}$ -resorcinol	1.90 <sup>b</sup>	-12.6 <sup>a</sup> , -12.2 <sup>b</sup>	-14.7 <sup>a</sup> , -16.1 <sup>b</sup>
$L_{II}$ -phthalic acid	1.90 <sup>b</sup>	-13.0 <sup>a</sup> , -15.0 <sup>b</sup>	-14.9 <sup>a</sup> , -17.5 <sup>b</sup>

<sup>a</sup>calculations at STO-3G, <sup>b</sup>at 6-31G theoretical level.

It can be concluded that protonation of **L**<sub>1</sub> has taken place at two pyridyl nitrogens. The stabilization energies of the first and second protonations should be -239 and -209 kcal mol<sup>-1</sup>, respectively. On the other hand, proton can interact with oxygen atoms of calix[4]arene with the energy of -128 kcal mol<sup>-1</sup>. Methanol can only interact with **L** in the axis of N-pyridine. It cannot react with oxygen atoms of calix[4]arene the way proton does. We also found that among metal ions, only Na<sup>+</sup> displays a cation- $\pi$  interaction with the calix[4]arene unit of ligand **L**. Other metals form a usual metal-oxygen interaction. This may result from the appropriate size of the sodium ion to fit into the  $\pi$  cavity of calix[4]arene.

The quantum calculations also show that in the gas phase inclusion of resorcinol and phthalic acid into methylpyridyl framework cannot occur which disagrees with the NMR results performed in CDCl<sub>3</sub>. The controversy indicates that hydrophobic force in the latter case has an enormous influence on the complexation behavior of **L**.



สถาบันวิทยบริการ  
จุฬาลงกรณ์มหาวิทยาลัย

## REFERENCES

1. Olson, D.C. and Vasilevskis, *J. Inorg. Chem.* 10, **1971**: 1228.
2. Micheloni, A. Saoatini and Paoletti, P., *J. Chem. Soc. Perkin. Trans. II* 2, **1978**: 828.
3. Lehn, J.M. and Sauvage, J.P., *J. Am. Chem. Soc.* 97, **1975**: 6700.
4. Lehn, J.M., *Struct. Bonding.* (Berlin) 16, **1973**:1.
5. Cabbiness, D.K. and Margerum, D.W., *J. Am. Chem. Soc.* 91, **1969**: 9540.
6. Fabbrizzi, L., Paoletti, P. and Clay, R.M., *Inorg. Chem.* 17, **1978**: 1043.
7. McDougall, G.J., Hancock, R.D. and Boeyens, J.C.A., *J. Chem. Soc. Dalton Trans.* **1978**:1043.
8. Hancock, R.D. and McDougall, *Adv. Mol. Int. Proc.* 18, **1980**:99.
9. Bush, D.H., Farmery, K., Goedken, V., Katovic, V., Melnyk, A.C., Sperati, C.R. and Tokel, N., *Adv. Chem. Soc.* 100, **1971**:44.
10. Cram, D.J. and Cram, J.M., *Acc Chem. Res.* 11, **1978**:8; D.J. Cram, *Pure Appl. Chem.* 50, **1978**:817.
11. Christensen, J.J., Eatough, D.J. and Izatt, R.M., *Chem. Rev.* 74, **1974**:315.
12. Izatt, R.M., Nelson, D.P., Rytting, J.H., Haymore, B.L. and Christensen, J.J., *J. Am. Chem. Soc.* 93, **1971**:1619.
13. Ikeda, A. and Shinkai, S., *Chem. Rev.* 97, **1997**:1713.
14. Gutsche, C.D., *Acc. Chem. Res.* 16, **1983**:161.
15. Jeffrey, G.A., *An Introduction to Hydrogen Bonding*, Oxford University Press, Oxford **1997**, pp 12-15.
16. Lindoy, L.F., *The Chemistry of Macrocyclic Ligand Complexes*, Cambridge University Press, Cambridge **1989**, pp 1-269.
17. Fischer, S., Grootenhuis, P.D.J., Groenen, L.C., van Hoorn, W.P., van Vaggel, F.C.J.M., Reinhoudt, D.N., Karplus, M., *J. Am. Chem. Soc.* 117, **1995**:1611.



18. Gruttner, C., Bohmer, V., Vogt, W. Thondorf, I., Biali, S.E. and Grynszpan, F., *Tetrahedron Lett* 35, **1994**:6267.
19. Biali, S.E., Bohmer, V., Brenn, J., Frings, M., Thondorf, I., Vogt, W. and Wohnert, J., *J. Org. Chem.* 62, **1997**:8350.
20. Thondorf, I., *J. Chem. Soc., Perkin Trans II* **1999**:1971.
21. Van Hoorn, W.P., Briels, W.J., van Dughoven, J.P.M., van Veggel, F.C.J.M. and Reinhoudt, D.N., *J. Org. Chem.* 63, **1998**:1299.
22. Tuntulani, T., Thumcharern, G. and Ruangpornvisuti, V., *J. Inclu. Phenom.* 38 ,**2000**:123.
23. Gaussian 94 (Revision D.1), Frisch, M.J., Trucks, G.W., Schlegel, H.B., Gill P.M. WJohnson, B.G., Robb M.A., Cheeseman, J.R., Keith, T.A., Petersson, G.A., Montgomery, J.A., Raghavachari, K., Al-Laham, M.A., Zakrzewski, V.G., Ortiz, J.V., Foresman, J.B., Peng, C.Y., Ayala, P.Y., Wong, M.W., Andres, J.L., Replogle, E.S., Gomperts, R., Martin, R.L., Fox, D.J., Binkley, J.S., Defrees, D.J., Baker, J., Stewart, J.P., Head-Gordon, M., Gonzalez, C., and Pople, J.A., Gaussian, Inc., Pittsburgh PA, **1995**.
24. *HyperChem Release 5.0 for Windows*, Hypercube Inc., October 1996.
25. Gordon, M.S., Binkley, J.S., Pople, J.A., Pietro, W.J. and Hehre, W.J. *J. Am. Chem. Soc.* 104, **1982**:2797.
26. Pietro, W.J., Francl, M.M., Hehre, W.J., Defrees, D.J., Pople, J.A. and Binkley, J.S., *J. Am. Chem. Soc.* 104, **1982**:5039.
27. Dobbs and Hehre, W.J., *J. Comp. Chem.* 7, **1986**:359.
28. Dobbs and Hehre, W.J., *J. Comp. Chem.* 8, **1987**:861.
29. Dobbs and Hehre, W.J., *J. Comp. Chem.* 8, **1987**:880.
30. Ditchfield, R., Hehre, W.J and Pople, J.A., *J. Chem. Phys.* 54, **1971**:724.
31. Hehre, W.J, Ditchfield, R. and Pople, J.A., *J. Chem. Phys.* 56, **1972**:2257.
32. Hariharan P.C. and Pople, J.A., *Mol. Phys.* 27, **1974**:209.
33. Gordon, M.S., *Chem. Phys. Lett.* 76, **1980**:163.
34. Hariharan P.C. and Pople, J.A. *Theo. Chim. Acta.* 28, **1973**:213.

35. Dunning, T.H., Jr. and Hay, P.J., *In Modern Theoretical Chemistry*, Ed.H.F. Schaefer III, Plenum, Newyork, **1976**.
36. McLean, A.D. and Chandler, G.S., *J. Chem. Phys.* 72, **1980**:5639.
37. Krishnan, R., Binkley, J.S., Seeger, R. and Pople, J.A., *J. Chem. Phys.* 72, **1980**:650.
38. James B. Foresman, Aeleen Frisch, *Exploring Chemistry with Electronic Structure Methods*, 2<sup>nd</sup> Edition, Faussian, Inc. Pittsburgh, PA, **1996**.
39. Harada, T., Rudzinski, J.M., Osawa, E., Shinkai, S., *Tertahedron* 49, **1993**: 5941.
40. Harada, T., Ohseto, F., Shinkai, S., *Tertahedron* 50, **1994**: 13377.
41. Harada, T., S. Shinkai, S., *J. Chem. Soc., Perkin Trans. 2*, **1995**: 2231.
42. Gutshe, C.D., Vauer, L.J., *J. Am. Chem. Soc.* 107, **1985**: 6052.
43. Wachters, A.J.H., *J. Chem. Phys.* 52, **1970**:1033.
44. Hey, P.J., *J. Chem. Phys.* 66, **1977**:4377.
45. Raghavachari, K. and Trucks, G.W., *J. Chem. Phys.* 9, **1989**:1062.
46. Binning, R.C., Jr. and Curtiss, L.A., *J. Comp. Chem.* 11, **1990**:1206.
47. Petersson, G.A., Bennett, A., Tensfeldt, T.G., Al-Laham, M.A., Shirley, W.A. and Mantzaris, J., *J. Chem. Phys.* 89, **1988**:2193.
48. Petersson, G.A. and Al-Laham, M.A., *J. Chem. Phys.* 94, **1991**:6081.
49. McGrath, M.P. and Radom, L., *J. Chem. Phys.* 94, **1991**:511.
50. Pulay, P. *J. Comp. Chem.* 3, **1982**:556.
51. Almlhoff, J., Korsell, K. and Faegri, K.Jr., *J. Comp. Chem.* 3, **1982**:385.

## APPENDIX A

**Table A1** Interaction data for the ligand L<sub>I</sub> and proton.

Distance (Å)	E <sub>H</sub> (Hartree)	ΔE (kcal.mol <sup>-1</sup> )	Dipole moment (Debye)	CPU times (h:m:s)
0.60	-2536.05023	44.0	27.64	1:35:15
0.63	-2536.13547	-9.5	27.75	1:35:00
0.75	-2536.41153	-182.7	28.26	1:27:03
0.88	-2536.52405	-253.4	28.65	1:26:52
0.90	-2536.53546	-260.5	28.72	1:26:12
0.95	-2536.5506	-270.0	28.86	1:27:44
1.00	-2536.55759	-274.4	28.99	1:26:38
1.05	-2536.55842	-274.9	29.13	1:27:28
1.10	-2536.5545	-272.5	29.27	1:27:42
1.15	-2536.54716	-267.9	29.41	1:26:00
1.25	-2536.52502	-254.0	29.70	1:27:51
1.375	-2536.48986	-231.9	30.11	1:27:00
1.50	-2536.45129	-207.7	30.56	1:26:36
1.75	-2536.37634	-160.7	31.60	1:34:55
2.00	-2536.31249	-120.6	32.81	1:37:17
2.25	-2536.26322	-89.7	34.09	1:38:29
2.50	-2536.2310	-69.5	31.93	3:10:06 <sup>a</sup>
3.00	-2536.2103	-56.5	33.45	4:43:07 <sup>a</sup>
5.00	-2536.1572	-23.1	34.05	10:53:21 <sup>a</sup>
10.00	-2536.1410	-13.0	34.21	7:02:52:53 <sup>a</sup>

<sup>a</sup>Long CPU times cause from the convergency problem of mono valence species.

**Table A2** Interaction data obtained from *ab initio* calculations with 6-31G basis set, at orientation of proton locating in the Z-axis.

Distance (Å)	$E_H$ (Hartree)	$\Delta E$ (kcal.mol <sup>-1</sup> )	Dipole moment (Debye)	CPU times (h:m:s)
-7.00	-2536.100769	-12.26	30.1884	3:38:57
-5.00	-2536.080085	-25.24	6.4665	3:33:48
-2.00	-2536.24325	-77.15	5.2478	1:33:34
-1.50	-2536.25686	-85.69	4.8718	1:29:41
-1.00	-2536.26675	-91.90	4.6441	1:28:34
-0.50	-2536.26420	-90.30	4.4220	1:28:47
0.50	-2536.30318	-114.8	0.20	1:16:31
0.75	-2536.32783	-130.2	0.29	1:09:47
1.00	-2536.34506	-141.0	0.59	1:14:24
1.22	-2536.35105	-144.8	0.85	1:14:24
1.25	-2536.35113	-144.8	0.88	1:14:20
1.28	-2536.35107	-144.8	0.92	1:14:02
1.30	-2536.35092	-144.7	0.94	1:13:46
1.50	-2536.34533	-141.2	1.16	1:15:28
1.75	-2536.32914	-131.0	1.42	1:15:16
2.00	-2536.30613	-116.6	1.62	1:16:27
2.50	-2536.26052	-88.0	1.71	1:20:25
3.00	-2536.23593	-72.6	2.09	1:27:18
4.00	-2536.21601	-60.1	3.03	1:38:11
5.00	-2536.20638	-54.0	4.06	5:36:49
6.00	-2536.20223	-51.4	6.13	4:32:20
7.00	-2536.2002	-50.1	8.56	7:10:23 <sup>a</sup>

<sup>a</sup>Long CPU times cause from the convergency problem of mono valence species.

สถาบันวิทยบริการ  
จุฬาลงกรณ์มหาวิทยาลัย

**Table A3** Interaction data obtained from *ab initio* calculations with 6-31G basis set, which methanol locating on the axis along a nitrogen atom of the pyridine plane.

Distance (Å)	$E_{\text{MeOH}}$ (Hartree)	$\Delta E$ (kcal.mol <sup>-1</sup> )	Dipole moment (Debye)	CPU times (h:m:s)
1.25	-2649.62977	24.9	6.04	1:14:13
1.35	-2649.64901	12.9	5.67	1:15:13
1.50	-2649.66563	2.4	5.17	1:14:12
1.60	-2649.67153	-1.3	4.89	1:12:56
1.70	-2649.67491	-3.4	4.65	1:13:17
1.75	-2649.67595	-4.0	4.54	1:12:47
1.80	-2649.67663	-4.5	4.44	1:13:02
1.85	-2649.67705	-4.7	4.35	1:12:34
1.95	-2649.67729	-4.9	4.20	1:12:57
2.00	-2649.67721	-4.8	4.13	1:12:39
2.25	-2649.67587	-4.0	3.90	1:12:01
2.50	-2649.67423	-3.0	3.77	1:12:15
3.00	-2649.67208	-1.6	3.66	1:12:50
4.00	-2649.67057	-0.7	3.60	1:11:01
5.00	-2649.67007	-0.4	3.53	1:11:15
7.00	-2649.66971	-0.1	3.55	1:11:02
9.00	-2649.66959	-0.1	3.54	1:11:10
10.00	-2649.66957	-0.0	3.52	1:10:53

**Table A4** Interaction data obtained from *ab initio* calculations with 6-31G basis set, at orientation of methanol locating in the Z-axis.

Distance (Å)	$E_{\text{MeOH}}$ (Hartree)	$\Delta E$ (kcal.mol <sup>-1</sup> )	Dipole moment (Debye)	CPU times (h:m:s)
1.50	-2649.32276	217.6	4.66	1:26:48
1.75	-2649.46589	127.8	4.33	1:19:29
2.00	-2649.53723	83.0	4.04	1:18:56
2.50	-2649.59801	45.0	3.57	1:16:59
3.00	-2649.62823	26.0	3.36	1:15:05
4.00	-2649.66036	5.7	3.39	1:12:59
5.00	-2649.66814	0.9	3.41	1:11:11
7.00	-2649.66903	0.3	3.39	1:09:24
9.00	-2649.66927	0.1	3.38	1:09:25
10.00	-2649.66934	0.1	3.37	1:09:45

สถาบันวิทยบริการ  
จุฬาลงกรณ์มหาวิทยาลัย

**Table A5** Interaction data obtained from *ab initio* calculations with 6-31G basis set, at orientation of methanol which points the methoxy unit towards the calix[4]arene framework locating in the Z-axis.

Distance (Å)	$E_{\text{MeOH}}$ (Hartree)	$\Delta E$ (kcal.mol <sup>-1</sup> )	Dipole moment (Debye)	CPU times (h:m:s)
0	-2648.945592	457.07	3.7917	1:14:03
1	-2649.230012	278.60	2.9931	1:06:57
3	-2649.499405	109.55	3.8057	1:22:37
5	-2649.647246	16.78	3.1180	1:17:47
7	-2649.662734	7.06	3.1701	1:15:17
10	-2649.662943	6.93	3.1691	1:14:26

สถาบันวิทยบริการ  
จุฬาลงกรณ์มหาวิทยาลัย



**Table A6** Interaction data obtained from *ab initio* calculations with 6-31G basis set, which lithium locating on the axis along a nitrogen atom of the pyridine plane.

Distance (Å)	$E_{Li}$ (Hartree)	$\Delta E$ (kcal.mol <sup>-1</sup> )	Dipole moment (Debye)	CPU times (h:m:s)
1.25	-2543.22047	22.1	32.69	1:19:00
1.38	-2543.30964	-33.8	33.48	1:19:14
1.50	-2543.35307	-61.1	34.15	1:19:20
1.55	-2543.36442	-68.2	34.43	1:19:42
1.60	-2543.37254	-73.3	34.69	1:19:16
1.65	-2543.38381	-80.4	34.96	1:19:06
1.75	-2543.38468	-80.9	35.48	1:19:47
1.80	-2543.38577	-81.6	35.75	1:20:36
1.83	-2543.38591	-81.7	35.90	1:17:17
1.85	-2543.38584	-81.6	36.01	1:20:31
1.87	-2543.38562	-81.5	36.12	1:17:29
1.90	-2543.38509	-81.2	36.27	1:20:20
1.95	-2543.38367	-80.3	36.54	1:20:21
2.00	-2543.38172	-79.0	36.80	1:20:01
2.05	-2543.37940	-77.6	37.07	1:20:11
2.25	-2543.36711	-69.9	38.18	1:19:11
2.50	-2543.34912	-58.6	39.66	1:19:18
3.00	-2543.31470	-37.0	42.93	1:17:44
4.00	-2543.27615	-12.8	49.70	1:10:59
5.00	-2543.26556	-6.2	55.29	1:10:13
6.00	-2543.26204	-4.0	60.31	1:10:07
7.00	-2543.26024	-2.8	65.21	1:09:42
10.00	-2543.25783	-1.3	79.68	1:09:31

**Table A7** Interaction data obtained from *ab initio* calculations with 6-31G basis set, at orientation of lithium locating in the Z-axis.

Distance (Å)	$E_{Li}$ (Hartree)	$\Delta E$ (kcal.mol <sup>-1</sup> )	Dipole moment (Debye)	CPU times (h:m:s)
0.00	-2543.45264	-123.5	1.45	1:18:51
0.25	-2543.46658	-132.3	0.87	1:25:40
0.50	-2543.47604	-138.2	0.35	1:24:56
0.70	-2543.48065	-141.1	0.11	1:25:45
0.90	-2543.48190	-141.9	0.54	1:25:18
0.95	-2543.48194	-141.9	0.69	1:26:30
1.00	-2543.48191	-141.9	0.78	1:25:16
1.10	-2543.48172	-141.8	1.03	1:24:56
1.15	-2543.48158	-141.7	1.16	1:24:29
1.22	-2543.48138	-141.6	1.34	1:24:08
1.23	-2543.48130	-141.5	1.40	1:26:42
1.25	-2543.48126	-141.5	1.46	1:26:52
1.28	-2543.48118	-141.5	1.54	1:26:07
1.30	-2543.48122	-141.5	2.28	1:26:54
1.55	-2543.48010	-140.8	3.78	1:17:43
1.80	-2543.47690	-138.8	2.90	1:20:46
2.05	-2543.46539	-131.5	3.05	1:22:36
2.30	-2543.45006	-121.9	4.53	1:26:05
2.80	-2543.39959	-90.3	6.72	1:18:57
3.30	-2543.34969	-58.9	9.41	1:17:44
3.80	-2543.31506	-37.2	12.40	1:16:40
4.30	-2543.29449	-24.3	15.40	1:15:39
5.30	-2543.27231	-10.4	21.32	1:20:01
6.30	-2543.26068	-3.1	27.24	1:17:55
8.30	-2543.25534	0.3	38.26	1:10:28
10.30	-2543.25594	0.0	39.23	1:15:11

**Table A8** Interaction data obtained from *ab initio* calculations with 6-31G basis set, which sodium locating on the axis along a nitrogen atom of the pyridine plane.

Distance (Å)	$E_{\text{Na}}$ (Hartree)	$\Delta E$ (kcal.mol <sup>-1</sup> )	Dipole moment (Debye)	CPU times (h:m:s)
1.50	-2695.79479	69.1	35.03	1:30:52
1.70	-2695.91783	-8.1	35.96	1:29:33
1.80	-2695.94763	-26.8	36.46	1:29:53
1.90	-2695.96479	-37.6	36.99	1:29:24
2.00	-2695.97346	-43.0	37.56	1:22:20
2.05	-2695.97546	-44.3	37.85	1:20:52
2.12	-2695.97639	-44.8	38.27	1:19:26
2.17	-2695.97597	-44.6	38.58	1:17:56
2.20	-2695.97538	-44.2	38.77	1:20:05
2.50	-2695.96202	-35.8	40.73	1:19:12
3.00	-2695.93827	-20.9	43.94	1:18:21
4.00	-2695.92013	-9.5	49.37	1:20:08
5.00	-2695.91432	-5.9	54.35	1:17:40
7.00	-2695.90956	-2.9	64.02	1:17:22
10.00	-2695.90716	-1.4	78.25	1:17:14

**Table A9** Interaction data obtained from *ab initio* calculations with 6-31G basis set, at orientation of sodium locating in the Z-axis.

Distance (Å)	$E_{\text{Na}}$ (Hartree)	$\Delta E$ (kcal.mol <sup>-1</sup> )	Dipole moment (Debye)	CPU times (h:m:s)
0.00	-2695.99920	-59.2	2.22	1:24:54
0.20	-2696.00305	-61.6	1.63	1:25:01
0.25	-2696.00339	-61.8	1.47	1:25:32
0.35	-2696.00299	-61.5	1.16	1:25:09
0.50	-2695.99942	-59.3	0.72	1:25:26
0.75	-2695.98631	-51.1	0.02	1:26:01
1.00	-2695.96915	-40.3	0.78	1:25:33
1.10	-2695.96410	-37.1	1.08	1:29:53
1.25	-2695.95996	-34.5	6.45	1:27:44
1.27	-2695.95975	-34.4	1.59	1:29:00
1.29	-2695.95964	-34.3	1.65	1:29:33
1.38	-2695.96019	-34.7	1.93	1:28:58
1.42	-2695.96096	-35.2	2.05	1:28:22
1.45	-2695.96175	-35.7	7.50	1:26:56
1.55	-2695.96394	-37.0	2.47	1:26:53
1.80	-2695.97645	-44.9	3.53	1:26:21
1.95	-2695.98379	-49.5	3.91	1:26:00
2.05	-2695.98731	-51.7	4.31	1:31:20
2.15	-2695.98929	-52.9	4.59	1:26:05
2.18	-2695.98954	-53.1	4.71	1:22:27
2.20	-2695.98961	-53.1	4.80	1:26:13
2.21	-2695.98953	-53.1	5.00	1:23:20
2.22	-2695.98962	-53.1	4.89	1:22:20
2.30	-2695.98950	-53.1	5.02	1:26:08
2.45	-2695.98479	-50.1	5.95	1:25:33
2.55	-2695.98027	-47.3	6.45	1:25:06
2.80	-2695.96531	-37.9	7.77	1:25:01
3.05	-2695.94953	-28.0	9.14	1:24:11
3.30	-2695.93671	-20.0	10.54	1:23:07
3.55	-2695.92822	-15.0	11.91	1:23:29
3.80	-2695.92329	-11.5	13.27	1:22:32
4.30	-2695.91809	-8.3	15.99	1:21:26

**Table A9** (Continued)

Distance (Å)	$E_{\text{Na}}$ (Hartree)	$\Delta E$ (kcal.mol <sup>-1</sup> )	Dipole moment (Debye)	CPU times (h:m:s)
5.30	-2695.90918	-2.7	21.60	1:19:57
6.30	-2695.90495	-0.0	27.09	1:18:53
7.30	-2695.90424	0.4	32.38	1:18:25
8.30	-2695.90444	0.3	37.54	1:17:25
10.30	-2695.90505	-0.1	47.60	1:17:20



สถาบันวิทยบริการ  
จุฬาลงกรณ์มหาวิทยาลัย

**Table A10** Interaction data obtained from *ab initio* calculations with 6-31G basis set, at orientation of potassium locating in the Z-axis.

Distance (Å)	$E_{\text{Be}}$ (Hartree)	$\Delta E$ (kcal.mol <sup>-1</sup> )	Dipole moment (Debye)	CPU times (h:m:s)
-7.00	-3129.13670	-4.43	28.1807	1:52:48
-3.00	-3129.17307	-27.25	10.9512	2:16:37
-2.00	-3129.20285	-45.94	7.4453	2:18:53
-1.00	-3129.22227	-58.12	4.5467	2:21:15
-0.63	-3129.22343	-58.86	3.5541	2:11:45
-0.55	-3129.22238	-58.20	3.3505	2:12:14
0.00	-3129.17933	-31.18	2.1012	2:10:14
0.50	-3129.04079	55.76	0.9990	2:08:27
1.00	-3128.85899	169.83	0.5010	2:10:41
2.00	-3129.01426	72.41	3.9388	2:06:32
2.75	-3129.15863	-18.19	6.8581	2:05:55
3.00	-3129.15787	-17.72	8.0987	2:03:28
3.64	-3129.13807	-5.29	11.7196	2:02:10
4.37	-3129.13828	-5.42	15.8756	1:58:54
5.00	-3129.14048	-6.80	19.3067	1:55:21
7.00	-3129.12976	-0.08	30.3213	1:51:11

**Table A11** Interaction data obtained from *ab initio* calculations with 6-31G basis set, which beryllium locating on the axis along a nitrogen atom of the pyridine plane.

Distance (Å)	$E_{\text{Be}}$ (Hartree)	$\Delta E$ (kcal.mol <sup>-1</sup> )	Dipole moment (Debye)	CPU times (h:m:s)
1.00	-2549.58178	-13.6	44.97	3:51:34
1.16	-2549.86412	-190.8	42.04	2:39:46
1.35	-2549.99187	-271.0	41.03	2:09:38
1.50	-2550.02280	-290.4	40.15	3:38:33
1.65	-2550.02621	-292.5	37.94	5:08:55
1.68	-2550.02196	-289.8	38.75	3:36:40
1.70	-2550.02223	-290.0	33.24	4:37:08
1.75	-2550.02037	-288.8	36.59	5:22:06
1.95	-2549.99530	-273.1	31.26	5:27:04
2.00	-2549.99531	-273.2	31.12	10:22:52
3.00	-2549.6909	-82.1	30.13	23:15:11 <sup>a</sup>
7.00	-2549.6164	-35.3	30.05	23:55:12 <sup>a</sup>

<sup>a</sup>Long CPU times cause from the convergency problem of mono valence species.



**Table A12** Interaction data obtained from *ab initio* calculations with 6-31G basis set, at orientation of beryllium locating in the Z-axis.

Distance (Å)	$E_{\text{Be}}$ (Hartree)	$\Delta E$ (kcal.mol <sup>-1</sup> )	Dipole moment (Debye)	CPU times (h:m:s)
0.00	-2550.04646	-305.2	1.69	1:26:13
0.25	-2550.08237	-327.8	0.05	1:25:59
0.50	-2550.12276	-353.1	1.67	1:22:07
0.70	-2550.14939	-369.8	2.73	1:21:58
1.00	-2550.17540	-386.1	4.09	1:21:27
1.15	-2550.18025	-389.2	4.66	1:25:27
1.22	-2550.18094	-389.6	4.94	1:25:29
1.30	-2550.18014	-389.1	5.27	1:25:29
1.50	-2550.17069	-383.2	6.14	1:25:00
1.75	-2550.14168	-365.0	7.44	1:20:36
2.00	-2550.09866	-338.0	8.90	1:24:50
2.50	-2549.99135	-270.6	12.20	1:33:16
3.00	-2549.90096	-213.9	9.54	2:22:03
5.00	-2549.70902	-93.5	6.46	22:12:49
7.00	-2549.6032	-27.1	4.53	7:23:37:17 <sup>a</sup>
10.00	-2549.5873	-17.1	4.33	7:22:25:14 <sup>a</sup>

<sup>a</sup>Long CPU times cause from the convergency problem of mono valence species.

**Table A13** Interaction data obtained from *ab initio* calculations with 6-31G basis set, which magnesium locating on the axis along a nitrogen atom of the pyridine plane.

Distance (Å)	$E_{Mg}$ (Hartree)	$\Delta E$ (kcal.mol <sup>-1</sup> )	Dipole moment (Debye)	CPU times (h:m:s)
1.25	-2732.43229	125.5	66.93	1:29:47
1.38	-2732.65845	-16.4	68.40	1:29:06
1.50	-2732.77476	-89.4	69.65	1:30:33
1.65	-2732.84851	-135.7	71.18	1:28:56
1.75	-2732.87013	-149.3	72.19	1:28:52
1.88	-2732.87807	-154.3	73.51	1:28:48
1.90	-2732.87784	-154.1	73.71	1:28:55
1.95	-2732.87596	-153.0	74.22	1:28:27
2.00	-2732.87250	-150.8	74.73	1:31:26
2.01	-2732.87164	-150.2	74.83	1:27:47
2.25	-2732.84043	-130.6	77.32	1:30:21
2.50	-2732.80499	-108.4	67.08	3:08:48
3.00	-2732.75619	-77.8	56.45	5:15:45
5.00	-2732.72109	-55.7	48.12	7:02:12:53 <sup>a</sup>
10.00	-2732.67360	-26.0	40.13	7:01:15:22 <sup>a</sup>

<sup>a</sup>Long CPU times cause from the convergency problem of mono valence species.

**Table A14** Interaction data obtained from *ab initio* calculations with 6-31G basis set, at orientation of magnesium locating in the Z-axis.

Distance (Å)	$E_{Mg}$ (Hartree)	$\Delta E$ (kcal.mol <sup>-1</sup> )	Dipole moment (Debye)	CPU times (h:m:s)
0.00	-2732.95516	-202.6	2.24	1:33:50
0.25	-2732.98852	-223.6	0.30	1:34:39
0.50	-2733.00706	-235.2	1.20	1:35:52
0.65	-2733.01069	-237.5	1.69	1:35:59
0.75	-2733.01411	-239.6	2.62	1:36:52
0.88	-2733.01433	-239.8	2.98	1:33:48
1.00	-2733.01350	-239.2	3.72	1:34:16
1.25	-2733.01053	-237.4	5.05	1:33:38
1.50	-2733.00799	-235.8	6.54	1:33:05
1.75	-2733.00339	-232.9	8.18	1:32:12
2.00	-2732.98869	-223.7	10.13	1:32:43
2.20	-2732.97205	-213.2	11.76	1:39:22
2.30	-2732.95929	-205.2	12.64	1:39:02
2.80	-2732.87905	-154.9	17.50	1:37:41
3.41	-2732.79642	-103.0	23.96	1:28:28
4.00	-2732.75652	-78.0	29.83	1:29:01
5.00	-2732.71828	-54.0	26.92	2:06:13
7.00	-2732.644117	-7.5	34.50	7:03:43:40 <sup>a</sup>
9.00	-2732.64401	-7.4	44.98	7:04:25:59 <sup>a</sup>

<sup>a</sup>Long CPU times cause from the convergency problem of mono valence species.

**Table A15** Interaction data obtained from *ab initio* calculations with 6-31G basis set, at orientation of resorcinol locating in the Z-axis.

Distance (Å)	$E_{\text{Resorcinol}}$ (Hartree)	$\Delta E$ (kcal.mol <sup>-1</sup> )	Dipole moment (Debye)	CPU times (h:m:s)
1.25	-2911.65049	30.8	15.03	1:42:04
1.60	-2911.70390	-2.7	13.06	1:28:34
1.80	-2911.71853	-11.9	11.45	1:29:39
1.90	-2911.71964	-12.6	10.92	1:29:20
2.00	-2911.71858	-11.9	10.08	1:25:42
2.20	-2911.71540	-9.9	9.45	1:04:31
3.00	-2911.70794	-5.2	8.60	1:02:42
5.00	-2911.70553	-3.7	8.36	1:26:59
7.00	-2911.70256	-1.8	8.07	1:03:53
9.00	-2911.70077	-0.7	8.07	1:03:53

สถาบันวิทยบริการ  
จุฬาลงกรณ์มหาวิทยาลัย

**Table A16** Interaction data obtained from *ab initio* calculations with 6-31G basis set, at orientation of resorcinol which points the molecular unit below the calix[4]arene framework locating in the Z-axis.

Distance (Å)	$E_{\text{Resorcinol}}$ (Hartree)	$\Delta E$ (kcal.mol <sup>-1</sup> )	Dipole moment (Debye)	CPU times (h:m:s)
1.25	-2911.65049	30.8	15.03	1:42:04
1.60	-2911.70390	-2.7	13.06	1:28:34
1.80	-2911.71853	-11.9	11.45	1:29:39
1.90	-2911.71964	-12.6	10.92	1:29:20
2.00	-2911.71858	-11.9	10.08	1:25:42
2.20	-2911.71540	-9.9	9.45	1:04:31
3.00	-2911.70794	-5.2	8.60	1:02:42

สถาบันวิทยบริการ  
จุฬาลงกรณ์มหาวิทยาลัย

**Table A17** Interaction data obtained from *ab initio* calculations with 6-31G basis set, at orientation of phthalic acid locating in the Z-axis.

Distance (Å)	$E_{\text{phthalic acid}}$ (Hartree)	$\Delta E$ (kcal.mol <sup>-1</sup> )	Dipole moment (Debye)	CPU times (h:m:s)
1.25	-3134.10530	54.2	11.85	1:48:07
1.60	-3134.20375	-7.6	9.40	1:46:22
1.80	-3134.21205	-12.8	8.21	1:45:08
1.90	-3134.21238	-13.0	7.83	1:45:58
2.00	-3134.21138	-12.4	7.31	1:44:30
2.20	-3134.20803	-10.3	6.67	1:43:40
3.00	-3134.19774	-3.8	5.65	1:43:13
5.00	-3134.19282	-0.7	5.25	1:17:26
7.00	-3134.19205	-0.2	5.14	1:17:37
9.00	-3134.19180	-0.1	5.09	1:42:47

สถาบันวิทยบริการ  
จุฬาลงกรณ์มหาวิทยาลัย

**Table A18** Interaction data obtained from *ab initio* calculations with 6-31G basis set, at orientation of phthalic acid locating in the Z-axis.

Distance (Å)	$E_{\text{phthalic acid}}$ (Hartree)	$\Delta E$ (kcal.mol <sup>-1</sup> )	Dipole moment (Debye)	CPU times (h:m:s)
1.25	-3134.10530	54.2	11.85	1:48:07
1.60	-3134.20375	-7.6	9.40	1:46:22
1.80	-3134.21205	-12.8	8.21	1:45:08
1.90	-3134.21238	-13.0	7.83	1:45:58
2.00	-3134.21138	-12.4	7.31	1:44:30
2.20	-3134.20803	-10.3	6.67	1:43:40
3.00	-3134.19774	-3.8	5.65	1:43:13

สถาบันวิทยบริการ  
จุฬาลงกรณ์มหาวิทยาลัย



## APPENDIX B

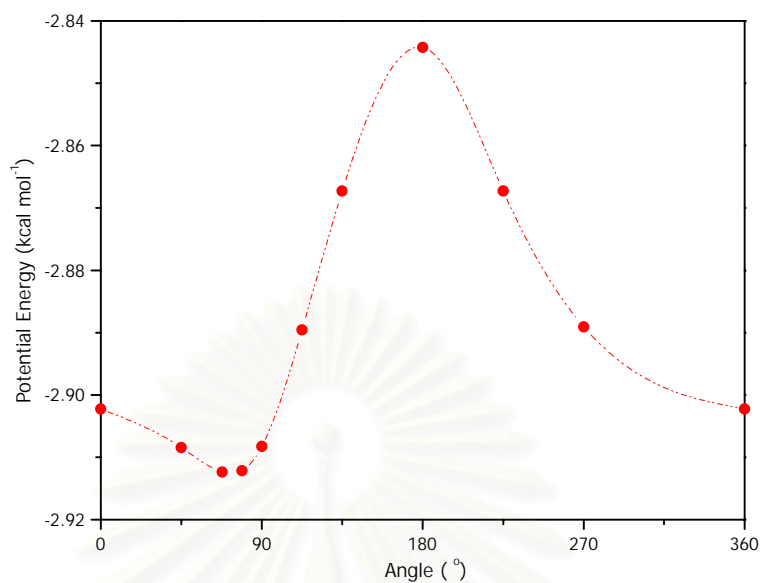


**Figure B1** Rotational barrier curve of methanol and the ligand L<sub>1</sub>.

**Table B1** Rotational barrier data obtained from *ab initio* calculations with STO-3G basis set, of interaction between methanol and the ligand L<sub>1</sub>.

Angle (°)	E <sub>H</sub> (Hartree)	ΔE (kcal.mol <sup>-1</sup> )	Dipole moment (Debye)	CPU times (h:m:s)
0.00	-2649.674125	-2.90	3.4875	1:13:29
45.00	-2649.674135	-2.91	3.4248	1:13:45
65.00	-2649.674140	-2.91	3.4466	1:12:43
68.00	-2649.674141	-2.91	3.4470	1:13:23
79.00	-2649.674141	-2.91	3.4475	1:12:35
90.00	-2649.674135	-2.91	3.4213	1:13:14
112.50	-2649.674105	-2.89	3.4698	1:12:02
135.00	-2649.674069	-2.87	3.4698	1:13:20
180.00	-2649.674033	-2.84	3.4912	1:12:35
225.00	-2649.674069	-2.87	3.4698	1:13:18
270.00	-2649.674104	-2.89	3.4205	1:13:33
360.00	-2649.674125	-2.90	3.4875	1:13:29

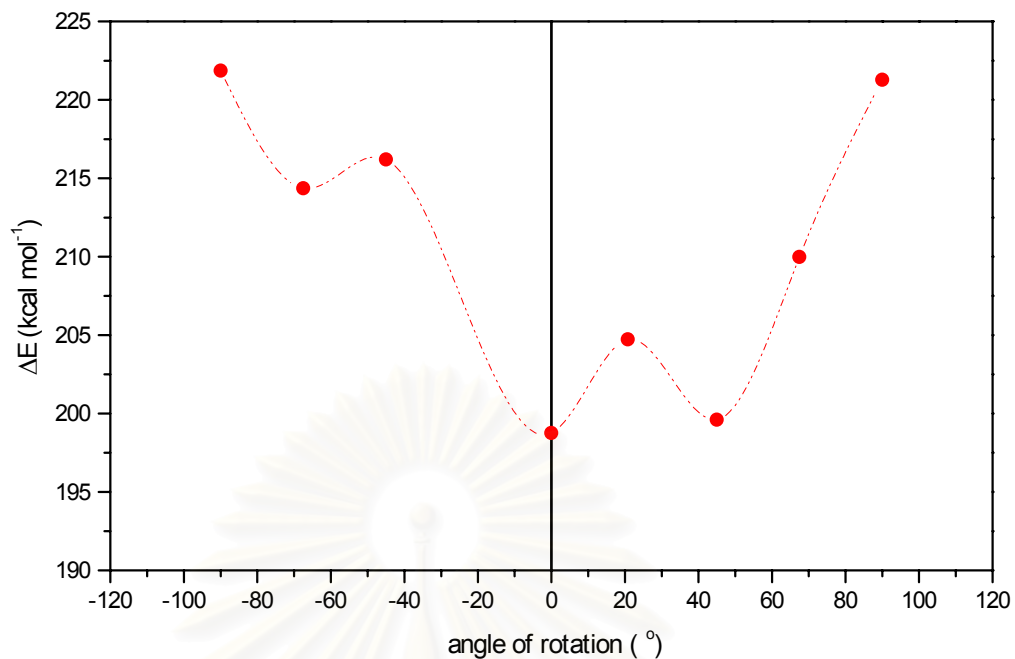


**Figure B2** Rotational barrier curve of methanol which but points the methoxy unit towards the calix[4]arene framework and the ligand L<sub>II</sub>.

**Table B2** Rotational barrier data obtained from *ab initio* calculations with STO-3G basis set, of interaction between methanol which but points the methoxy unit towards the calix[4]arene framework and the ligand L<sub>II</sub>.

Angle (°)	$E_H$ (Hartree)	$\Delta E$ ( $\text{kcal mol}^{-1}$ )	Dipole moment (Debye)	CPU times (h:m:s)
-90	-2649.315933	221.87	4.4178	1:25:19
-67.5	-2649.327894	214.36	4.5649	1:24:42
-45	-2649.324966	216.20	4.6645	1:26:27
0	-2649.352766	198.75	4.3778	1:26:23
20.8	-2649.343253	204.72	4.7611	1:33:04
45	-2649.351397	199.61	5.0184	1:26:10
67.5	-2649.334862	209.99	4.6562	1:25:08
90	-2649.316863	221.28	4.4081	1:25:52

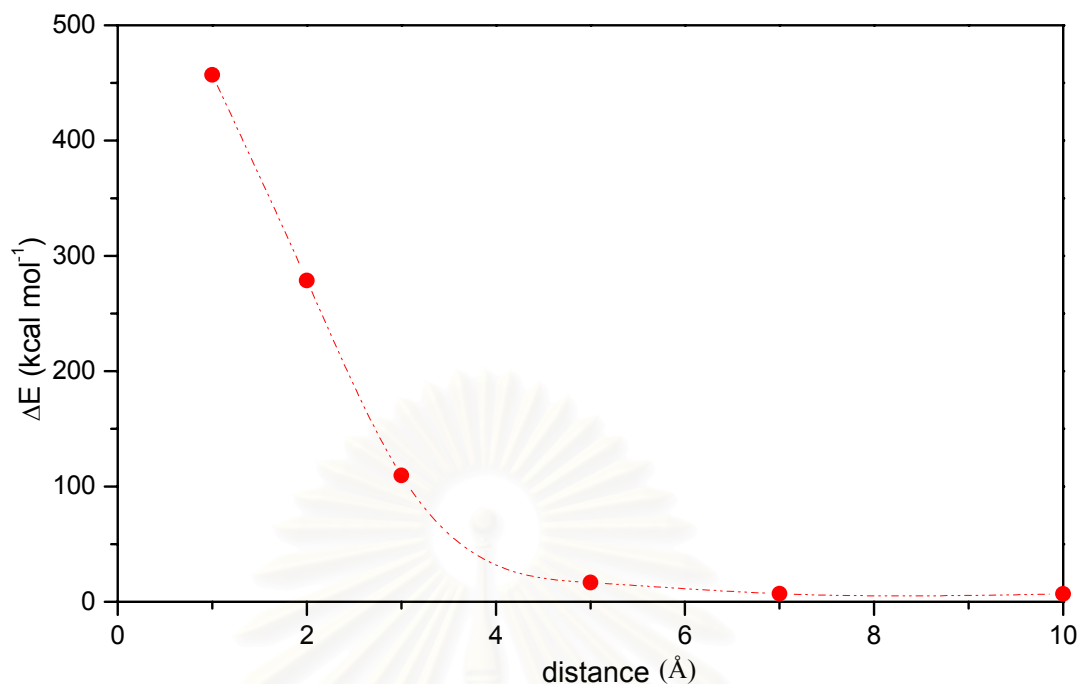


**Figure B3** Potential curve of methanol which but points the methoxy unit towards the calix [4]arene framework and the ligand L<sub>II</sub>.

**Table B3** Inclusion data obtained from *ab initio* calculations with STO-3G basis set, of interaction between methanol which but points the methoxy unit towards the calix[4]arene framework and the ligand L<sub>I</sub>.

Distance (Å)	E <sub>H</sub> (Hartree)	ΔE (kcal.mol <sup>-1</sup> )	Dipole moment (Debye)	CPU times (h:m:s)
0	-2648.945592	457.07	3.7917	1:14:03
1	-2649.230012	278.60	2.9931	1:06:57
3	-2649.499405	109.55	3.8057	1:22:37
5	-2649.647246	16.78	3.1180	1:17:47
7	-2649.662734	7.06	3.1701	1:15:17
10	-2649.662943	6.93	3.1691	1:14:26

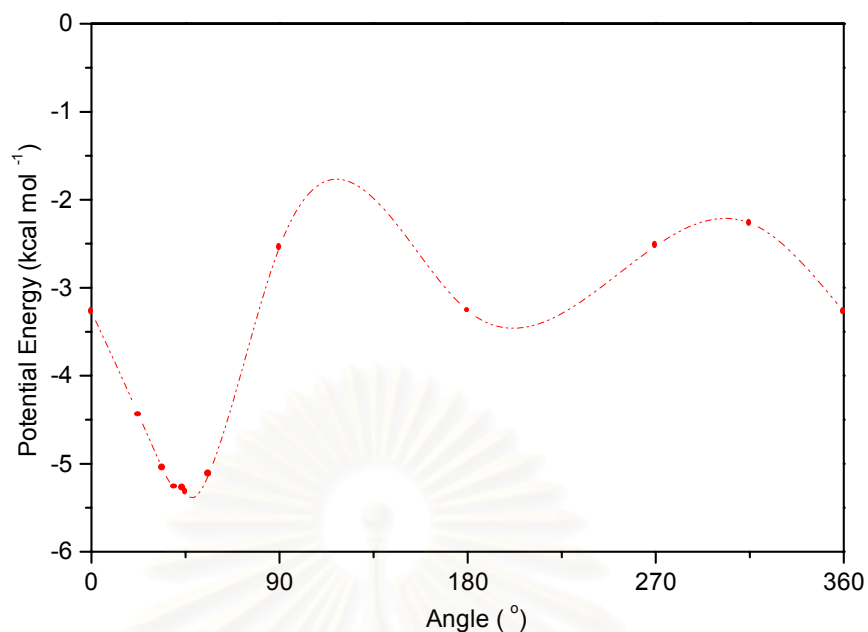


**Figure B4** Rotational barrier curve of resorcinol and the ligand L<sub>II</sub>.

**Table B4** Rotational barrier data obtained from *ab initio* calculations with STO-3G basis set, of interaction between resorcinol and the ligand L<sub>II</sub>.

Angle (°)	E <sub>H</sub> (Hartree)	ΔE (kcal.mol <sup>-1</sup> )	Dipole moment (Debye)	CPU times (h:m:s)
0.00	-2911.7048367	-3.27	8.3376	1:26:50
22.50	-2911.7066989	-4.44	8.4621	1:27:10
33.75	-2911.7076604	-5.04	8.539	1:26:52
40.00	-2911.7080112	-5.26	8.5774	1:27:40
43.75	-2911.7080310	-5.28	8.595	1:27:35
45.00	-2911.7081117	-5.33	8.6091	1:03:34
56.25	-2911.7077740	-5.12	8.6229	1:27:12
90.00	-2911.7036643	-2.54	8.5206	1:27:08
180.00	-2911.7048145	-3.26	8.3291	1:26:38
270.00	-2911.7036438	-2.52	8.5151	1:26:45
315.00	-2911.7032280	-2.26	8.298	1:03:37
360.00	-2911.7048367	-3.27	8.3376	1:26:50

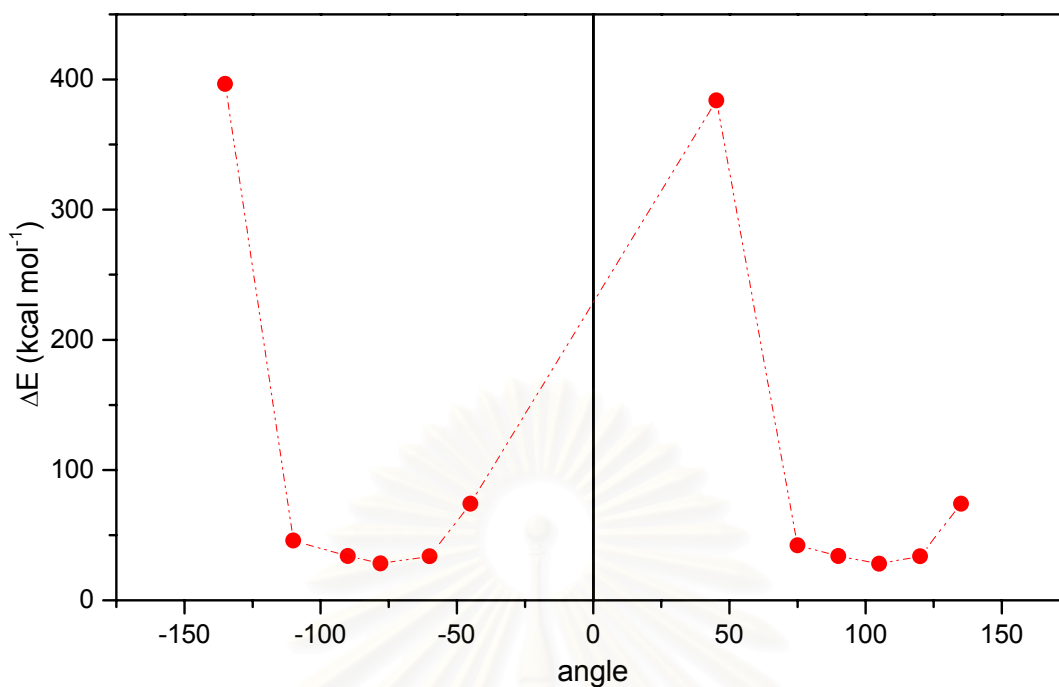


**Figure B5** Rotational barrier curve of resorcinol which points the molecular unit below the calix[4]arene framework included in ligand L<sub>II</sub>.

**Table B5** Rotational barrier data obtained from *ab initio* calculations with STO-3G basis set, of interaction between resorcinol which points the molecular unit below the calix[4]arene framework and the ligand L<sub>II</sub>.

Angle (°)	E <sub>H</sub> (Hartree)	ΔE (kcal.mol <sup>-1</sup> )	Dipole moment (Debye)	CPU times (h:m:s)
135	-2911.581521	47.80	6.7484	2:03:14
120	-2911.645810	32.80	6.8817	2:03:13
105	-2911.654964	17.80	6.8916	1:56:12
90	-2911.645691	2.80	7.1075	1:55:41
75	-2911.632526	-12.20	7.0281	1:56:21
45.27	-2911.087836	-41.930	6.9266	2:07:15
-45	-2911.581521	-132.20	6.7484	2:03:17
-60	-2911.645812	-147.20	6.8817	2:04:17
-78	-2911.654389	-165.20	6.9313	1:55:29
-90	-2911.645691	-177.20	7.1075	1:45:42
-110	-2911.626452	-197.20	6.9632	1:56:44
-135	-2911.067618	-222.20	6.9260	1:38:03

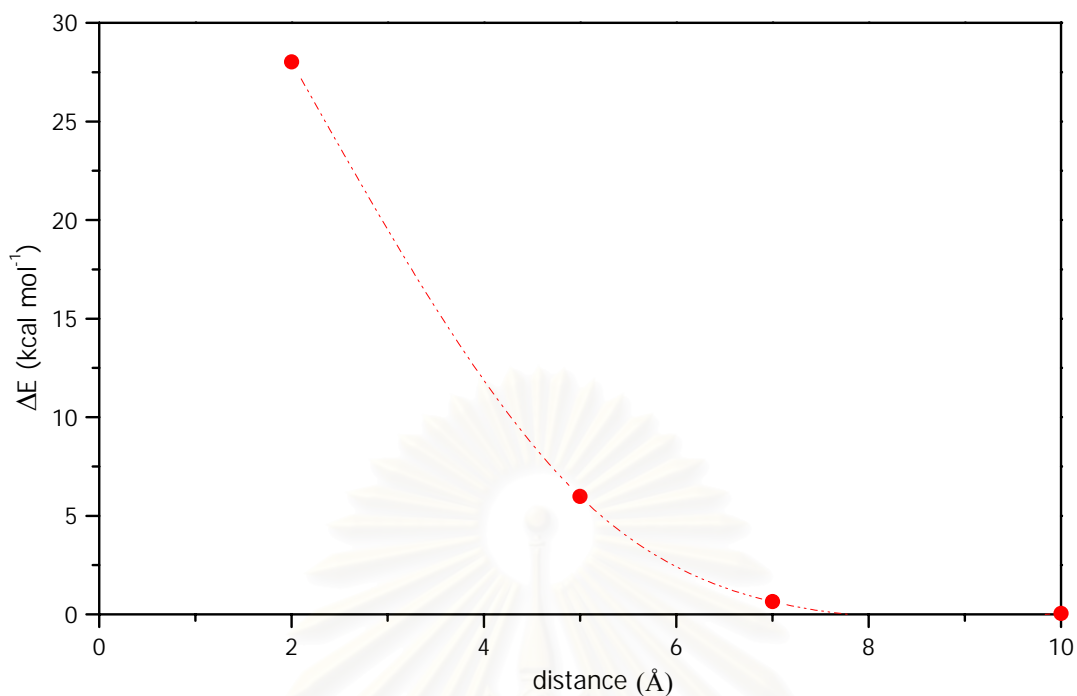


**Figure B6** Potential curve of resorcinol which points the molecular unit below the calix[4]arene framework and the ligand L<sub>II</sub>.

**Table B6** Energies data obtained from *ab initio* calculations with STO-3G basis set, of interaction between resorcinol which points the molecular unit below the calix [4]arene framework and the ligand L<sub>II</sub>.

Distance (Å)	E <sub>H</sub> (Hartree)	ΔE (kcal.mol <sup>-1</sup> )	Dipole moment (Debye)	CPU times (h:m:s)
2	-2911.654964	28.02	6.8916	1:56:12
5	-2911.690084	5.98	7.8088	1:34:38
7	-2911.698598	0.64	7.6398	1:29:12
10	-2911.699548	0.05	7.5791	1:26:32

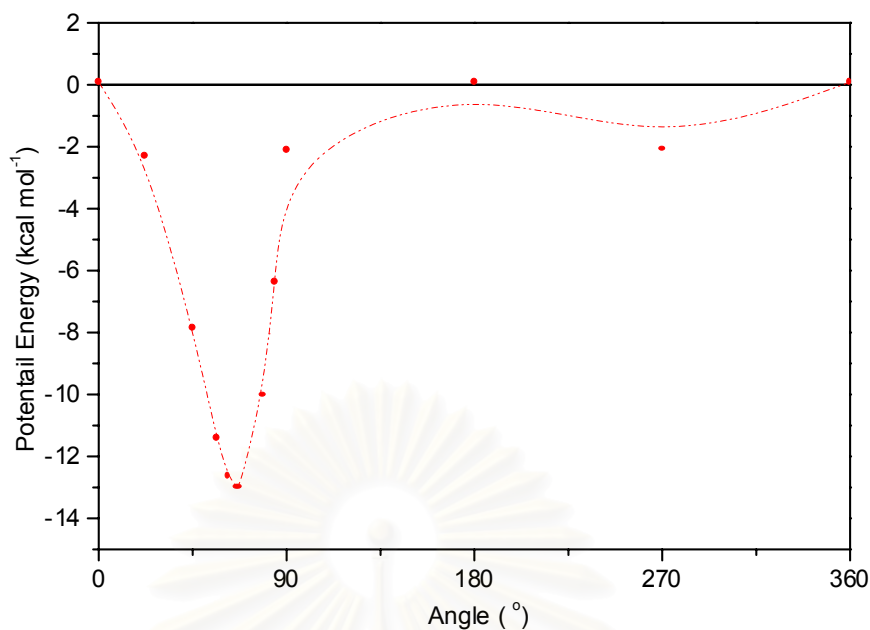


**Figure B7** Rotational barrier curve of phthalic acid and the ligand L<sub>II</sub>.

**Table B7** Rotational barrier data obtained from *ab initio* calculations with STO-3G basis set, of interaction between phthalic acid and the ligand L<sub>II</sub>.

Angle (°)	E <sub>II</sub> (Hartree)	ΔE (kcal.mol <sup>-1</sup> )	Dipole moment (Debye)	CPU times (h:m:s)
0.00	-3134.1915334	0.09	5.4857	1:44:17
22.50	-3134.1953656	-2.31	5.6798	1:45:14
45.00	-3134.2042124	-7.86	6.4214	1:46:25
56.50	-3134.2098715	-11.41	7.1285	1:45:57
62.00	-3134.2117887	-12.62	7.5159	1:45:40
66.00	-3134.2123629	-12.98	7.7750	1:43:56
67.50	-3134.2123884	-12.99	7.8667	1:44:32
78.50	-3134.2076353	-10.01	8.2823	1:45:47
84.38	-3134.2017972	-6.35	8.2843	1:45:11
90.00	-3134.1950422	-2.11	8.1653	1:44:33
180.00	-3134.1915111	0.11	5.4825	1:46:28
270.00	-3134.1949890	-2.07	8.1540	1:43:44
360.00	-3134.1915334	0.09	5.4857	1:44:17



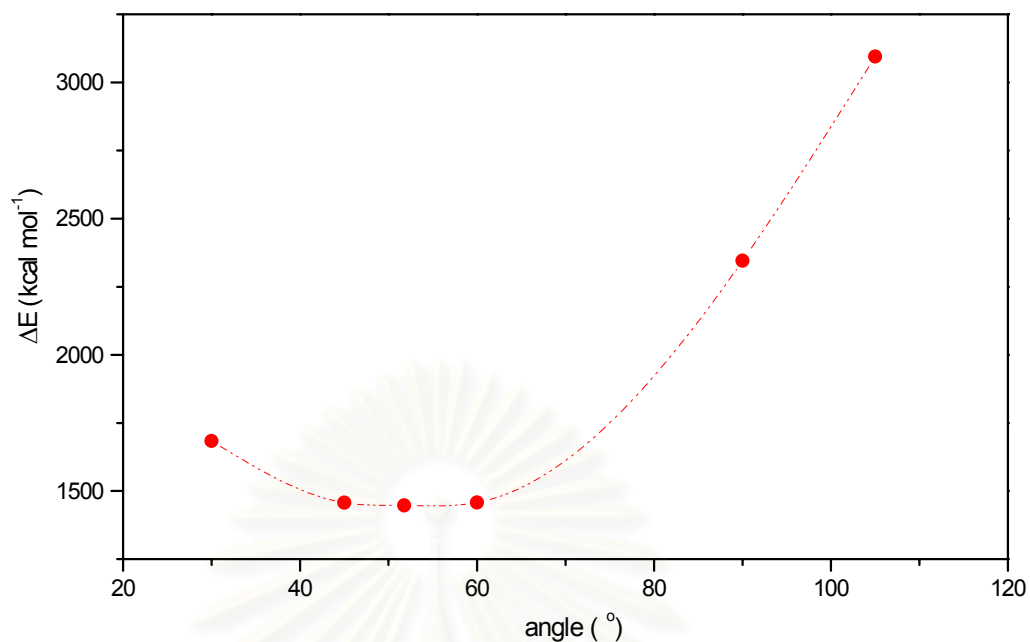


**Figure B8** Rotational barrier curve of phthalic acid which points the aromatic unit towards the calix[4]arene framework and the ligand L<sub>II</sub>.

**Table B8** Rotational barrier data obtained from *ab initio* calculations with STO-3G basis set, of interaction between phthalic acid which points the aromatic unit towards the calix[4]arene framework and the ligand L<sub>II</sub>.

Angle (°)	$E_H$ (Hartree)	$\Delta E$ (kcal.mol <sup>-1</sup> )	Dipole moment (Debye)	CPU times (h:m:s)
30	-3131.508653	1683.63	4.1131	3:42:33
45	-3131.869492	1457.20	4.4628	2:49:49
51.78	-3131.885548	1447.12	8.4973	3:06:41
60	-3131.868324	1457.93	11.5055	2:52:11
90	-3130.454169	2345.33	19.4778	3:50:09
105	-3129.259947	3094.71	12.6271	12:58:10

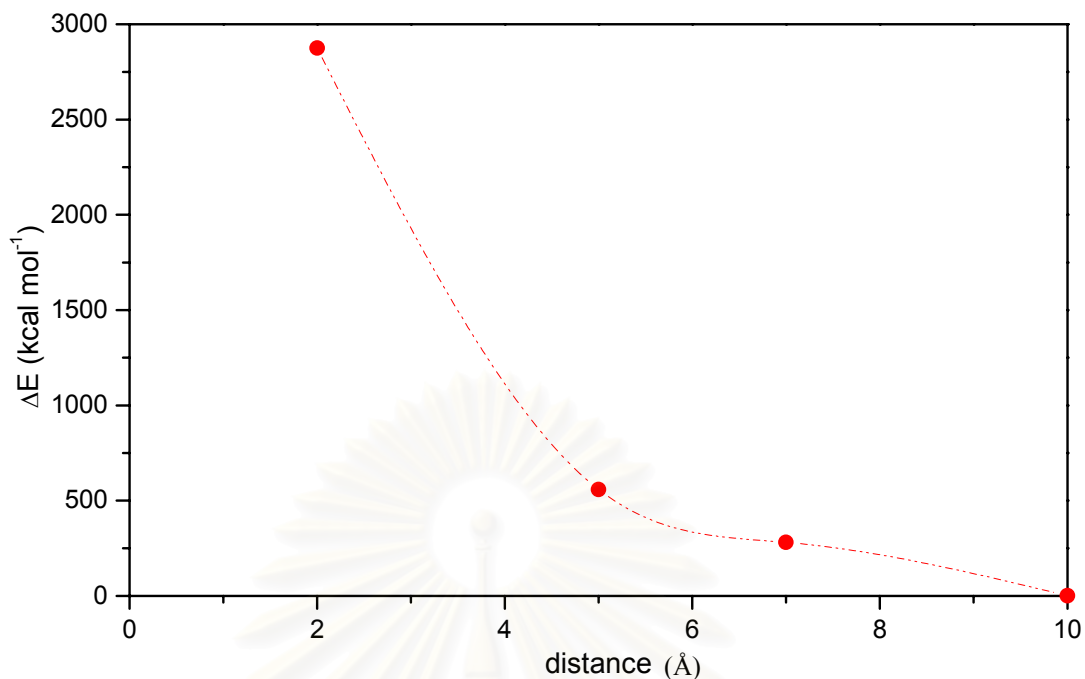


**Figure B9** Potential curve of phthalic acid which points the aromatic unit towards the calix [4]arene framework and the ligand L<sub>II</sub>.

**Table B9** Energies data obtained from *ab initio* calculations with STO-3G basis set, of interaction between phthalic acid which points the aromatic unit towards the calix[4]arene framework and the ligand L<sub>II</sub>.

Distance (Å)	E <sub>H</sub> (Hartree)	ΔE (kcal.mol <sup>-1</sup> )	Dipole moment (Debye)	CPU times (h:m:s)
2	-3129.609528	2875.35	6.6934	6.6934
5	-3133.302112	558.21	6.8428	6.8428
7	-3133.743588	281.18	6.9725	6.9725
10	-3134.190351	0.84	7.3493	7.3493

## VITA

Pratan Ruekmetha was born on August 16, 1974 in Bangkok, Thailand. He received the Bachelor of Science in Chemistry from Chulalongkorn University, in 1997. Since 1997 he has been a graduate student at the Department of Chemistry, Chulalongkorn University, studying in the field of inorganic chemistry leading to a Master of science degree.



สถาบันวิทยบริการ  
จุฬาลงกรณ์มหาวิทยาลัย